Geotechnical Engineering Masters Projects   Civil and Environmental Engineering

2018

Influence of Reconsolidation Procedure on Small Strain Shear Modulus and Undrained Shear Behavior of Silts Subjected to Tube Sampling Disturbance

Shreya Pandey
University of Massachusetts Amherst

INFLUENCE OF RECONSOLIDATION PROCEDURE ON SMALL STRAIN SHEAR MODULUS AND UNDRAINED SHEAR BEHAVIOR OF SILTS SUBJECTED TO TUBE SAMPLING DISTURBANCE

A Master Project Presented

By

Shreeya Pandey

Master of Science in Civil Engineering

Department of Civil and Environmental Engineering University of Massachusetts Amherst, MA 01003

AUGUST 2018

INFLUENCE OF RECONSOLIDATION PROCEDURE 0N SMALL STRAN SHEAR MODULUS AND UNDRAINED SI-ÆAR BEHAVIOR OF SILTS SUBJECTED TO TUBE SAMPLING DISTURBANCE

A Masters Project Presented

by

Shreeya Pandey

Approved as to style and content by:

_____

Dr Don J. DeGroot, Chairperson

_____

Dr. Guoping Zhang, Member

_____
Sanjay Arwade
Civil and Environmental Engineering Department

ACKNOWLEGEMENTS

I would like to extend my thanks and appreciation to the following people for their assistance to this project: Professor Don DeGroot, advisor and mentor, for his guidance and support throughout the project; Professor Guoping Zhang for serving as a committee member and for his insights and advice; William Lukas for training and guiding me to run the triaxial test; my classmate for all their support and my family for their support and encouragement.
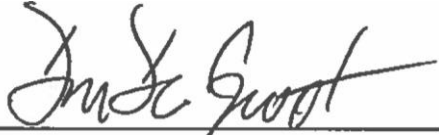
ABSTRACT

**INFLUENCE OF RECONSOLIDATION PROCEDURE ON SMALL STRAIN
SHEAR MODULUS AND UNDRAINED SHEAR BEHAVIOR OF SILTS
SUBJECTED TO TUBE SAMPLING DISTURBANCE**

AUGUST 2018

Shreeya Pandey, B.S., Asian Institute of Technology

M.S., University of Massachusetts Amherst

Directed by: Dr. Don J. DeGroot

This thesis presents results of a laboratory testing program that studied the effects of

laboratory simulated tube sampling disturbance on the undrained shear strength behavior

of reconstituted low plasticity silts at overconsolidation ratios of 1.0 and 3.6. The three

test soils consisted of two different mixtures of kaolin clay and silica silt and a

reconstituted natural Dedham silt. Triaxial tests with bender elements were conducted

on the reconstituted samples using the Ideal Sampling Approach (ISA) followed by

post-ISA reconsolidation and undrained shear. The specimens were subjected to $\pm$ 1%

and $\pm$ 3% ISA axial strain cycles. Changes in shear wave velocity and small strain shear

modulus during simulation of tube sampling was used to develop a better understanding

of the effects of sample disturbance on the undrained stress-strain-strength behavior of

silts.

Laboratory simulated tube sampling disturbance changed the undrained shear

behavior of the low plasticity silts from contractive to dilative. The reconstituted silt

samples experienced significant loss in effective stress due to ISA disturbance which

decreased with an increase in overconsolidation ratio and plasticity. The normalized

undrained shear behavior of the tested reconstituted silt samples did not show any

dependency on the consolidation stress level, however, an increase in the consolidation

stress level increased the tendency for the low plasticity silts to exhibit dilative behavior. The effect of Recompression and SHANSEP consolidation procedures on recovering the undisturbed behavior was found to be dependent on the plasticity of the soil, to some extend on the pre-ISA consolidation stress, level of ISA disturbance experienced by the specimen and the overconsolidation ratio.

The measured shear wave velocity and small strain shear modulus at various stress states showed significant reduction during ISA disturbance which could be used as an indicator of sample disturbance in similar types of silts. However, after reconsolidating the specimens back to the initial effective stress state the shear wave velocity and small strain shear modulus values were mostly recovered indicating little to no influence of sample disturbance. The amount of reduction in shear wave velocity and small strain shear modulus was found to be dependent on plasticity of soil, level of disturbance and overconsolidation ratio.

Table of Contents

LIST OF FIGURES

CHAPTER 1: INTRODUCTION

1.1 Introduction

Sampling of undisturbed soil from the subsurface is essential for measuring engineering properties of the soil. During the process of retrieving soil from the subsurface, transporting it to laboratory and installing it in a testing device the soil is disturbed which changes the in-situ properties of soil. Tube sampling is commonly used to collect samples from the subsurface. Stress relief and distortion of the soil structure are irrecoverable forms of sample disturbance during tube sampling. It also causes significant shearing between the soil and the sampler wall changing the in-situ stress-strain behavior of the soil and the resultant laboratory measurement of the sample can be significantly different than the in-situ behavior for highly disturbed samples.

Many studies have been conducted on clays that have resulted in the development of methods to assess the effects of sample disturbance. However, there is a lack of similar such methods to quantify the effects of sample disturbance on intermediate soils such as sandy clays, silty clays, clayey silt, and silty sands. Sampling undisturbed silt is difficult, previous studies have reported densification of loose silts during sampling and there is lack of laboratory testing experience in determining the in-situ strength of silts due to its tendency to exhibit dilative behavior upon undrained shearing. Unlike clays, the undrained shear behavior of silts is more uncertain and there is lack of understanding of the influence of sample disturbance on determination of design parameters from laboratory tests.

The goal of this research was to study the effect of tube sample disturbance on the undrained shear strength behavior of silts by laboratory simulation of tube sampling on reconstituted silt samples. Triaxial tests with bender elements were conducted on

reconstituted silts samples using the Ideal Sampling Approach (Baligh et al. 1987). Changes in shear wave velocity, V_s and small strain shear modulus, G_{max}, during simulation of tube sampling was used to develop a better understanding of the effects of sample disturbance on the undrained stress-strain-strength behavior of silts.

1.2 Objectives and Scope of Research

The primary objective of this research was to study the effect of tube sampling disturbance on the undrained shear behavior of reconstituted silt samples by conducting triaxial testing. The reconstituted samples tested consists of 85S15K and 50S50K prepared by varying the percentage of kaolin clay (K) and silica silt (S) by dry mass. The third soil tested was Dedham Silt which is a natural glacially deposited silt from Dedham, Massachusetts. This research program incorporated triaxial cells embedded with bender elements to monitor the change in shear wave velocity, V_s, and small strain shear modulus, G_{max}, throughout all phases of testing.

The scope of this research included advanced laboratory testing of reconstituted silt samples and included the following tasks: -

1. Index and classification tests such as grain-size distribution, specific gravity and Atterberg limits.

2. Preparation of reconstituted specimens for triaxial testing using the vacuum split mold technique similar to Wang et al. (2011).

3. Stimulation of tube sampling disturbance on test specimens using the ideal sampling approach.

4. Evaluation of the effect of two reconsolidation procedures namely, Recompression and SHANSEP to mitigate the effects of sample disturbance in silts.

5. Evaluation of the influence of consolidation stress level on undrained shear behavior and normalized undrained shear strength of silts.

6. Evaluation of the Brandon et al. (2006) failure criteria for selection of undrained shear strength of silts that exhibit dilative behavior during undrained shear.

7. Evaluation of the influence of ISA straining, post-ISA Recompression and SHANSEP consolidation procedures after ISA disturbance on shear wave velocity and small strain shear modulus of the test soils.

1.3 Thesis Organization

Chapter 2 presents a brief review of the literature on sample disturbance and effects of sampling on clays and silts. Topics include: ISA method for stimulating tube sampling disturbance, Recompression and SHANSEP reconsolidation procedures, criteria used to define failure for dilating soils and shear wave velocity – stress state framework.

Chapter 3 presents the methods of investigation which includes index test and triaxial test procedure, sample preparation, equipment description and a brief description of bender elements used to measure the shear wave velocity and small strain shear modulus of the test soils.

Chapter 4 is subdivided into three sections. Section 4.1 presents the results from anisotropically consolidated undrained triaxial compression tests (CAUC) performed at various consolidation stress levels on test soils 50S50K, 85S15K and Dedham Silt. This section discusses the influence of stress level on the normalized undrained shear strength and Brandon et al. (2006) failure criteria for selection of undrained shear strength of dilating soils. Section 4.2 presents and analyzes results from laboratory triaxial tests conducted on the test soils to study the effect of the

Recompression and SHANSEP consolidation procedures on post ISA behavior of the test soils. Section 4.3 presents and analyzes results of shear wave velocity and small strain shear modulus measurements obtained from laboratory triaxial cells equipped with bender elements.

CHAPTER 2. BACKGROUND

This chapter presents a brief summary of background information and prior research on sample disturbance and effect of sampling on the behavior of different types of soils. Topics include: ISA method for stimulating sample disturbance, Recompression and SHANSEP reconsolidation procedures, criteria used to define failure for dilating soils and shear wave velocity – stress state framework.

2.1 Sample disturbance

Engineering properties of soil are typically measured by conducting laboratory testing on undisturbed soil samples collected from the subsurface. However, during the process of retrieving soil from the subsurface, transporting it to laboratory and installing it in a testing device changes the in-situ properties such as water content, structure of the soil and changes in stress can occur which is referred to as sample disturbance. The three main sources of sample disturbance are stress relief due to drilling and collection of samples, sampling equipment and handling and storage of the sample before testing. Figure 2.1 shows the complex hypothetical stress path for a low OCR clay during drilling, tube sampling and specimen preparation (Ladd and DeGroot 2003). The stress path shows the change in stress that the sample undergoes during sample disturbance. As shown in the Figure 2.1 during drilling the specimen experiences removal of deviator stress q at constant effective horizontal stress σ'_{ho}, this resultant isotropic stress is known as the perfect sampling stress σ'_{ps}. However, the sample undergoes a series of stress changes during tube sampling, transport, extrusion and trimming causing the sampling effective stress σ'_s to typically be much less than the σ'_{ps}. The degree of sampling stress relief is dependent on the stress history and plasticity of the soil (Hight & Leroueil 2003).

5

Apart from stress relief, distortion of the soil structure during tube sampling is a irrecoverable form of sample disturbance. Tube sampling causes significant shearing between the soil and the sampler inner wall. This changes the condition of the sample and the resultant laboratory measurement of its undrained stress-strain behavior can by far different from its in-situ behavior for severely disturbed samples.

Extensive research has been conducted to study sample disturbance in various type of soils especially, clays and sands. These studies identified that stress relief during sampling is unavoidable and quantified the effect of sample disturbance on the shear strength measured in the laboratory to explain the observed behavior of "disturbed" samples (Santagata & Germaine 2002). The effect of sample disturbance has been extensively studied on natural and resedimented clays (e.g. Baligh et al. 1987, Santagata and Germaine 2002, 2005, 2006, Ladd and Lambe 1963, Clayton et al. 1992, Siddique et al. 2000). Lunne et al. (2006) investigated the effect of sample disturbance on measured shear strength behavior of low plasticity soft marine Norwegian clays. The study concluded that sample disturbance causes decrease in shear strength and elastic modulus and an increase in strain at failure.

Unlike clays, less research has been conducted to study the effect of sample disturbance on intermediate soils such as silts, clayey silts and sandy silts mainly due to the difficulty in sampling these soils. Therefore, often reconstituted silt specimens are used by researchers for testing the behavior of intermediate soils. Fleming and Duncan (1990) tested reconstituted samples of Alaskan silts and found that sample disturbance increased the measured shear strength in CIUC and CAUC tests whereas the shear strength decreased in UU tests. Sandven (2003) found that loose and normally consolidated Norwegian silts tend to densify during tube sampling which causes the measured strength and stiffness of the soil to be higher than its in situ values. Similarly,

Long (2006a) studied Athlone laminated clay/silts and reported that tube sampling disturbance resulted in strong post-peak dilation and increase in stiffness and undrained strength of the soil. Carroll (2013) reported that low and non-plastic silts are more susceptible to densification during sampling. Carroll (2013) simulated tube sample disturbance on several Irish silts and observed dilative behavior during shear as opposed to the anticipated contractive behavior for an undisturbed specimen. Carroll (2013) also concluded that both actual and stimulated disturbance resulted in an increase in strength and stiffness of the soil, which would lead to selection of unconservative soil parameters for most design problems.

2.2 ISA Method of Stimulating Sample Disturbance

Two models or frameworks that quantify the effect of sample disturbance are the perfect sampling approach (PSA, Ladd & Lambe 1963) and the ideal sampling approach (ISA, Baligh et al 1987). The perfect sampling approach simulates sample disturbance experienced during ideal block sampling. PSA framework identifies the release of the in-situ shear (or deviator) stress as the only unavoidable disturbance during sampling. However, for tube sampling there are additional factors that significantly contribute to sample disturbance, most notably penetration of the sampling tube into the soil and its subsequent extraction. Baligh et al (1987) introduced the ISA using the strain path method to simulate disturbance due to tube sampling.

The ISA takes into account the disturbance due to undrained tube penetration at the centerline of an ideal sample of varying geometry. The soil undergoes axial compression during penetration followed by undrained triaxial extension as the soil enter the tube sampler. This compression and extension straining are presented in Figure 2.2. The soil is also subjected to shear strain along the wall of the sampler where the soil

is remolded generating excess pore pressure. The vertical strain induced by the tube

sampler is given by the following equation: -

$$\varepsilon_{zz} = -\ln(1 + \frac{2t}{OD} \frac{\frac{z}{OD}}{[1+4(\frac{z}{OD})^2]^{3/2}} \qquad (2.2.1)$$

$$\varepsilon_{zz,max} = 0.385 \frac{t}{D_t} \qquad (2.2.2)$$

where
t = sampler wall thickness (mm)

D_t = external sampler diameter (mm)

z = distance from the tip of the sampler (mm)

$\varepsilon_{zz,max}$ = maximum vertical strain

     ISA also considers the disturbance due to sample retrieval and extrusion, which

is idealized by an undrained release of the post ISA disturbance shear stresses in the soil

from final anisotropic stress condition in the tube to the final isotropic stress state before

testing. Another part of the tube sampling that contributes to sample disturbance is the

geometry of the cutting shoe of the sampler. Clayton et al (1998) investigated the

influence of various geometric designs of the cutting shoe of the sampler on sample

disturbance and concluded that: -

1. increasing the area ratio of the sampling tube resulted in a significant increase in the

peak compressive strain ahead of the sampler but only a slight increase in the peak

extension strain;

2. increasing the inside clearance ratio resulted in an increase in the peak extension

strain with a slight reduction in the peak compressive strain;

3. the inside cutting-edge angle only effected the peak extension strain; and

4. increasing the outside cutting angle resulted in a significant increase in the peak compressive strain and a slight increase in the peak extension strain.

5. using a more realistic cutting shoe geometric rather than a blunt sampler by Baligh (1985) resulted in significantly lower peak axial strain during sampling as presented in Figure 2.2.2.

Clayton et al (1998) recommended that a good sampler for clays is one with an area ratio not exceeding 10% and a cutting-edge angle less than or equal to $10°$.

2.3 SHANSEP and Recompression Methods

The stress history and normalized soil engineering properties (SHANSEP) and Recompression methods were developed to consider the effects of sample disturbance, anisotropy and strain rate undrained shear behavior of clays. The Recompression method developed by Bjerrum (1972) and SHANSEP developed by Ladd and Foott (1974) both recommend using CK_0U tests with consolidation to known stress states, shearing at different modes of failure and with appropriate strain rates to account for anisotropy and strain rate effects (Ladd & DeGroot 2003). The two methods, however differ significantly on how to deal with sample disturbance.

Figure 2.3.1 shows the Recompression and SHANSEP consolidation procedures for laboratory CK_0U testing. The Recompression method anisotropically consolidates specimens to the estimated in situ state of stress σ'_{vo} and σ'_{ho}. This method is preferred for high quality samples because Recompression to in situ stress state for less disturbed specimen does not cause much decrease in water content and hence should result in a measure of the undrained shear strength (s_u) that is representative of in situ conditions. The Recompression method is also preferred for highly structured clays, cemented clays and high OCR clays (Ladd & DeGroot 2003). However, this method cannot be used for

truly normally consolidated soil as it might cause significant reduction of water content and overestimate the undrained s_u. Santagata and Germaine (2005) also reported that for NC RBBC soil Recompression to in situ stresses overestimated the s_u of the soil. Similarly, for NC RBBC specimen subjected to ISA 1% and 2% resulted in significant overestimation of undrained s_u.

The SHANSEP method is based on experimental observation and field data that the normalized undrained stress-strain-strength behavior of clays is a function of the stress history of the clay deposit. This method assumes perfectly normalized behavior for all values of σ'_{vc}, mode of shear and uses mechanical overconsolidation to represent all preconsolidation mechanism (Ladd & DeGroot 2003). The perfectly normalized behavior or SHANSEP equation is given by the following: -

$$\frac{s_u}{\sigma'_{vc}} = S \ (OCR)^m$$

(2.3.1)

where,

$\frac{s_u}{\sigma'_{vc}} =$ normalized undrained shear strength

OCR = Overconsolidation ratio

S and m = SHANSEP parameters

To measure the normally consolidated behavior specimens are K_0 consolidated to stress level greater than σ'_p as shown in point A and B of Figure 2.3. The overconsolidated behavior is measured by unloading the specimen to the required OCR (point C and D). SHANSEP parameters S is computed from OCR =1 and m from varying OCR >1. SHANSEP method does not work for highly structured clays and

highly desiccated clay crust. For structured clays it underpredicts the in situ undrained stiffness of the soils and for desiccated crust the mechanical overconsolidation does not represent the primary overconsolidation mechanism (Ladd & DeGroot 2003).

Santagata and Germaine (2005) reported that SHANSEP method on NC RBBC subjected to ±1% & ±2% ISA produced reliable conservative undrained shear strength, however, for higher degree of disturbance (± 5% ISA) the disturbance was not recovered.

2.4 Failure Criteria for Selection of Undrained Shear Strength of Dilating Silts

The dilative behavior tendency of low-plasticity silts when performing undrained triaxial test makes it difficult to evaluate the undrained shear strength and to define the failure point of the soil. Various criteria as listed in Table 2.4.1 have been proposed for soils such as dilating silts using as shown in an idealized stress path in Figure 2.4. Depending on the type of triaxial test performed, the strength parameter to be determined and the stress-strain-volume change behavior of the soil, the failure criteria is selected (Brandon et al. 2006). As given in Table 2.4 the peak deviator stress and limiting strain can be used for any type of triaxial test performed. The remaining criteria are used for tests where pore pressures and effective stress are known.

Brandon et al. (2006) performed CU tests on undisturbed Yazoo silt, remolded OC Yazoo silt, remolded NC Yazoo silt and remolded OC LMVD (Lower Mississippi Valley division) silt and used all six failure criteria to evaluate the undrained shear strength. It was reported that the peak deviator stress failure criteria resulted in wide scatter of the undrained shear strength of the silts. Using the peak deviator stress failure criteria, the normalized undrained shear strength (s_u/σ'_{vc}) for undisturbed and remolded NC Yazoo silt ranged from 1.0 to 1.4, and 1.6 and >4.5 for remolded OC Yazoo and

remolded OC LMVD. Similarly, Long et al (2010) also reported high values of undrained shear strength of Norwegian glaciomarine silts using peak deviator stress failure criterion.

The second criterion which is the peak principle stress ratio $(\sigma_1'/\sigma_2')_{max}$ also gave a wide scatter of undrained shear strength. The s_u/σ'_{vc} for undisturbed and remolded NC Yazoo silt ranged from 0.88 to 0.96, and 1.0 to 1.90 for remolded OC Yazoo and remolded OC LMVD. Brandon et al. (2006) concludes that the scatter is because the stress path lies very close to the failure envelope, and the exact value of deviator stress where the principle stress ratio is maximum is uncertain It was also observed that the principal stress ratio might be constant over a wide range of deviator stresses.

The peak pore pressure u_{max} showed the least deviation in s_u/σ'_{vc} and gave the lowest undrained shear strength. Using u_{max} failure criteria the s_u/σ'_{vc} for undisturbed, remolded NC Yazoo silt and remolded OC LMVD was 0.49 and for OC Yazoo was 0.48. Carroll (2013) also reported that u_{max} failure criteria resulted in s_u/σ'_{vc} ranging from 0.44 to 0.45 for Irish silts. The u_{max} failure criteria gives conservative undrained shear strength because u_{max} often occurs before full mobilization of the effective stress properties (Brandon et al. 2006).

For $\bar{A}=0$ or $\Delta u=0$ failure criteria the undrained shear strength is equal to the drained strength. This ensures reliability of the strength value as the strength that results from negative change in pore pressure is not taken into consideration. The s_u/σ'_{vc} reported by Brandon et al. (2006) are consistent ranging from 1.47 to 1.58 for remolded and undisturbed NC Yazoo silt, and 1.43 and 1.38 for remolded OC Yazoo and remolded OC LMVD silt respectively. However, the $\bar{A}=0$ failure criterion is not applicable when the pore pressure does not fall below zero as found in Norwegian

glaciomarine silts reported by Long et al. (2010). Brandon et al. (2006) recommends that

Ā=0 failure criteria to be used for low plasticity silts such as Mississippi Valley silts that

experiences less dilation upon shearing.

Similar to peak principle stress ratio criteria, the K_f line criteria produces scatter

as the exact value of deviator stress that touches the K_f line is not clear. Using the K_f line

failure criteria the s_u/σ'_{vc} for undisturbed and remolded NC Yazoo silt ranged from 0.88

to 0.96, and 1.0 to 1.90 for remolded OC Yazoo and remolded OC LMVD.

The limiting strain criteria used in literature ranges from 5% to 15%. It is not

known what percent of ε_f is ideal as limiting strain criteria for low plasticity silts.

Brandon et al (2006) suggest using $\varepsilon_f = 10\%$ for low plasticity silts, however, the

reported s_u/σ'_{vc} values are not consistent ranging from 1.24 to 3.5.

2.5 Shear Wave Velocity – Stress State Framework

The following presentation of the shear wave velocity – stress state framework is

abstracted from Lukas (2017). Hardin and Blandford (1989) presented an equation that

relates the small strain shear modulus G_0 to several state parameters and soil properties

as

$$G_{0ij} = V_{ij}{}^2\rho_t = S_{ij}F(e)OCR^k\sigma'_{ref}{}^{1-ni-nj}\sigma'_i{}^{ni}\sigma'_j{}^{nj} \qquad \text{Eq. 2.5.1}$$

where

G_{0ij} = small strain stiffness

V_{ij} = shear wave velocity

ρ_t = total density

S_{ij} = "structure" term

$F(e)$ = function accounting for void ratio change

OCR = overconsolidation ratio

13

σ'_{ref} = reference stress

σ'_{ij} = effective stress

i = direction of wave propagation

j = direction of wave polarization

For measurement of the shear wave velocity in the vertical (v) direction with a horizontally (h) polarized wave and with σ'_{ref} set equal to 1 kPa reduces Equation 2.5.1 to:

$$G_{vh} = V_{vh}{}^2 \rho_t = S_{vh} F(e) OCR^k {\sigma'_v}^{nv} {\sigma'_h}^{nh} \qquad \text{Eq. 2.5.2}$$

Laboratory data shows that the coefficient k = 0 and that the coefficients 'nv' and 'nh' are equal to each other and constant (e.g., Jamiolkowski et al. 1995, Pennington et al. 1997). Several different forms of the void ratio function have been proposed with $F(e) = e^{-m}$ being a common one (Jamiolkowski et al. 1995). This further simplifies Equation 2.5.2 to:

$$G_{vh} = V_{vh}{}^2 \rho_t = S_{vh} e^{-m} (\sigma'_v \sigma'_h)^n \qquad \text{Eq. 2.5.3}$$

To determine the coefficients S_{vh}, m, and n the shear wave velocity should be measured at known states of σ'_v, σ'_h, and e for: 1) various stress states but with little change in void ratio to determine n, i.e. unload cycles, 2) the same effective stress state but at different void ratios to determine m, and 3) normalization of G_{vh} by $F(e)$ to confirm n and to determine S_{vh}. These known states can all be achieved by performing a K_0-consolidated test in a triaxial stress path cell equipped with bender elements with multiple unload-reload loops and frequent measurement of the shear wave velocity.

Use of the shear wave velocity – stress state framework presumes that a disturbed state for soft clays will plot in a region below the backbone curve as shown schematically in Figure 2.5. This is based on sample disturbance in soft clays results in a reduction in effective stress and shear wave velocity due to the combined effects of

sampling stress relief and distortion (e.g., Hight and Leroueil 2003, Ladd and DeGroot 2003, Lunne et al. 2006, Landon et al. 2007, Donohue and Long 2010). No such similar framework has been developed for studying the effects of sample disturbance in silts which may contract or dilate during sampling depending on the initial in situ state conditions, sampling induced disturbance and whether that disturbance is drained or undrained. As such Lukas (2017) will shift the backbone the G_{vh}-e-σ'^2 backbone curve for a given soil as shown schematically in Figure 2.5 which is a modification of the Figure 2.4 framework for soft clays. For initially loose non-cemented low PI to non-plastic intermediate soils where densification can occur during sampling, G_{vh} will increase since it is a direct function of void ratio; similarly an initially dense soil may dilate (loosen) during sampling, resulting in a decrease in G_{vh}. Hence, disturbed sample conditions for silts may occur above or below Figure 4.4 Line O-A.

Table 2. 1 Summary of Failure Criteria for Triaxial Tests (Brandon et al. 2006)

Failure criterion	Test applicability
Peak deviator stress, $(\sigma_1 - \sigma_2)_{max}$	UU, CU, CD
Peak principle stress ratio, $(\sigma_1' / \sigma_2')_{max}$	CU, DD
Peak pore pressure, u_{max}	CU
$\bar{A}=0$ or $\Delta u=0$	CU
Reaching the K_f line	CU, CD
Limiting strain	UU, CU, CD
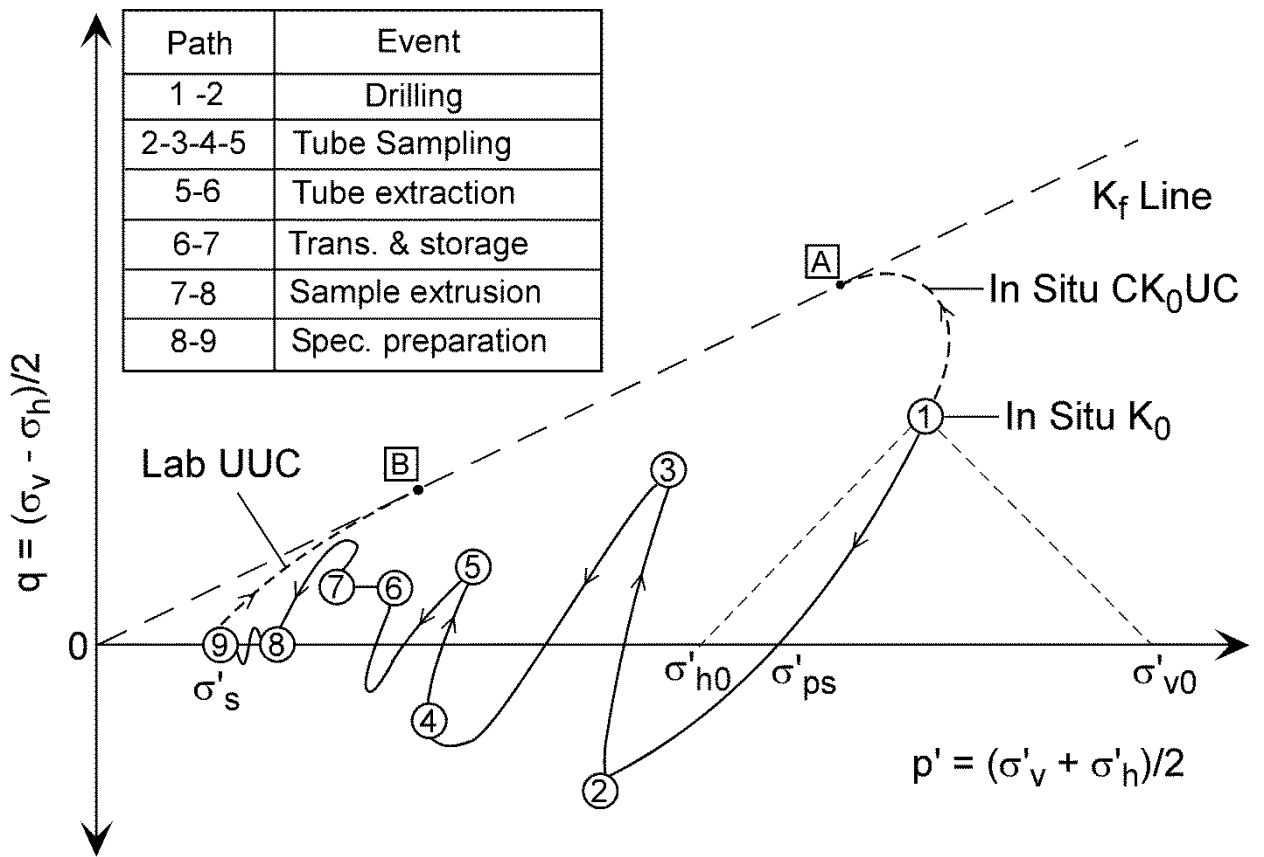
Figure 2. 1 Hypothetical stress path during tube sampling and specimen preparation of centerline element of low OCR clay (Ladd and DeGroot 2003)
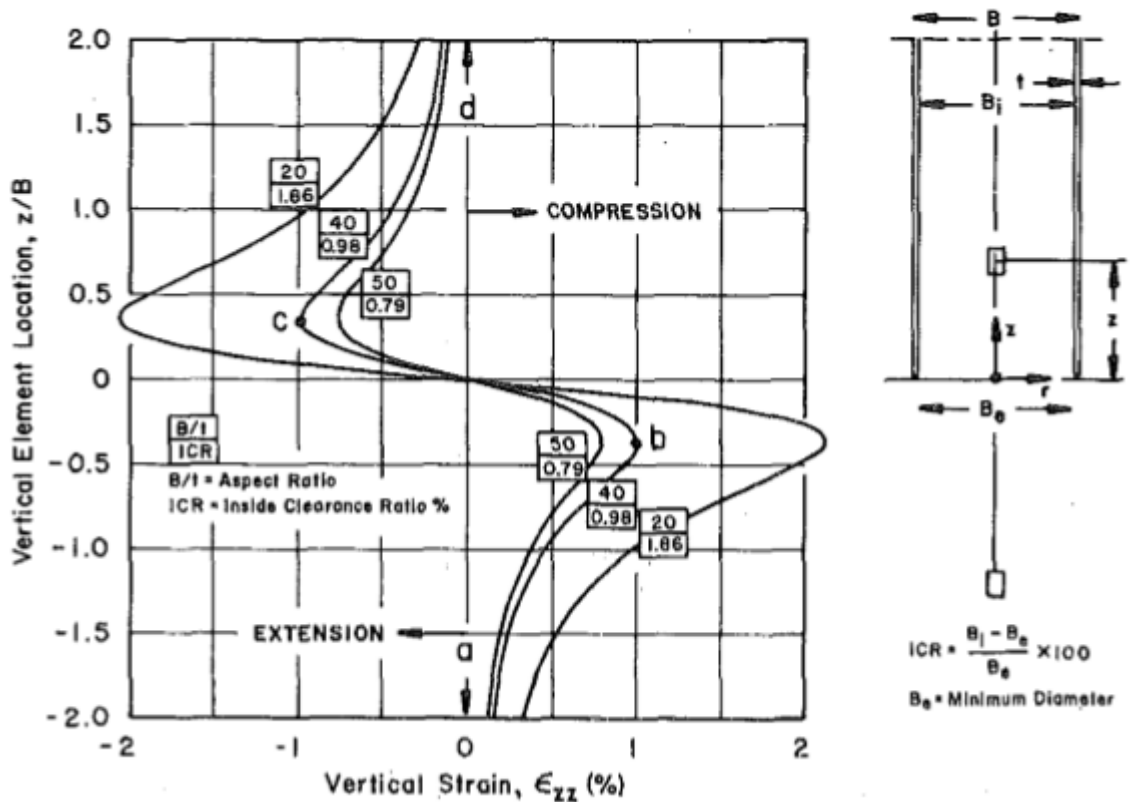
Figure 2. 2 Strain history at the centerline of different simple samplers (Baligh et al. 1987).
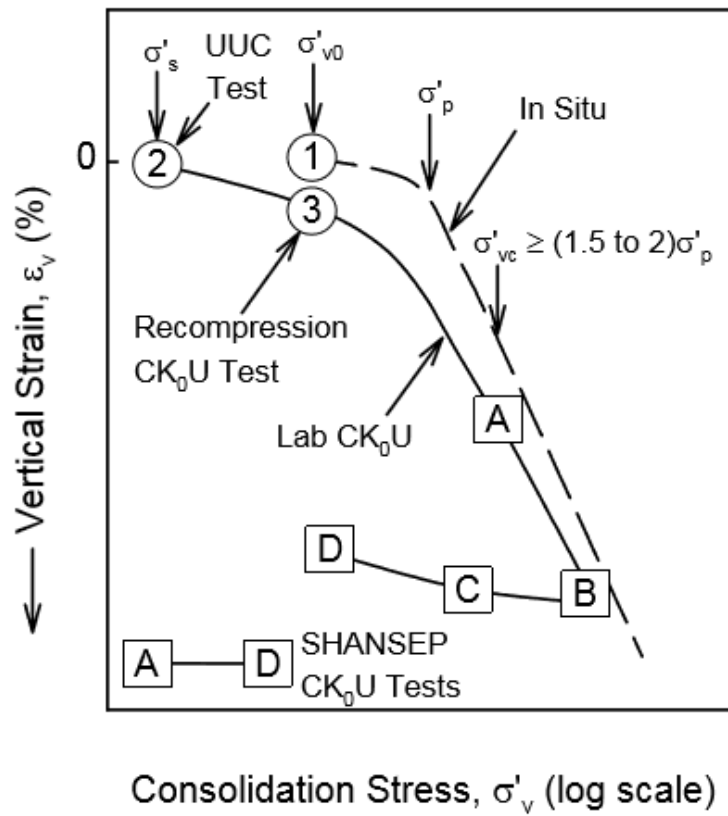
Figure 2. 3 Recompression and SHANSEP Consolidation Procedure for Laboratory CK0U Testing (after Ladd 1991)
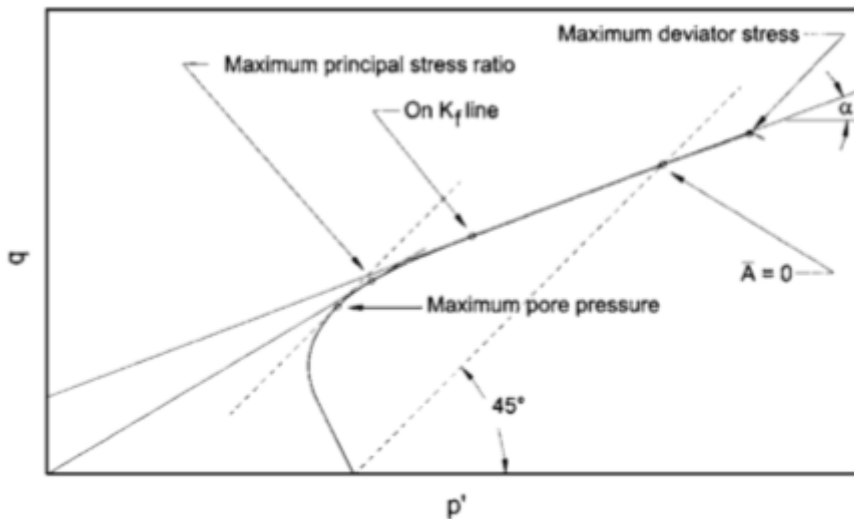
Figure 2. 4 Idealized stress path showing stresses at failure for different failure criteria (Brandon et al. 2006)
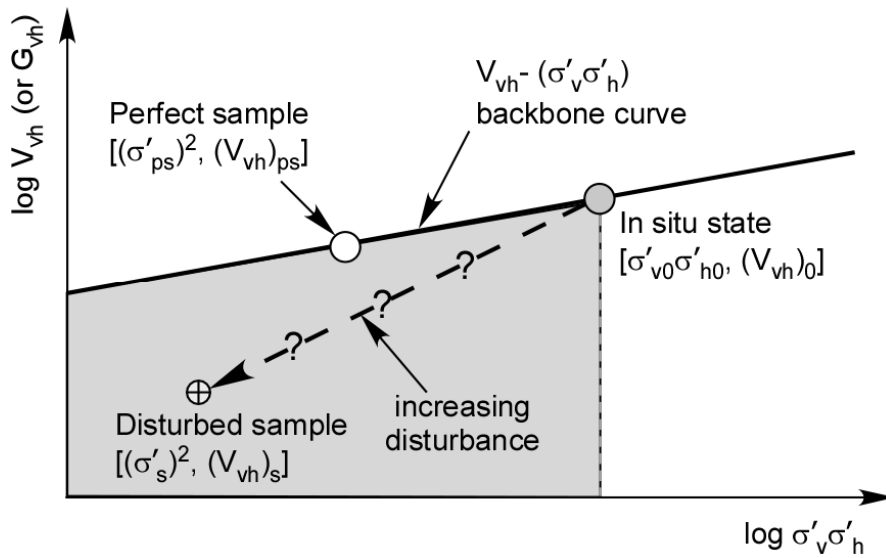
Figure 2. 5 Schematic of shear wave velocity V_{vh} (or small strain shear modulus G_{vh}) – stress state $\sigma'_v\sigma'_h$ framework and reduction in sample state for the perfect sample and a disturbed sample (after DeGroot et al. 2010).
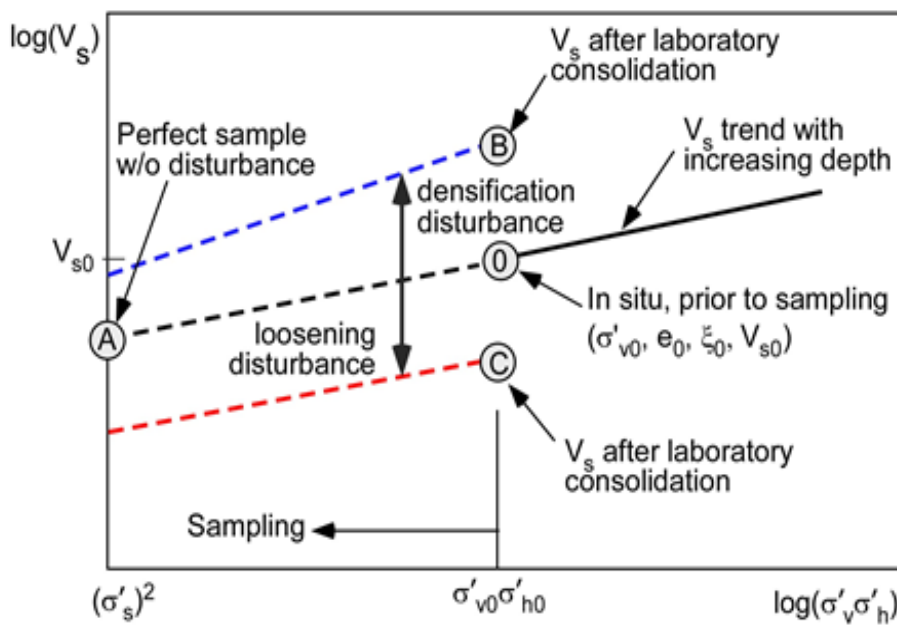
Figure 2. 6 Proposed framework to assess sample quality using shear wave velocity V_{vh} and stress state $\sigma'_v\sigma'_h$ for silts (from Lukas 2017).

CHAPTER 3. METHODS OF INVESTIGATION

This chapter describes the methods used to perform laboratory soil
characterization of the soils tested. This is followed by a description of the triaxial
apparatus used, specimen preparation and triaxial test procedures. Methods used to
conduct bender element tests to measure the shear wave velocity, V_s.

3.1 Basic Index and Classification Tests

This section includes the methods used to characterize and classify the three
different soils used which included: 85S15K (85% silt and 15 % kaolin), 50S50K (50%
silt and 50% kaolin) and natural Dedham Silt. The index tests conducted on the above
soils were Atterberg limits, grain-size analysis and specific gravity.

3.1.1 Water Content

The water content of the soils was measured in general accordance to *ASTM
D2216-10 Standard Test Method for Laboratory Determination of Water (Moisture)
Contents of Soil and Rock by Mass.* Two water content samples were collected after
trimming 50S50K to obtain the wet mass and then oven dried at 110 °C for 24 hours to
obtain the dry mass of the samples. The water content of the soil is determined as

$$w_c = \frac{M_t - M_s}{M_s} \times 100$$

(3.1)

where:

M_t = total soil mass (g)

M_s = mass of solids (g)

w_c = water content (%)

Similarly, water content was measured after completion of the triaxial test to obtain the final water content of the soil.

3.1.2 Grain-Size Analysis

The Hydrometer test was conducted on the soils in general accordance to *ASTM D7928-17 Standard Test Method for Particle-Size Distribution (Gradation) of Fine-Grained Soils Using the Sedimentation (Hydrometer) Analysis.* 5 g of sodium hexemetaphosphate was added to 100 mL of distilled water. The solution was then added to 50 g of soil and mixed in a malt mixer for 1 minute. The slurry was then transferred to a 1000 mL cylinder and was filled with distilled water to the 1000 mL mark. The slurry in the cylinder was mixed by shaking the cylinder up and down for a minute and tempered for at least 16 hours. A reference solution was also prepared using 5 g of sodium hexemetaphosphate mixed with distilled water in a 1000 mL cylinder and tempered for 16 hours. After the 16 hours period the slurry in the cylinder was mixed by shaking the cylinder up and down for a minute. The cylinder is then placed on the bench and using a 151H hydrometer schedule readings was taken for both the soil and the reference solution over a period of 24 hours.

After the test, the slurry was passed through #200 sieve and collected for oven drying to obtain the mass of solids. The mass of solids retained on the #200 is used to measure the percentage of sand fraction, the percentage of clay fraction is computed from the mass of solids less than 2 μm and the percentage of silt is equivalent to 100 subtracted from the sum of % clay fraction and % sand.

3.1.3 Atterberg Limits

Atterberg limits on the soils was performed in general accordance to *ASTM D4318 Standard Test Methods for Liquid Limit, Plastic Limit and Plasticity Index of*

Soils. The soil was first mixed with distilled water until the 15th blow on a calibrated Casagrande cup closed the groove. The soil was allowed to sit overnight in the humid room. The soil was taken out of the humid room and allowed to come back to room temperature before beginning the test. The soil was placed in the Casagrande cup and a groove was cut through the soil. The cup was dropped at the rate of 2 blows per second until the groove closed about 13 mm. A soil sample was taken and placed in the oven to measure the water content. The procedure was repeated to obtain 5 water contents at different blow counts. The water content at the 25th blow was determined as the liquid limit of the soil.

For the plastic limit about 25 g of soil was spread in a glass plate before performing the liquid limit on the soil. The soil was rolled into a 0.32 cm diameter strand. The soil was repeatedly rolled until it starts to crumble at 0.32 cm diameter. The crumbles were collected and placed in the oven to measure the water content. This procedure was repeated three times and the plastic limit is determined as:

$$PL = \frac{w_{c1} + w_{c2} + w_{c3} + w_{c4}}{4}$$
(3.2)

where:

w_c = water content (%)

PL = Plastic Limit

3.1.4 Specific Gravity

Specific gravity test was performed on the soils in general accordance to *ASTM D854-14 Standard Methods for Specific Gravity of Soil Solids by Water Pycnometer*. The test was conducted in a controlled temperature box using ASTM Method B. 50 g of soil was mixed with deaired water in a malt mixer for a minute. The slurry was

transferred to the calibrated pycnometer and deaired water was added until the water level was between one third and half of the depth of the main body of the pycnometer. The slurry was deaired using vacuum for at least 2 hours. A small diameter flexible tube was used to fill the pycnometer with deaired water until the calibrated mark. The pycnometer was left overnight in a controlled temperature box. The pycnometer is weighed and the temperature was recorded. The slurry was collected in a ceramic bowl and oven dried. The specific gravity was determined as:

$$G_t = \frac{M_s}{M_{\rho w,t} - M_{\rho ws,t} - M_s}$$

(3.3)

$$G_{20°C} = k \times G_t$$

(3.4)

where:

M_s = mass of the oven dry soil solids (g)

$M_{\rho w,t}$ = mass of pycnometer and water at the test temperature (g)

$M_{\rho ws,t}$ = mass of pycnometer, water and soil solids at test temperature (g)

G_t = specific gravity of soil solids at test temperature

K = temperature coefficient

$G_{20°C}$ = specific gravity of soil solids at 20°C

3.2 Triaxial Testing

Triaxial test was performed on split mold samples of 85S15K and Dedham Silt and intact samples of 50S50K in general accordance to *ASTM D4767-11 Standard Method for Consolidated Undrained Triaxial Compression Test for Cohesive Soils*. This section includes apparatus description, specimen preparation (using split mold and consolidometer) and test procedures.

3.2.1 Triaxial Apparatus

The triaxial tests were conducted using the GEOTAC TruePath automated stress path system for triaxial testing software. The triaxial apparatus consisted of a GEOTAC load frame, flow pumps, pore pressure transducer, cell pressure transducer, LVDT, internal and external load cell and triaxial test cell chamber. An internal load cell was used to determine the stress on the specimen avoiding the need for piston friction correction. The load frame was used for loading and unloading the specimen at a constant stress or strain rate. The LVDT attached to piston measured the change in the height of the specimen throughout the test. The pore pressure pump provided back pressure and maintained constant pressure during consolidation while the cell pressure pump controlled the cell pressure. The cell pressure in the triaxial cell chamber and pore pressure in the specimen were measured using two pressure transducers mounted directly on the triaxial cell. The TruePath software allowed the user to control and monitor each phase of the triaxial test.

3.2.1 Specimen Preparation

Two mixtures of synthetic soil 85S15K and 50S50K were prepared by varying the percentage of kaolin clay and silica silt by dry mass. The third soil tested was Dedham Silt, which is a natural glacially deposited silt from Dedham, Massachusetts. The index properties and the Unified Soil Classification System of the test soils from Lukas (2018) are presented in Table 3.1 and Figure 43.1. The reconstituted specimen of 85S15K (85% silt and 15 % kaolin) and Dedham Silt may be subjected to liquefaction during trimming, therefore the specimens were prepared in a split mold under vacuum. For the split mold specimens, the amount of distilled water added was 2-2.5 times the liquid limit of the soil. All specimens tested were 35.6 mm in diameter and 71.2 mm tall.

The spilt mold was set up on the triaxial base with an extender on the top to accommodate more soil as shown in Figure 3.2. The slurry was transferred to the split mold with a membrane already in place under vacuum. For low plasticity soil (85S15K) a small vacuum is applied to the specimen at the triaxial base and allowed to self-consolidate overnight. Dedham silt which is non-plastic no vacuum was applied to the specimen and was left to self- consolidate for a few hours or overnight. The next day a total of 5 kg of dead weight was added to the specimen at the rate of 1 kg per hour and left to consolidate overnight. At the end of this preloading phase, the dead weights were removed, and the top cap was assembled on the specimen with the drainage lines attached to the top cap. Vacuum line was attached from the water trap and approximately 30 kPa of vacuum was applied to the specimen and left overnight under vacuum. The split mold was removed the next day, the dimensions of the specimen were measured and all the parts of a triaxial apparatus were assembled together and placed in the load frame. The vacuum applied to specimen was only removed after a seating cell pressure of 30 kPa was applied. This method of split mold set-up is described in more detail in Lukas (2018).

The soil 50S50K (50% silt and 50 % kaolin) which has enough clay content to be self-standing was prepared in a consolidometer. The soil was mixed with distilled water at 1.5-2 times the liquid limit and allowed to hydrate overnight. The parts of the consolidometer set up are shown in Figure 3.3. Vacuum grease was applied to the bottom of the consolidometer with an O ring attached to the bottom. An acrylic cylinder with an inside diameter of 102 mm was lubricated with silicon oil (200cs) and attached to the bottom of the consolidometer along with a porous stone. The soil slurry was transferred to the cylinder. The soil was mixed with a propeller mixing blade under vacuum to minimize trapping air bubbles in the soil cake. A drill attachment was

connected to the top cap of the consolidometer and a mixing blade was inserted through the bottom of the top cap and attached to the drill. The soil was mixed for 30 seconds under vacuum. The drill attachment was removed and a piston along with a cross bar was attached to the cylinder and locked to the bottom of the consolidometer. A GeoJac frame was used to perform 1-D consolidation by applying incremental stresses starting from 5 kPa to 200 kPa until the specimen was consolidated with one log cycle of secondary compression at the maximum applied stress. The soil cake was then extruded and coated with 50-50 mixture of petroleum jelly and paraffin wax and covered with plastic film dipped in the wax mixture. The soil cake was stored in a humid room with a controlled temperature of 11℃.

3.2.3 Test Procedure

TruePath automated stress path system for triaxial testing software was used to perform triaxial test on the test soils. 85S15K, 50S50K and Dedham silt specimens were anisotropically consolidated using controlled stress path to selected target K_0 values. The K_0 values presented in Table 3.2 were estimated by Lukas et al (2018) using Mesri and Hayat (1993) relationship among K_0, OCR and ϕ'_{mo} (effective stress friction angle at maximum obliquity). All specimens were normally consolidated to an effective vertical stress ranging from 100 to 800 kPa and unloaded, if an overconsolidated state was required, to the appropriate vertical stress and corresponding K_0 for a given target overconsolidation ratio (OCR).

An initial seating pressure of 30 kPa was applied to the specimen and backpressure saturation was performed by ramping up the back pressure to 300 kPa and maintain that pressure until a B value >0.95 was achieved. The specimen was anisotropically consolidated using controlled stress path to K_0 value as discussed above

at a strain rate of 0.2 %/hr for loading and 0.05%/hr for unloading. The specimen was allowed to creep overnight prior to undrained shearing for normally consolidated soil, ISA shearing or unloading in case of specimen with OCR 3.6. After consolidation, the specimen was subjected to undrained ISA shearing under strain-controlled mode with peak ISA strains of $\pm$ 1 % and $\pm$ 3 %. After completion of the ISA loading cycle, the specimen was unloaded to $q = 0$ (i.e., zero deviator stress) under undrained conditions and reaching an isotropic state after the removal of the deviator stress. Post-ISA, the specimen was anisotropically reconsolidated to pre-ISA vertical effective stress of 400 kPa for normally consolidated specimen or unloaded to vertical effective stress of 111 kPa for specimen with OCR 3.6 for the Recompression procedure. Finally, the specimen was sheared undrained in triaxial compression mode at the rate of 0.5%/hr until a maximum of 15% strain.

Post-ISA SHANSEP tests were also conducted, i.e., the specimen was reconsolidated past the pre-ISA vertical effective stress to 800 kPa and sheared undrained for normally consolidated soil or unloaded to an appropriate vertical effective stress for the OCR specimens.

3.3 Bender Elements

Bender elements were imbedded in the triaxial base and the top cap as shown in Figure 3.4. The construction system and configuration of bender elements is described in detail by Lukas (2018). The function generator used was a Wavetek model 29 19 MHz Direct Digital Synthesis (DSS). The transmitting bender was excited by the function generator with a ±10 V single sine wave of varying frequency generated every 100 ms. A PicoScope (Model 4226) oscilloscope along with PicoScope 6 software was used to read both the transmitted and received signals. The function generator, Wavetek

has different frequencies programmed in the system which can be recalled by clicking the RECALL button followed by the desired frequency, then ENTER button and OUTPUT button. The received and transmitted signals are displayed on the computer using the PicoScope interface. The data was recorded either by clicking the space bar or the go and stop button on the screen.

All the bender signals were transmitted at frequency of 5kHz which was determined to produce the best recorded signal by the receiving bender element. The shear wave velocity was computed using the shear wave travel time (Δt) estimated using the first zero crossover method also knows as the start-to-start method (Lukas, 2018). This was determined by taking the time interval between the start transmission wave and the pre-deviated received wave which is defined as when it first crosses the zero-voltage value as shown in Figure 3.5. The shear wave velocity was determined as:

$$V_{vh} = \frac{L_{tt}}{\Delta t} \tag{3.5}$$

where:

V_{vh} = shear wave velocity (v is the direction of wave propagation & h is the direction of wave polarization)

L_{tt} = tip to tip distance between the top and bottom benders

Δt = shear wave travelled time (using the zero-crossover method)

The small strain shear modulus G_{vh} was estimated using the following reduced equation from Hardin and Blandford (1989).

$$G_{vh} = V_{vh}^2 \rho_t = S_{vh} e^{-m} (\sigma_v' \, \sigma_h')^n$$

.6)

where:

ρ_t = total density

S_{vh} = "structure" term

e^{-m} = void ratio function

σ_v' = vertical effective stress

σ_h' = horizontal effective stress

S_{vh} , m and n coefficients were estimated by measuring the shear wave velocity at known states of σ'$_v$, σ'$_h$, and e of the test soils. The shear wave velocity was measured at various stress states by taking multiple bender readings while performing K_0-consolidation triaxial test with multiple unload-reload loops. The $G_{vh} - e - \sigma'^2$ backbone curve for low PI to non-plastic silts was also established from the bender readings taken during K_0-consolidation triaxial test with multiple unload-reload loops. The analysis procedure is described in more detail in Lukas (2018).

Table 3. 1 Index properties of synthetic intermediate soil samples (Lukas 2018)

Soil	LL (%)	PL (%)	PI (%)	Fine Content (%)	USCS
50S50K	31	15	16	88	CL
85S15K	19	15	4	79	CL-ML
Dedham Silt	19	NP	NP	100	ML

Note: LL = liquid limit, PL = plastic limit, Fines Content =%<0.075 mm

Table 3. 2 K0 values estimated by Lukas et al (2018) using Mesari and Hayat (1993) relationship

Soil	50S50K	85S15K	Dedham Silt
K_{NC} (-)	0.59	0.52	0.56
$K_{3.6}$ (-)	0.98	0.96	0.97
$\varphi'mo$ (°)	26.3	36.5	35.0

Note: ϕ'_{mo}=effective stress friction angle at maximum obliquity.
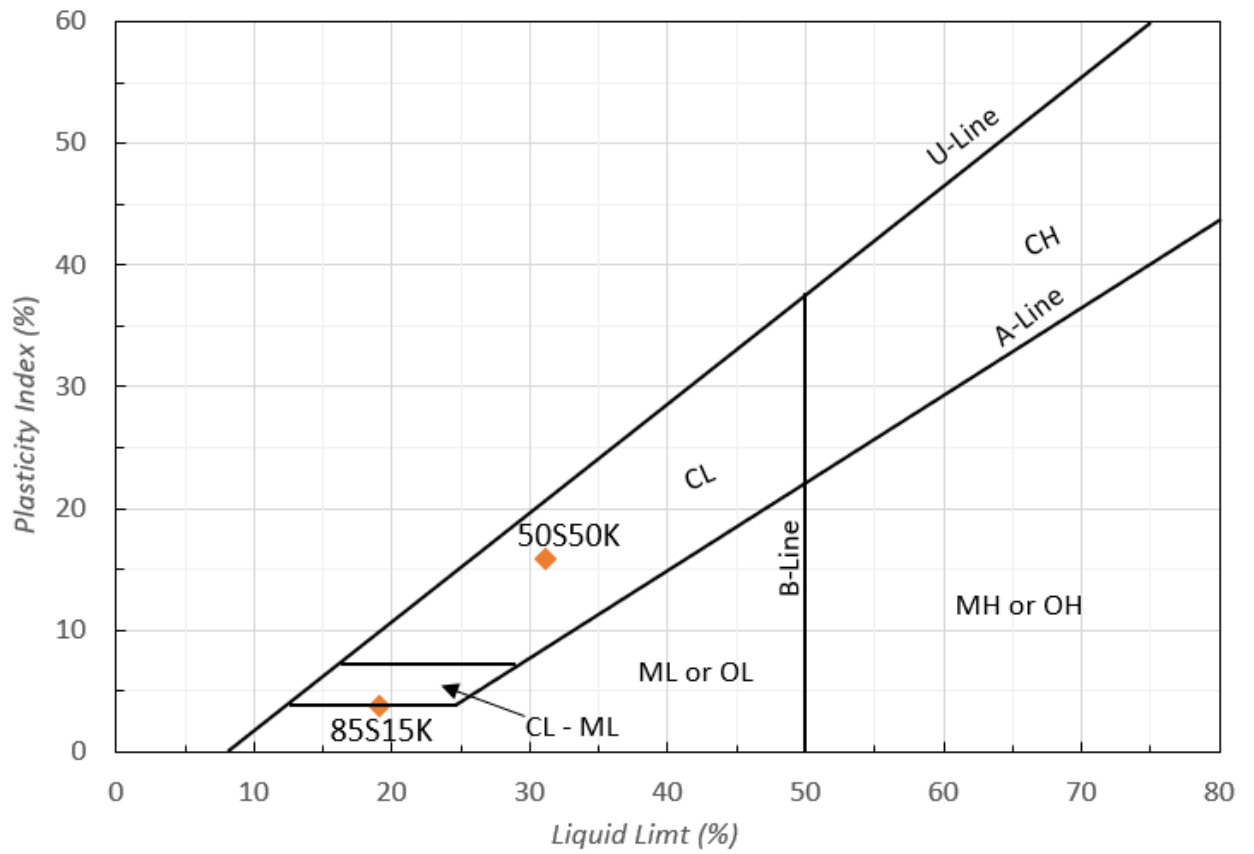
Figure 3. 1 Plasticity chart for test soils 50S50K and 85S15K (S=%Silt, K=%Kaolin)
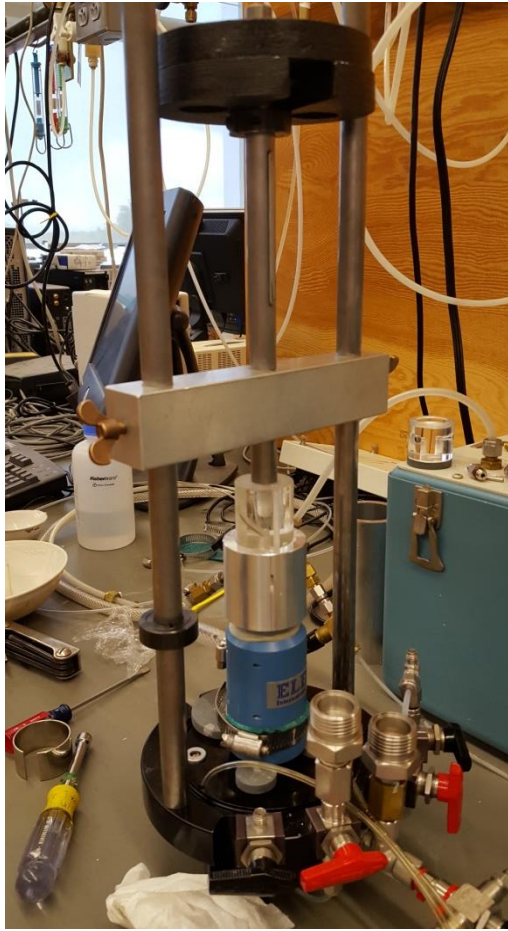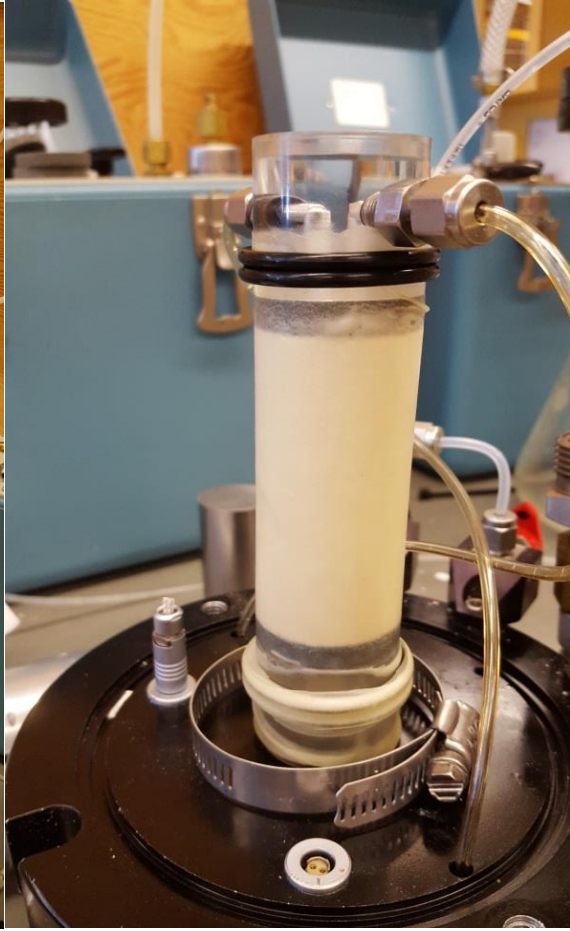
(a)   (b)

Figure 3. 2 Specimen preparation using a split mold under vacuum: (a) split mold set up
on a triaxial base, (b) specimen after the split mold is removed.

Figure 3. 3 Consolidometer used to make cakes of test soil 50S50K
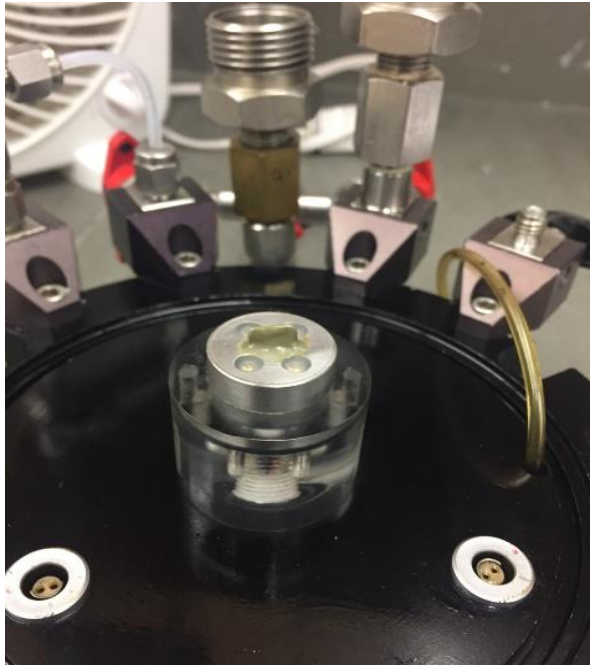
(a)   (b)

Figure 3. 4 Bender element: (a) bottom bender on the triaxial base, (b) top bender incorporated in the top cap.
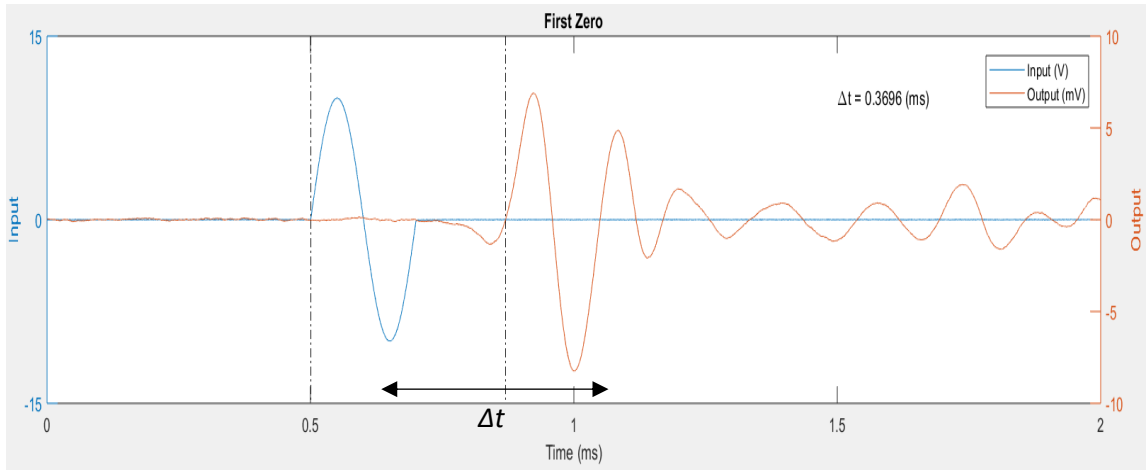
Figure 3. 5 Example for selection of travel time *Δt* using first zero crossover method.

CHAPTER 4. PRESENTATION AND INTERPRETATION OF RESULTS

This chapter presents and analyzes results from the laboratory triaxial test and shear wave velocity measurements using bender elements. This includes the influence of stress level on the normalized undrained shear strength, effects of SHANSEP and recompression on post ISA behavior, and evaluation of small strain modulus during ISA, Recompression and SHANSEP testing.

4.1 Normalization Results

This section presents the results from anisotropically consolidated undrained triaxial compression tests (CAUC) performed at various consolidation stress levels on test soils 50S50K, 85S15K and Dedham Silt. Preparation of the test specimens is described in Section 4.2.1. The testing program was conducted on NC specimens anisotropically consolidated using the K_o values presented in Table 2.2. The test soils were consolidated to vertical effective stresses of 100 kPa, 200 Pa, 400 kPa, 600 kPa and 800 kPa followed by undrained shear. Given that the Dedham silt exhibited dilating behavior the undrained shear strength of the test soils were all computed using the Brandon et al. (2006) failure criteria which are peak deviator stress ($\sigma_1 - \sigma_3$)$_{max}$, peak principal stress ratio (σ_1'/σ_3')$_{max}$, peak excess pore pressure Δu_{max}, reaching k_f line, limiting strain (5%) and $\overline{A}$ =0 or Δu=0 as shown in Figure 2.4 in chapter 2.

Table 4.1 summarizes the end of consolidation conditions for each of the test specimens and Figures 4.1 to 4.3 present the consolidation plots in terms of vertical (axial) strain and void ratio. Tables 4.2 to 4.4 summarizes the undrained shear strength and normalized undrained shear strength of the test soils consolidated to various vertical effective stress using Brandon et al. (2006) failure criterion.

Figures 4.4 to 4.9 present the stress-strain, shear induced pore pressure, and effective stress paths for the 85S15K, 50S50K and Dedham Silt specimens. The results show that the 50S50K soil exhibits contractive behavior (i.e., progressively increasing positive shear induced pore pressures) through the entire test for all preshear stress levels. In contract, the Dedham Silt specimens all exhibit dilative behavior with the effective stress path sharply migrating to the right and up the failure envelope. The 85S15K specimens initially all show contractive behavior but switch to dilative behavior at larger strains towards the end of the tests nominally coinciding with where the effective stress paths appear to reach the failure envelope. The peak shear stress of 85S15K and 50S50K is mobilized at <0.4 % strain followed by strain softening. It can also be observed that for 85S15K (P.I = 4), the post peak behavior is dependent on the preshear vertical effective stress. The 85S15K specimens consolidated to higher vertical effective stresses of 600 kPa and 800 kPa show a greater tendency towards dilative behavior, i.e., more rapid gain in shear strength with increasing strain. Dedham Silt which is a non-plastic soil does not reach a peak shear stress value and continues to migrate up the failure envelope with continued strain until the maximum strain level reached in a test.

Figures 4.7 to 4.9 present the results all normalized by the preshear vertical effective stress. The normalized shear stress versus axial strain plot of 85S15K shows that the normalized shear stress generally does not increase with an increase in stress level. However, the normalized shear stress for the specimen consolidated to stress level of 600 kPa is higher compared to specimen consolidated to stress level of 800 kPa. This specimen was used to develop the shear wave velocity framework (results presented in Section 4.2 below) and had three unload-reload loops prior to reaching the final consolidation stress of 600 kPa and it is possible this caused some changes in the

specimen structure resulting in a higher strength than if it had been consolidated directly to 600 kPa without any unload-reload loops.

Figure 4.10 plots the undrained shear strength versus preshear vertical effective stress with s_u taken as equal to q_{max} for the 85S15K and 50S50K soils which all show a distinct peak shear stress during the initial contractive behavior. Linear regression to the data with the intercept forced through zero results in the following S values, i.e., s_u/σ'_{vc} for OCR = 1 conditions:

85S15K: $S = s_u/\sigma'_{vc} = 0.30$

50S50K: $S = s_u/\sigma'_{vc}\ 0.26$

The near perfect linear regression fits indicate little to no dependency of the normalized undrained stress strength with consolidation stress level for these two soils

Given that the Dedham Silt exhibits dilative behavior from the start of shear the Brandon et al. (2006) criteria are used to evaluate the potential dependency of undrained shear strength with consolidation stress level. Figure 4.11 presents an example application of the Brandon et al. (2006) criteria for the Dedham Silt specimen tested with $\sigma'_{vc} = 200$ kPa. Tables 4.2 to 4.4 present s_u values for the Brandon et al. (2006) criteria for the test soils – note: the criteria are not intended for soils that exhibit contractive behavior but the results for the 85S15K and 50S50K soils are nevertheless presented here for comparative purposes. Figure 4.12 and 4.13 plots the Tables 4.2 to 4.4 results versus preshear vertical effective stress.

The post peak normalized shear stress behavior is also influenced by the preshear consolidated vertical effective stress depending on which criterion is used. For example, for 85S15K consolidated to vertical effective stress, $\sigma'vc > 400$ kPa, there is gain in post peak normalized shear stress with an increase in strain. If the specimen were subjected

to higher strain, then the post peak normalized shear stress would exceed the peak shear stress resulting from dilation. This demonstrates that the tendency for low plasticity silts to dilate increases with an increase in stress level. The normalized shear stress and post peak normalized shear stress behavior of 50S50K (P.I = 16) does not show an increase with the increase in the stress level.

For 85S15K, the results from the failure criteria methods show increase in normalized undrained shear strength with increase in stress level. However, the peak deviator stress method does not show an increase in normalized undrained shear strength with increase in stress level. The remaining four methods shows large deviation in the normalized undrained shear strength with increase in stress level. The peak excess pore pressure and k_f line methods shows consistency in increase in normalized undrained shear strength with increase in stress level. For 50S50K the normalized undrained shear strength results as shown in Figure 4.12 (b) does not show any trend with increase in stress level. The peak deviator stress method shows least deviation in the normalized undrained strength with increase in stress level.

The peak deviator stress method cannot be used for dilating soil such as Dedham Silt. In Figure 4.12 (c) all methods except peak excess pore pressure (Δu_{max}) show large deviation in the normalized undrained shear strength with increase in stress level. However, a decreasing trend in normalized undrained shear strength with increasing stress level is observed for peak deviator stress ($\sigma_1 - \sigma_3$)$_{max}$, peak principal stress ratio $(\sigma_1'/\sigma_3')_{max}$, k_f line and limiting strain (5%) failure criteria.

The axial strain at failure versus stress level is shown in figure 4.13. The axial strain at failure is constant with the increase in the stress level for 85S15K and 50S50K. The axial strain at peak stress and peak excess pore pressure are most consistent with

increase in stress level. It can be observed that the peak shear stress occurs at very small strain for both the soils. The axial strain at failure for Dedham Silt shows significant deviation with increase in stress level except for axial strain at peak excess pore pressure.

Table 4. 1 Summary consolidation and undrained shear results

Soil	σ'_{vc} (kPa)	K_c (-)	w_c (%)	e_c (-)	ε_a (%)	ε_v (%)	ε_f (-)	q_f (kPa)	q_f/σ'_{vc} (−)	ϕ' at q_f (°)	ϕ'_{mo} (°)
	108	0.55	20	0.683	1.6	0.8	0.14	29.8	0.276	21	21
	198	0.51	16	0.661	3.5	2.2	0.15	57.3	0.289	23	36
85S15K	401	0.52	24	0.615	5.2	5.1	0.15	117.5	0.293	23	37
	600	0.51	17	0.622	5.5	4.7	0.33	182.3	0.304	25	36
	808	0.51	18	0.556	5.0	6.0	0.29	236.8	0.293	25	37
	208	0.58	23	0.745	9.2	2.9	0.29	51.9	0.250	20	23
50S50K	397	0.57	24	0.591	7.1	7.0	0.22	101.9	0.257	20	27
	599	0.56	25	0.598	11.8	8.8	0.18	151.0	0.252	19	25
	803	0.56	28	0.579	13.0	10.2	0.37	210.7	0.262	21	26
	109	0.60	18	0.644	0.5	0.3	11.62	*159.7**	*1.465**	*33**	33
Dedham Silt	204	0.57	14	0.646	1.3	0.7	14.40	*232.8**	*1.141**	*34**	35
	400	0.56	22	0.560	3.5	2.4	11.02	*176.4**	*0.441**	*35**	35
	601	0.56	17	0.631	2.9	1.9	13.00	*356.6**	*0.593**	*33**	35

Note: * italics denotes specimen had not reached a peak q; the value listed is the final reading

Table 4. 2 Shear strength of 85S15K tests using Brandon et al. (2006) failure criteria

σ'_{vc} (kPa)	$(\sigma 1 - \sigma 3)_{max}$		$(\sigma'1/\sigma'3)_{max}$		u_{max}		K_f line		$\varepsilon_f = 5\%$
	q_f (kPa)	ε_f (%)	q_f (kPa)	ε_f (%)	q_f (kPa)	ε_f (%)	q_f (kPa)	ε_f (%)	q_f (kPa)
108	29.8	0.14	32.1	13.7	25.7	4.3	32	13.5	26.1
198	57.3	0.15	41.3	10	39.4	7	38	4.6	39
401	117.5	0.15	83	10.8	79.7	7.7	81	3.8	79.2
600	182.3	0.33	162.3	11.3	153.2	7.2	156	2.8	151.5
808	236.8	0.29	200.9	10.5	194.9	7.6	200	2.4	191.7

Table 4. 3 Shear strength of 50S50K tests using Brandon et al. (2006) failure criteria

σ'_{vc} (kPa)	$(\sigma1 - \sigma3)_{max}$		$(\sigma'1/\sigma'3)_{max}$		u_{max}		K_f line		ε_f=5%
	q_f (kPa)	ε_f (%)	q_f (kPa)	ε_f (%)	q_f (kPa)	ε_f (%)	q_f (kPa)	ε_f (%)	qf (kPa)
200	48.3	0.29	43.8	7.4	39.1	14.6	42	10.4	45.6
400	101.9	0.37	81.5	11.5	77.7	15.1	78	14.7	89.6
600	151	0.18	127.9	9.3	118.6	15	120	13.6	135.7
800	210.7	0.37	177.4	10	167.5	14.8	170	13.4	189.5

Table 4. 4 Shear strength of Dedham Silt tests using Brandon et al. (2006) failure criteria

σ'_{vc} (kPa)	$(\sigma1 - \sigma3)_{max}$		$(\sigma'1/\sigma'3)_{max}$		u_{max}		K_f line		$\bar{A}$=0		ε_f=5%
	q_f (kPa)	ε_f (%)	q_f (kPa)	ε_f (%)	q_f (kPa)	ε_f (%)	q_f (kPa)	ε_f (%)	q_f (kPa)	ε_f (%)	qf (kPa)
100	*159.5**	*14.9**	111.2	10.1	36.1	1.3	52	3.8	78	7	61.5
200	*232.8**	*14.4**	187	11.4	66.5	1.9	125	7.3	150	9.1	95.5
400	*176.4**	*11.2**	176.4	11.2	111.1	3.9	148	8.5	-	-	117.6
600	*356.6**	*10.5**	349.3	10.1	211.4	10.1	290	7.4	-	-	245.6

Note: * italics denotes specimen had not reached a peak q; the values listed are the final reading
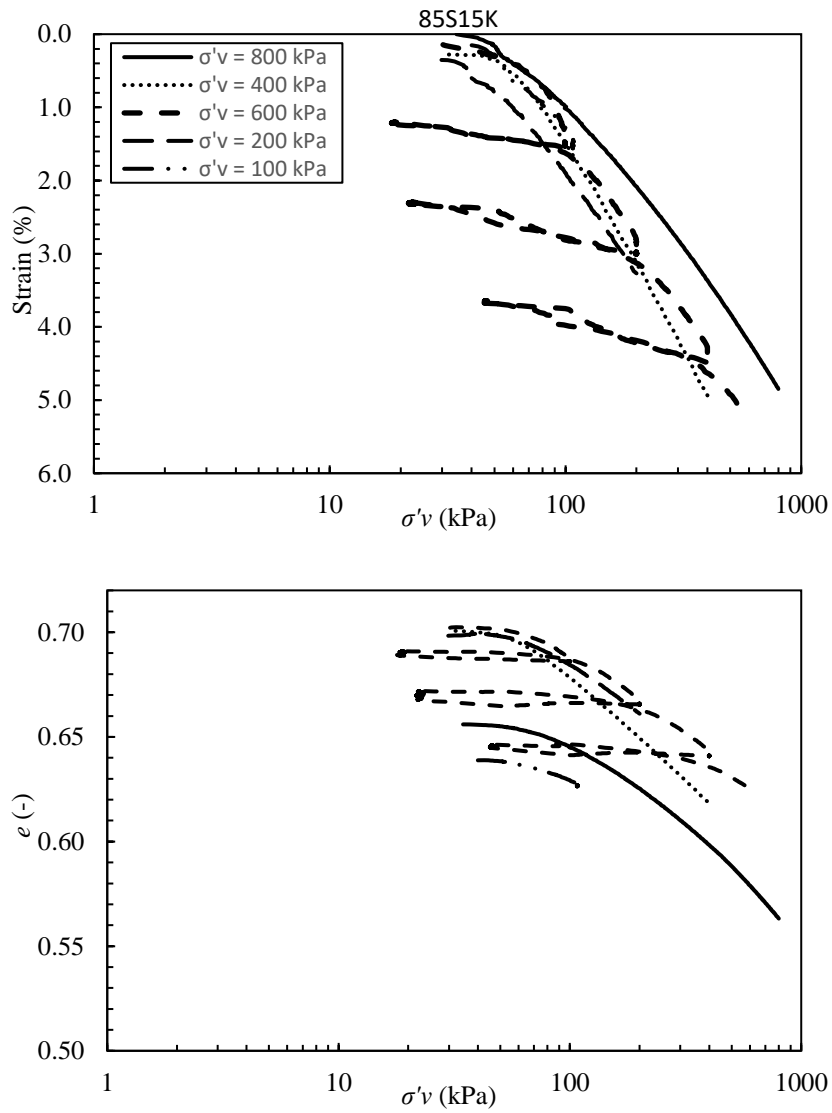
Figure 4. 1 Strain and void ratio versus vertical effective stress of 85S15K at different stress level
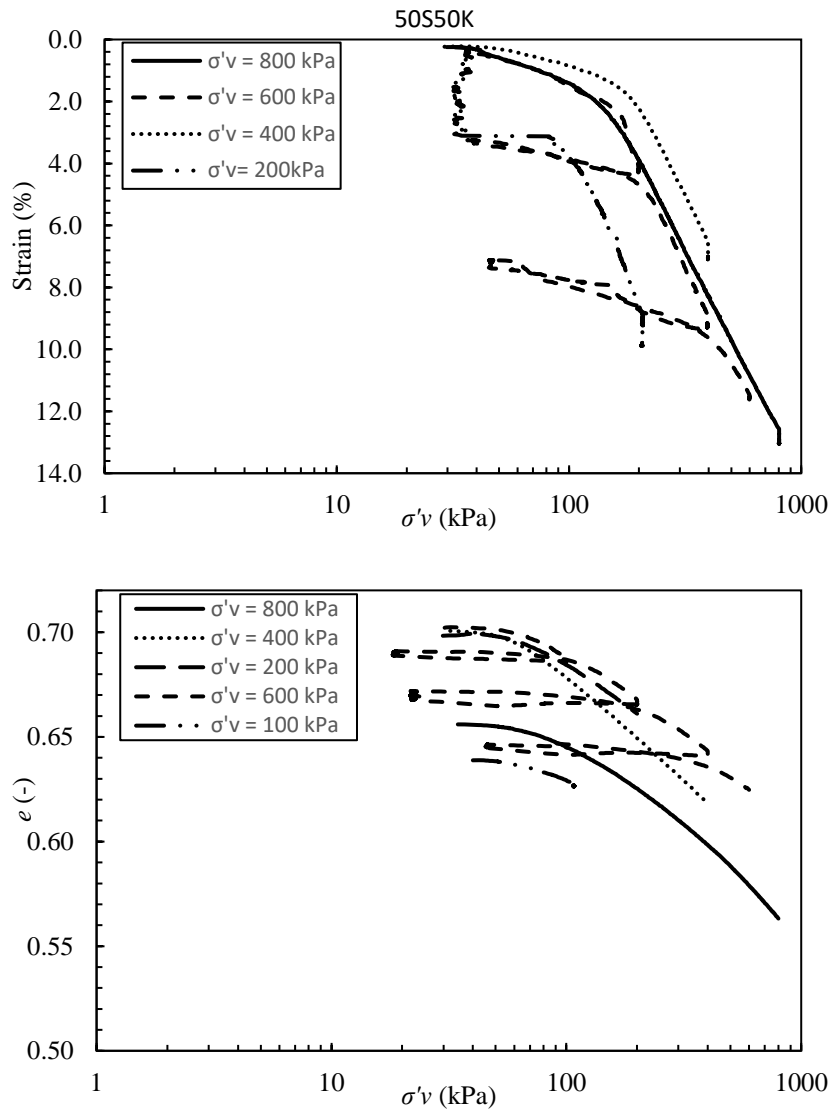
Figure 4. 2 Strain and void ratio versus vertical effective stress of 50S50K at different stress level
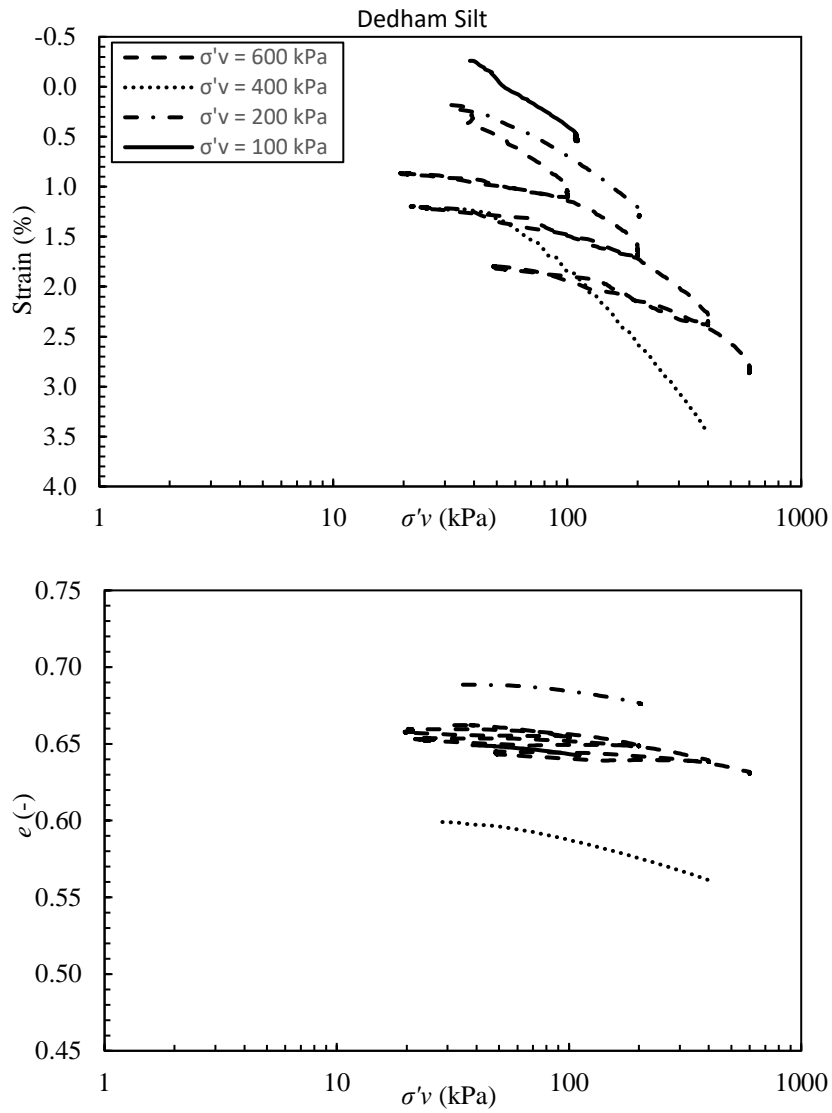
Figure 4. 3 Strain and void ratio versus vertical effective stress of Dedham Silt at different stress level
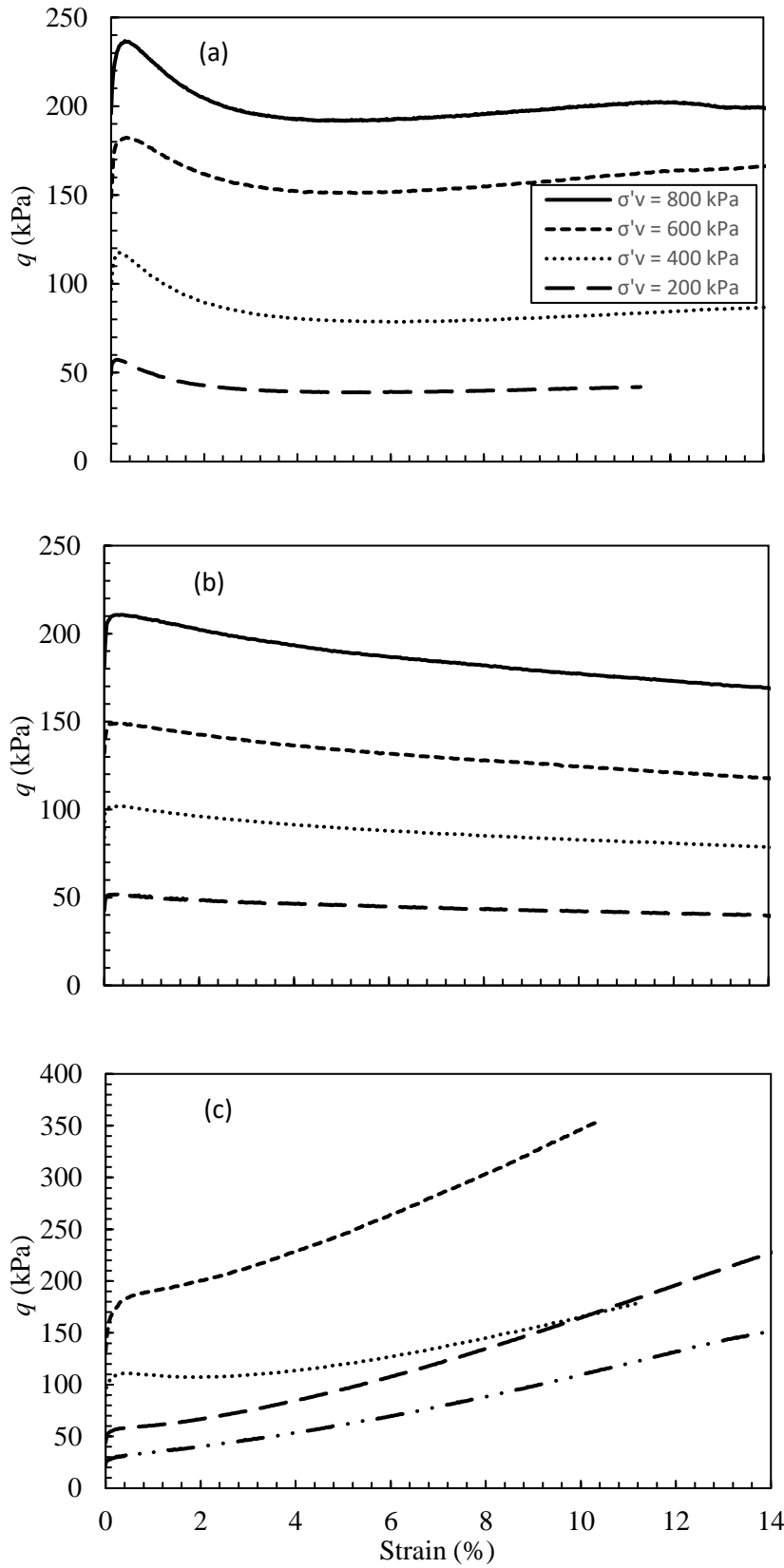
Figure 4. 4 Shear stress versus axial strain (a) 85S15K (b) 50S50K (c)Dedham Silt
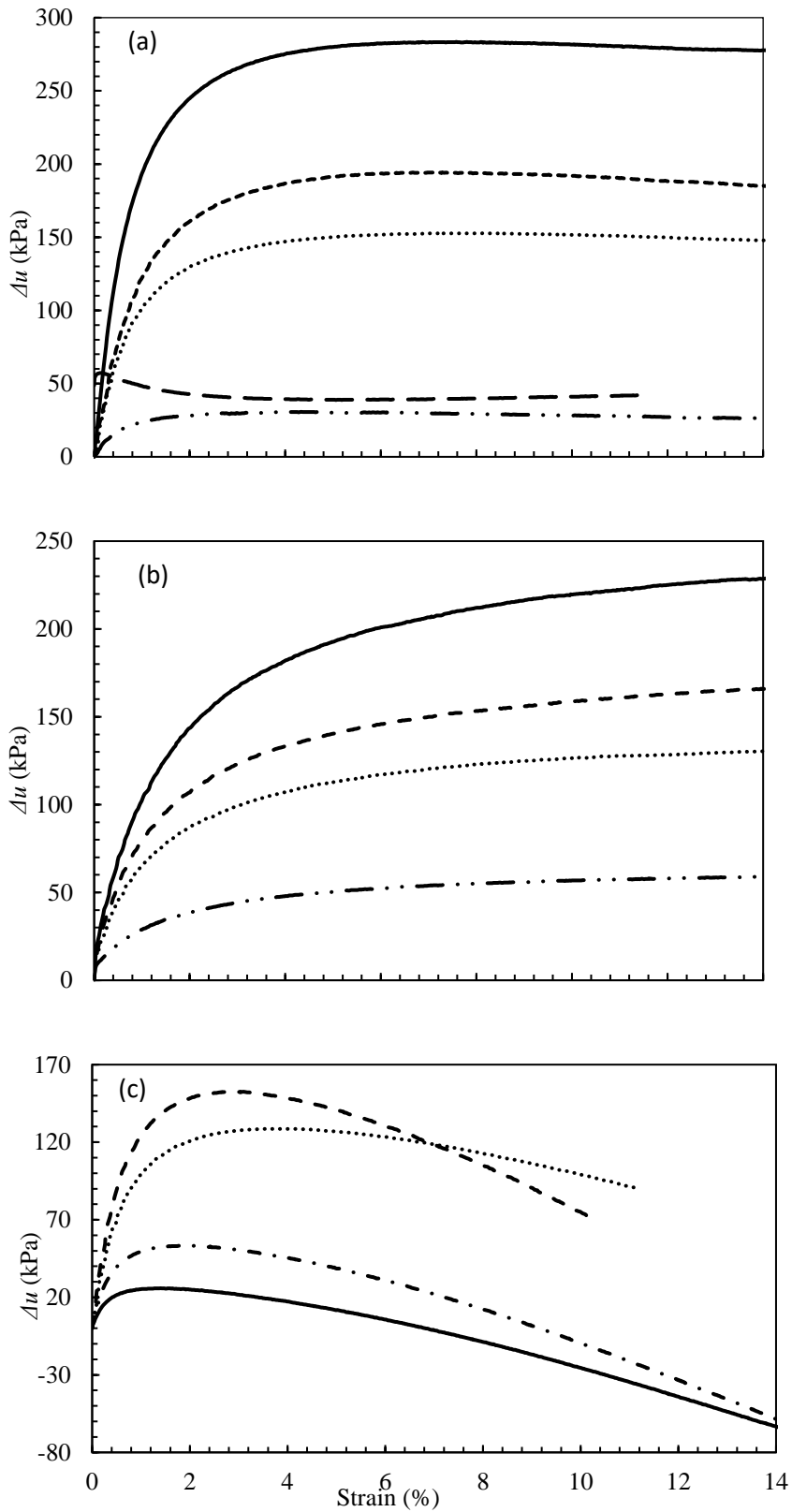
Figure 4. 5 Shear induced pore pressure versus axial strain (a) 85S15K (b) 50S50K (c)Dedham Silt
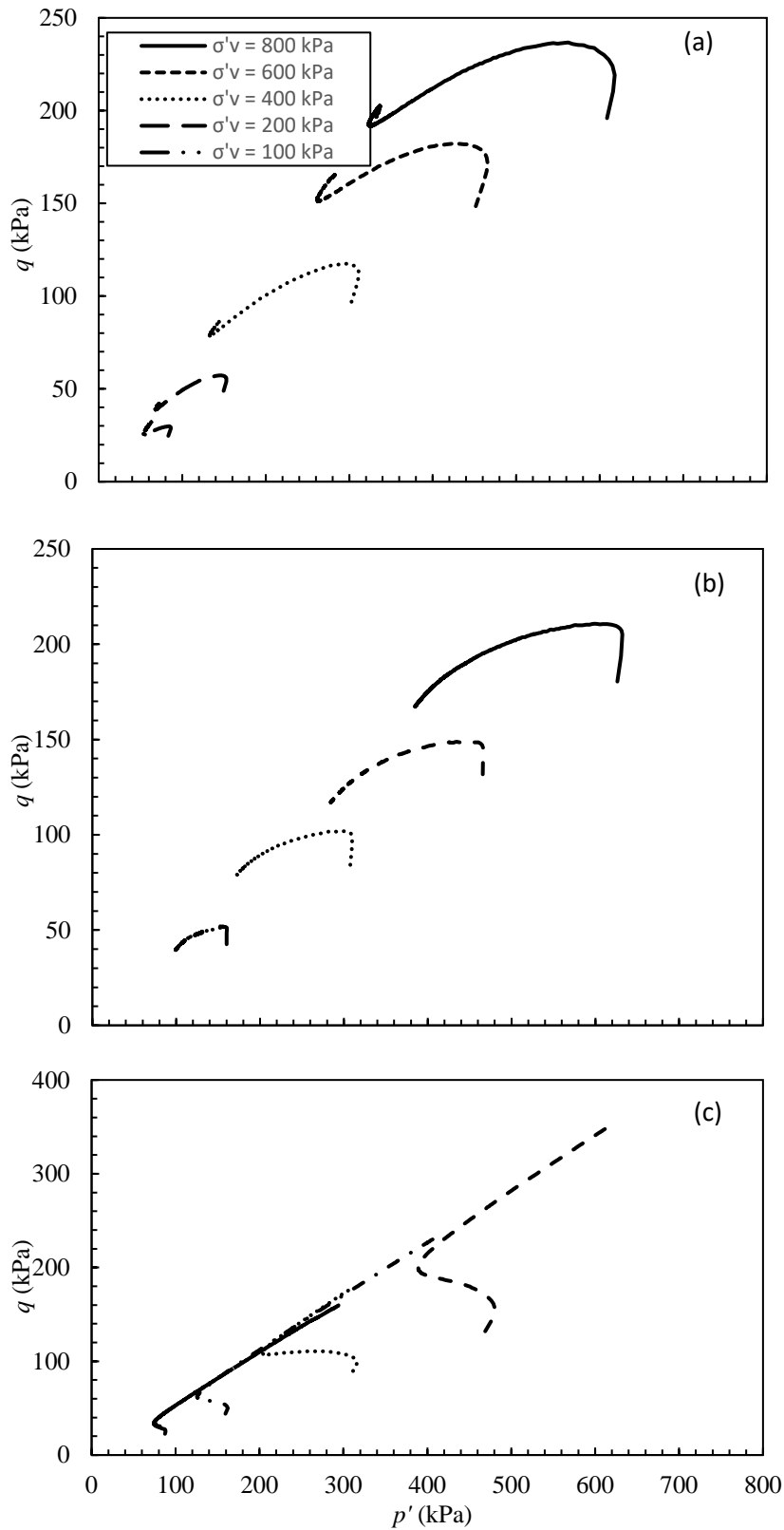
Figure 4. 6 Effective stress path (a) 85S15K (b) 50S50K (c)Dedham Sil
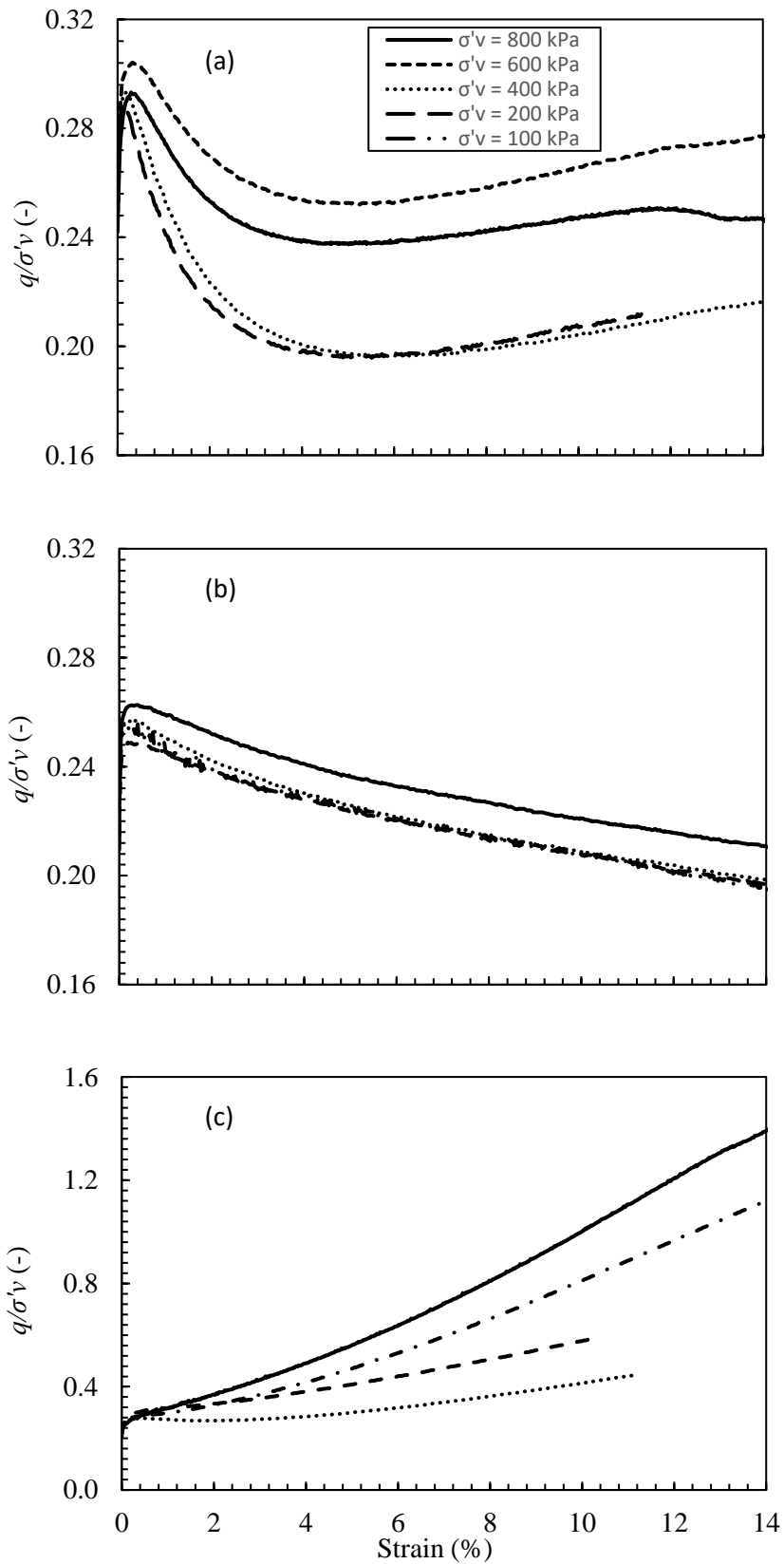
Figure 4. 7 Normalized shear stress versus axial strain (a) 85S15K (b) 50S50K (c)Dedham Silt
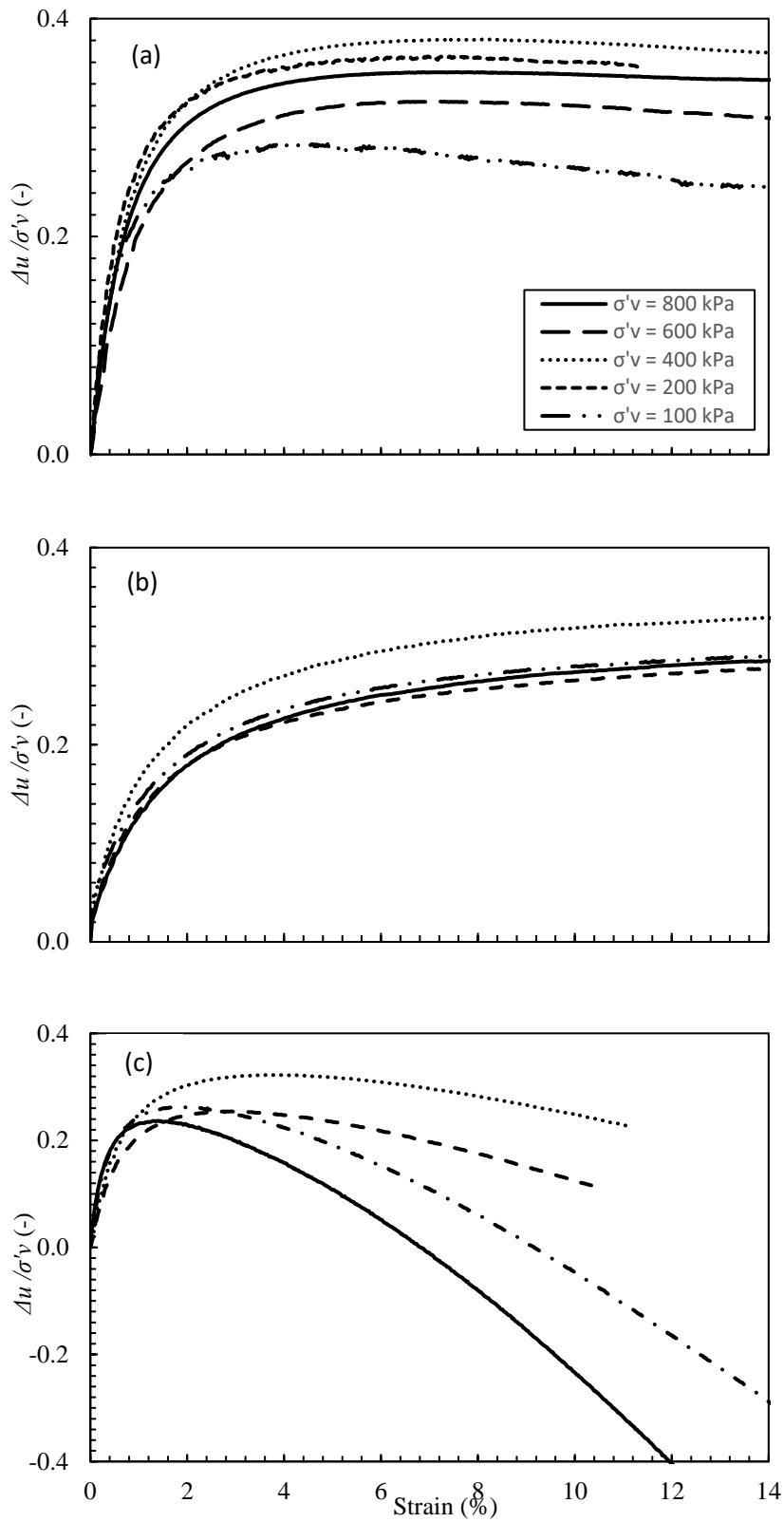
Figure 4. 8 Normalized shear induced pore pressure versus strain (a) 85S15K (b) 50S50K (c)Dedham Silt
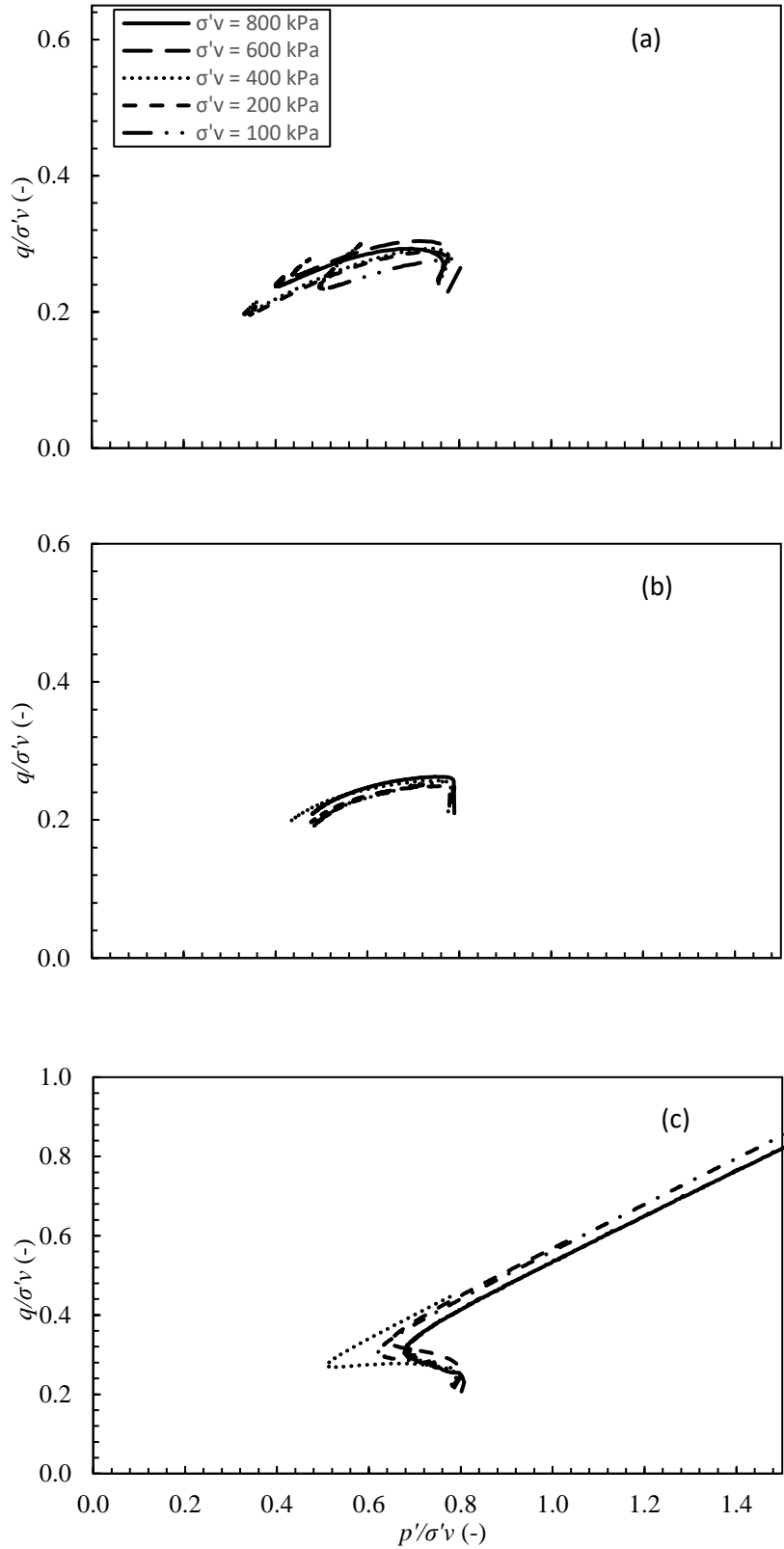
Figure 4. 9 Normalized shear effective stress path (a) 85S15K (b) 50S50K (c)Dedham Silt
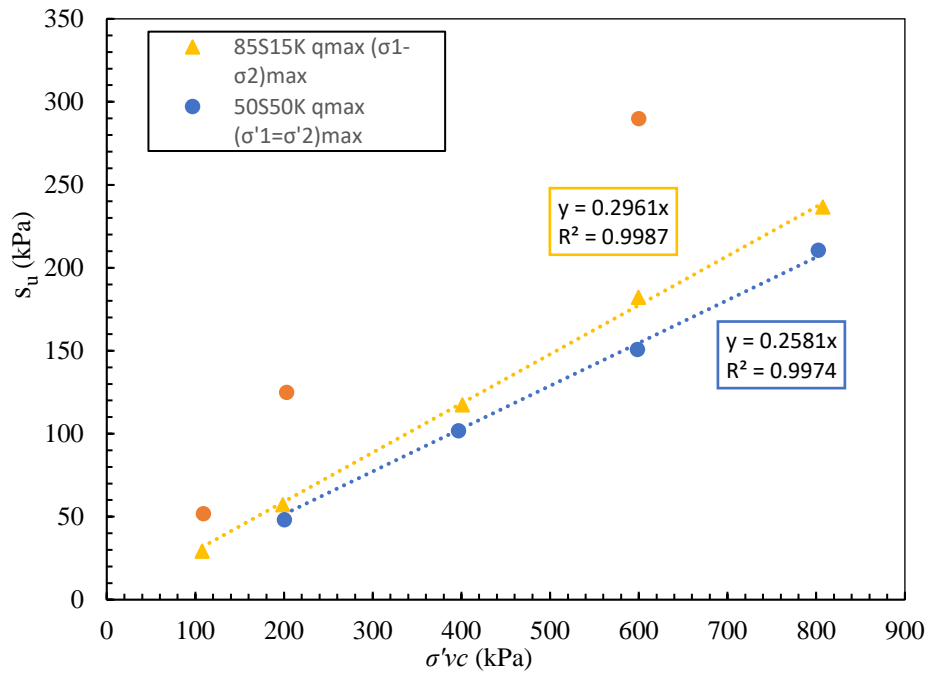
Figure 4. 10 Undrained shear strength at q_{max} versus effective stress for 85S15K, 50S50K and Dedham Silt (s_u at K_f line)
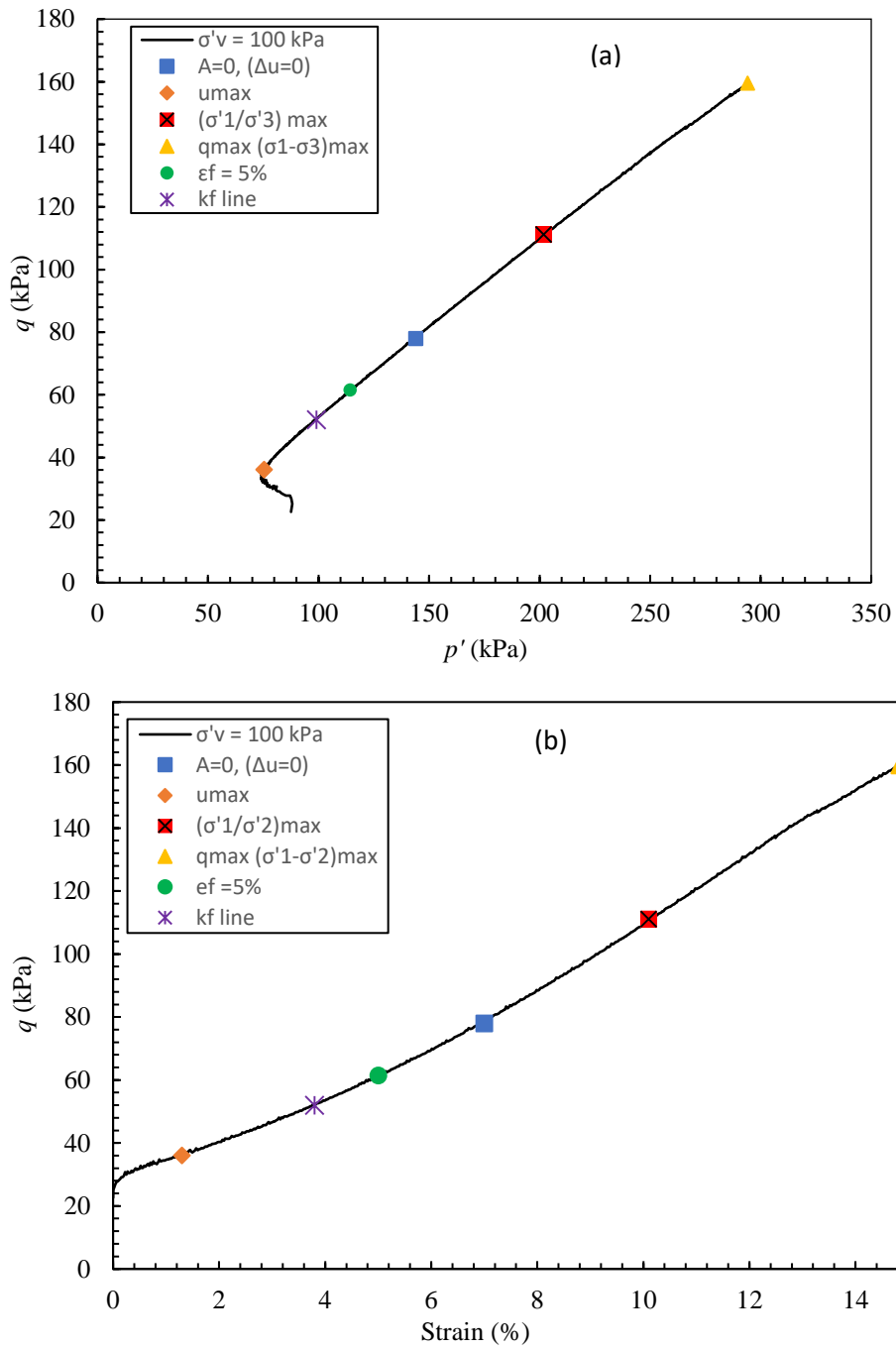
Figure 4. 11 Example of using Brandon et al (2006) failure criteria for Dedham Silt (σ'_{vc}=100 kPa) (a) Effective stress path (b) q versus strain
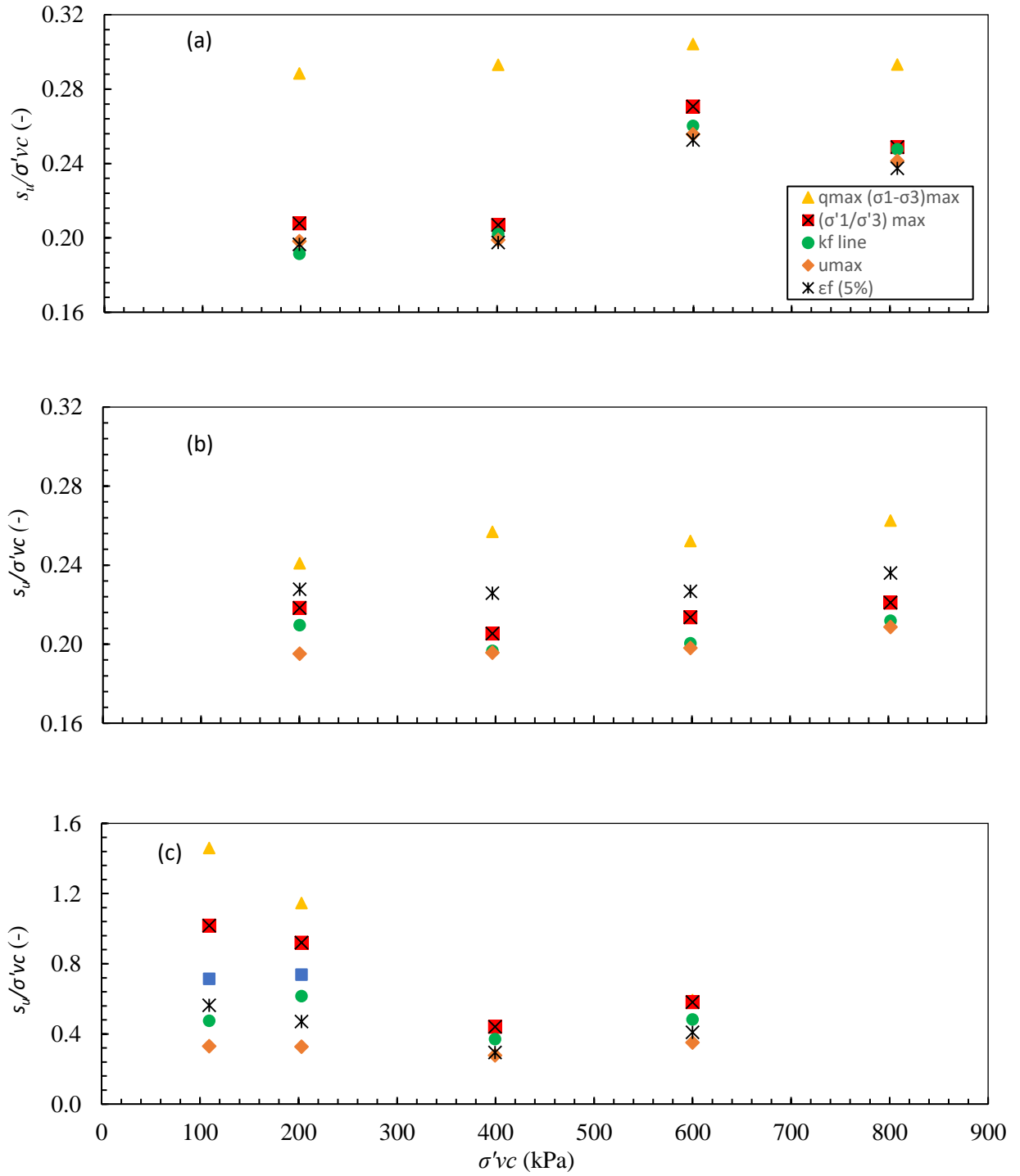
Figure 4. 12 Normalized undrained shear strength versus vertical effective stress using Brandon et al (2006) failure criteria (a) 85S15K (b) 50S50K (c)Dedham Silt
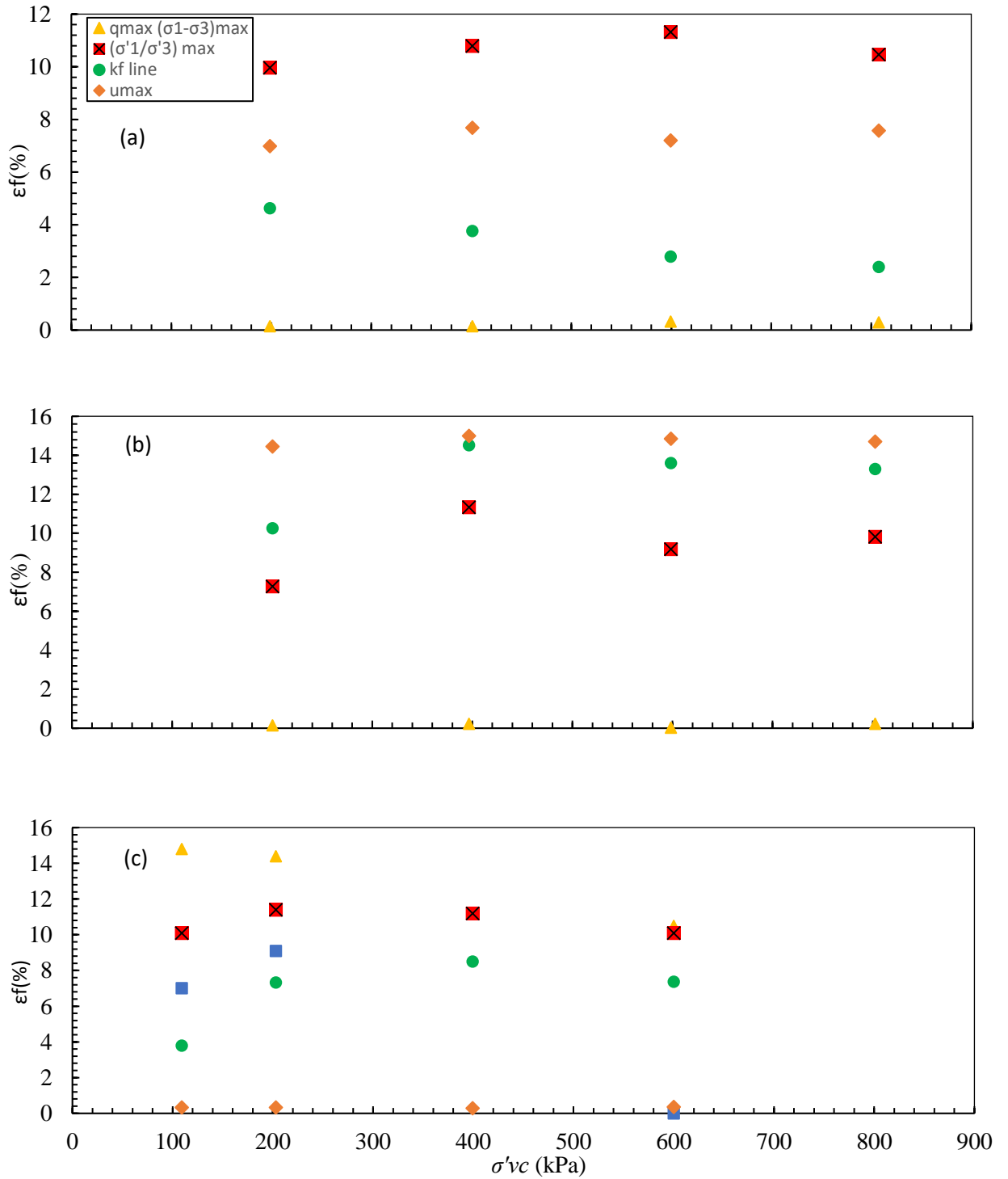
Figure 4. 13 Axial strain at failure versus vertical effective stress using Brandon et al (2006) failure criteria (a) 85S15K (b) 50S50K (c)Dedham Silt

4.2 SHANSEP versus Recompression

This section presents and analyzes results from laboratory triaxial tests conducted on reconstituted specimens of 85S15K, 50S50K and Dedham Silt to study the effect of recompression and SHANSEP consolidation procedures on post ISA behavior of the test soils. As described in the Methods Chapter, all specimens were first anisotropically consolidated using controlled stress path to the target K_0 value at a strain rate of 0.2 %/hr for loading and 0.05%/hr for unloading, followed by undrained ISA shearing. At completion of the ISA cycle, the specimens were either reconsolidated back to the pre-ISA effective stress state (i.e., Recompression method) or consolidated first well beyond the pre-ISA effective stress state as per the SHANSEP procedure to a final OCR equal to that of the pre-ISA stress state (i.e., OCR = 1 for NC and OCR = 3.6 for OC specimens). At the end of Recompression or SHANSEP reconsolidation procedure the specimens were sheared undrained at 0.5%/hr.

4.2.1 ISA Behavior

Figure 4.2.1 presents the stress strain, shear induced pore pressure versus strain and effective stress path for normally consolidated 85S15K and 50S50K specimens during ±1% & ±3% ISA shearing and Figure 4.2.2 presents the same plots for specimens of the same two soils with OCR =3.6. The undisturbed CAUC behavior is also plotted in Figures 4.2.1 and 4.2.2 for reference and Table 4.2.1 presents a summary of the undisturbed CAUC consolidation and undrained shear behavior. It can be observed that for OCR = 1 85S15K the loss in effective stress during ISA disturbance is significant in reference to the undisturbed behavior and is also much larger than the 50S50K specimen. For OCR=3.6, the loss in effective stress is much smaller than the OCR = 1 behavior for both soils. Dedham Silt, as shown in Figure 4.2.3, demonstrates similar

behavior to 85S15K in terms of significant loss in effective stress, which is also lower

for higher OCR.

4.2.2 OCR 1.0 Behavior for 50S50K and 85S15K

Figures 4.2.4 to 4.2.7 present examples for 50S50K and 85S15K of the complete

compression curve in void ratio (e) versus effective stress space and the complete

effective stress path during the full test sequence consisting of: initial consolidation to

OCR = 1, ISA shearing, post-ISA reconsolidation (either Recompression or SHANSEP),

and final undrained shear. Figures 4.2.4 and 4.2.5 compare results for 50S50K with

OCR = 1 and ± 1% ISA straining followed by either Recompression consolidation back

to the pre-ISA effective stress state with σ'_{vc} = 400 kPa versus SHANSEP consolidation

to a final post-ISA σ'_{vc} = 800 kPa. Figures 4.2.6 and 4.2.7 present results for the same

Recompression and SHANSEP test procedures for 85S15K.

Figure 4.2.8 to 4.2.11 present the final undrained shear stress-strain, normalized

stress-strain, shear induced pore pressure and effective stress paths for OCR = 1

undisturbed, ±1% & ±3% ISA Recompression and SHANSEP tests. The results for the

CAUC undisturbed behavior for each of the three soils are summarized in Table 4.2.1.

Table 4.2.2 presents a summary of the post-ISA Recompression and SHANSEP

undrained shear behavior for 50S50K. In all cases the normally consolidated 50S50K

specimens subjected to ISA disturbance exhibit contractive behavior throughout

undrained shear. The undisturbed 50S50K specimen had a peak shear stress at 0.37%

followed by contractive behavior until the end of shear. The OCR = 1 specimens

subjected to ±1% ISA followed by Recompression and SHANSEP consolidation

reached a peak shear stress at 1.08% and 0.18% strain respectively. The normalized

peak undrained shear stresses increased from 0.255 for the undisturbed to 0.287 for ±1%

ISA with Recompression post-ISA consolidation. However, the specimen with SHANSEP post-ISA consolidation had a value of 0.255 thus apparently mitigating the effect of ISA disturbance. Similarly, for ±3% ISA with Recompression post-ISA consolidation the peak normalized shear stress increased to 0.312 compared with 0.267 for the test with SHANSEP post-ISA consolidation. It can also be observed that normally consolidated 50S50K specimens subjected to ISA disturbance did not show dilative behavior.

For 85S15K OCR=1 the undisturbed CAUC specimen had a peak shear stress at small strain of 0.15% followed by contractive behavior until the specimen reached the failure envelope at which point it exhibited dilative behavior. For OCR 1, ±1% ISA and post-ISA Recompression consolidation the specimen reached a peak shear stress at 1.31 % strain followed by dilative behavior. The SHANSEP test with OCR 1 and ±1% ISA reached a peak shear stress at 0.47% strain slightly recovering the undisturbed contractive phase which is followed by dilative behavior.

For 85S15K two specimens were first normally consolidated to σ'_{vc}= 200 kPa followed by ±1% ISA for one and ±3% ISA for the other. Thereafter both specimens were SHANSEP consolidated to σ'_{vc} = 800 kPa. For ±1% ISA the specimen reached a lower peak shear stress than the specimen that was consolidated to σ'_{vc}= 400 kPa prior to ISA shearing and recovered the undisturbed contractive phase followed by dilative behavior. The normalized effective stress path, as shown in Figure 4.2.9, the specimen consolidated to σ'_{vc}= 200 kPa prior to ISA shearing followed closest to the undisturbed effective stress path and the tendency for dilative behavior was reduced compared to the specimen with pre-ISA σ'_{vc}= 400 kPa followed by SHANSEP consolidation to σ'_{vc} = 800 kPa.

Table 4.2.3 summarizes the post-ISA undrained shear results for 85S15K undisturbed and ±1% & ±3% ISA Recompression and SHANSEP tests. Overall, the undrained shear strength is significantly affected by ISA disturbance. For OCR=1, ±1% ISA disturbance the normalized peak shear stress increased from 0.290 at 0.15% strain for undisturbed to 0.353 at 1.31% strain for ±1% ISA with Recompression post-ISA consolidation. The SHANSEP post-ISA consolidation resulted in a normalized peak shear stress of 0.327 at 0.47% strain which is closer to the undisturbed normalized peak shear stress reducing some but not all of the effect of ISA disturbance. It can also be observed that SHANSEP consolidation reduced the tendency to develop dilative behavior. However, for ±3% ISA disturbance, SHANSEP consolidation does not counter act the disturbance and the specimens had a greater tendency towards post-ISA dilative behavior

4.2.3 OCR 3.6 Behavior for 50S50K and 85S15K

Figures 4.2.12 presents the complete compression curve and full test sequence for a 50S50K specimen with OCR = 3.6 and ± 1% ISA straining followed by Recompression post-ISA consolidation. Figure 4.2.13 presents the same plots for 85S15K with Recompression post-ISA consolidation and Figure 4.2.14 for SHANSEP post-ISA consolidation. Figures 4.2.15 to 4.2.18 present the final undrained shear stress-strain, normalized stress-strain, shear induced pore pressure and effective stress paths for OCR = 3.6 undisturbed, ±1% & ±3% ISA Recompression and SHANSEP (only for 85S15K) tests.

For 50S50K the post-ISA Recompression behavior closely resembles that of the undisturbed CAUC behavior for both ± 1% and ± 3% ISA, except for the slope of the stress-strain curve during the initial part of shear up to around 4% strain. For 85S15K

there are more noticeable differences in behavior among the undisturbed, Recompression and SHANSEP specimens. The normalized SHANSEP effective stress paths initially followed exactly that of the undisturbed specimens for both ± 1% and ± 3% which was not the case for the Recompression tests. However, neither reconsolidation procedures captured the initial peak shear stress followed by a brief contractive behavior and then dilative behavior shown by the undisturbed specimens (i.e., the S shape in the effective stress paths as they approach the failure envelope). Depending on how the undrained shear strength is defined there can be large differences among the test results for 85S15K unlike that found for the 50S50K soil.

4.2.4 Dedham Silt Behavior

Figures 4.2.19 presents the complete compression curve and full test sequence for a Dedham silt specimen with OCR = 1.0 and ± 1% ISA straining followed by Recompression post-ISA consolidation and Figure 4.2.20 presents the same plots for OCR = 3.6. Figures 4.2.21 and 4.2.22 present the final undrained shear stress-strain, normalized stress-strain, shear induced pore pressure and effective stress paths for OCR = 1.0 and 3.6 undisturbed, ±1% & ±3% (OCR = 3.6 only) ISA Recompression tests. The eventual behavior in all cases is highly dilative but ISA straining removes the initial contractive phase for the OCR = 1 behavior while it creates an initially softer response (i.e., lower slope in the stress-strain curve) for the OCR = 3.6 specimens with ±1% & ±3% ISA straining. Table 4.2.4 presents a summary of the undrained shear results.

4.2.5 Summary

Tables 4.2.5 and 4.2.6 present a comparison of results for post-ISA Recompression and SHANSEP consolidation procedures for OCR=1 and OCR=3.6 for

all three test soils. The effect of ISA disturbance is significant in the low plasticity 85S15K silt than the low plasticity 50S50K clay. For 85S15K, the ISA Recompression results in an increase in the undrained shear strength and eliminates the contractive behavior of the undisturbed specimen resulting in dilative behavior. The SHANSEP consolidation procedure recovers to some extent the undisturbed behavior and reduces the dilative behavior for OCR = 1 and ±1% ISA disturbance, however, it overestimated the undrained shear strength of the soil. For higher OCR and ISA disturbance SHANSEP consolidation does not counter act the ISA disturbance and the specimens have a greater tendency to post-ISA dilation. For 50S50K SHANSEP consolidation is more effective in recovering the undisturbed behavior compared to 85S15K but overestimates the undrained shear strength.

Table 4.2 1 Summary consolidation and undrained shear results from undisturbed CAUC tests

Soil	σ'_{vmax} σ'_{vc} (kPa)	OCR	K_c (-)	w_c (%)	e_c (-)	ε_a (%)	ε_{vol} (%)	ε_f-(%)	q_f (kPa)	q_f/σ'_{vc} (-)	ϕ' at q_f (°)	ϕ'_{mo} (°)
85S15K	401	1.0	0.52	24	0.615	5.2	5.1	0.15	118	0.293	23	36
	111	3.6	0.99	24	0.543	4.6	6.6	14.7*	91*	0.818	36	36
50S50K	397	1.0	0.57	24	0.591	7.1	7.1	0.37	102	0.257	21	26
	110	3.6	1.02	25	0.618	6.4	6.1	3.53	78	0.711	26	27
Dedham Silt	399	1.0	0.56	22	0.560	3.5	2.4	11.18*	176*	0.442	35	35
	111	3.6	0.98	23	0.678	2.2	1.7	14.7*	270*	2.430	35	35

Note: $K_c = \sigma'_{hc}/\sigma'_{vc}$, * denotes specimen had not reached a peak q; the values listed are the final reading

Table 4.2 2 50S50K Shear Results

Undisturbed - CAUC					Disturbed - Recompression							Disturbed - SHANSEP					
OCR	σ'_{vc} (kPa)	s_u (kPa)	ε_f (%)	ISA (%)	OCR	σ'_{vc} (kPa)	s_u (kPa)	ε_f (%)	$\Delta e/e_0$ (-)	ε_v (%)	OCR	σ'_{vc} (kPa)	s_u (kPa)	ε_f (%)	$\Delta e/e_0$ (-)	ε_v (%)
1.0	397	101.9	0.37	1	1.0	394	115	1.08	0.025	0.94	1.0	814	208	0.18	0.099	4.2
				3	1.0	404	126	3.01	0.047	1.86	1.0	811	216	0.89	0.110	4.3
3.6	104	78.2	3.53	1	3.6	107	75	3.83	0.002	0.06	-	-	-	-	-	-
				3	3.6	107	76	3.68	0.001	0.06	-	-	-	-	-	-

Table 4.2 3 85S15K Shear Results

	Undisturbed-CAUC			ISA (%)	Disturbed Recompression							Disturbed - SHANSEP						
						Initial Peak		q_{max}					Initial Peak		q_{max}			
OCR	σ'_{vc} (kPa)	s_u (kPa)	ε_f (%)		σ'_{vc} (kPa)	s_u (kPa)	ε_f (%)	s_u (kPa)	ε_f (%)	$\Delta e/e_0$ (-)	ε_v (%)	σ'_{vc} (kPa)	s_u (kPa)	ε_f (%)	s_u (kPa)	ε_f (%)	$\Delta e/e_0$ (-)	ε_v (%)
1.0	401	116.3	0.15	1	398	141	1.31	148*	10*	0.031	1.2	838	274	0.47	-	-	0.065	2.6
				3	408	-	-	227*	11*	0.067	2.6	833	-	-	391*	9.4*	3.559	0.09
3.6	106	84.98	0.85	1	109	-	-	102*	10*	0.011	0.4	223	-	-	253*	10*	0.054	2.1
				3	108	-	-	95*	5*	0.048	1.9	227	-	-	242*	10*	0.095	3.4

Note: * denotes specimen had not reached a peak q; the values listed are the final reading

Table 4.2 4 Dedham Silt Shear Results

| Undisturbed | | | | | | ISA (%) | Disturbed Recompression | | | | | | | |
| | | Initial Peak | | q_{max} | | | | | Initial Peak | | q_{max} | | | |
OCR	σ'_{vc} (kPa)	s_u (kPa)	ε_f (%)	s_u (kPa)	ε_f (%)		OCR	σ'_{vc} (kPa)	s_u (kPa)	ε_f (%)	s_u (kPa)	ε_f (%)	$\Delta e/e_0$ (-)	ε_v (%)
1.0	399	109.8	0.38	164*	10*	1	1.0	400	-	-	455*	10*	0.010	0.39
3.6	110	80.3	0.58	195*	10*	1	3.6	109	-	-	248*	10*	0.014	0.54
						3	3.6	111	-	-	401*	9*	0.046	1.65

Note: * denotes specimen had not reached a peak q; the values listed are the final reading

Table 4.2 5 Comparison of recompression and SHANSEP technique on normally consolidated 85S15K, 50S50K and Dedham Silt

Soil	Test Type		σ'_{vc} (kPa)	q_{peak} (kPa)	q_{peak}/σ'_{vc} (-)	ε_{peak} (%)	Dilative Beahvior
50S50K		Undisturbed	400	102	0.255	0.37	No
	ISA (±1%)	Recompression	400	115	0.287	1.08	No
		SHANSEP	814	208	0.255	0.18	No
	ISA (±3%)	Recompression	404	126	0.312	0.89	No
		SHANSEP	811	216	0.267	0.15	No
85S15K		Undisturbed	401	116	0.290	0.15	No
	ISA (±1%)	Recompression	398	141	0.353	1.31	Yes
		SHANSEP	838	274	0.327	0.47	No
	ISA (±3%)	Recompression	408	No peak			Yes
		SHANSEP	833	No peak			Yes
Dedham Silt		Undisturbed	399	110	0.275	0.38	Yes
	ISA (±1%)	Recompression	404	No peak			Yes
		SHANSEP	803	No peak			Yes

Table 4.2 6 Comparison of recompression and SHANSEP technique OCR=3.6 on 85S15K, 50S50K and Dedham Silt

Soil	Test Type		σ'_{vc} (kPa)	q_{peak} (kPa)	q_{peak}/σ'_{vc} (-)	ε_{peak} (%)	Dilative Beahvior
50S50K		Undisturbed	104	78	0.752	3.53	No
	ISA (±1%)	Recompression	107	75	0.700	3.83	No
		SHANSEP	-	-	-	-	-
	ISA (±3%)	Recompression	107	76	0.713	3.68	No
		SHANSEP	-	-	-	-	-
85S15K		Undisturbed	106	85	0.802	0.85	No
	ISA (±1%)	Recompression	109	No peak			Yes
		SHANSEP	223	No peak			Yes
	ISA (±3%)	Recompression	108	No peak			Yes
		SHANSEP	227	No peak			Yes

Note: No peak was observed for Dedham Silt OCR=3.6 recompression and SHANSEP tests.

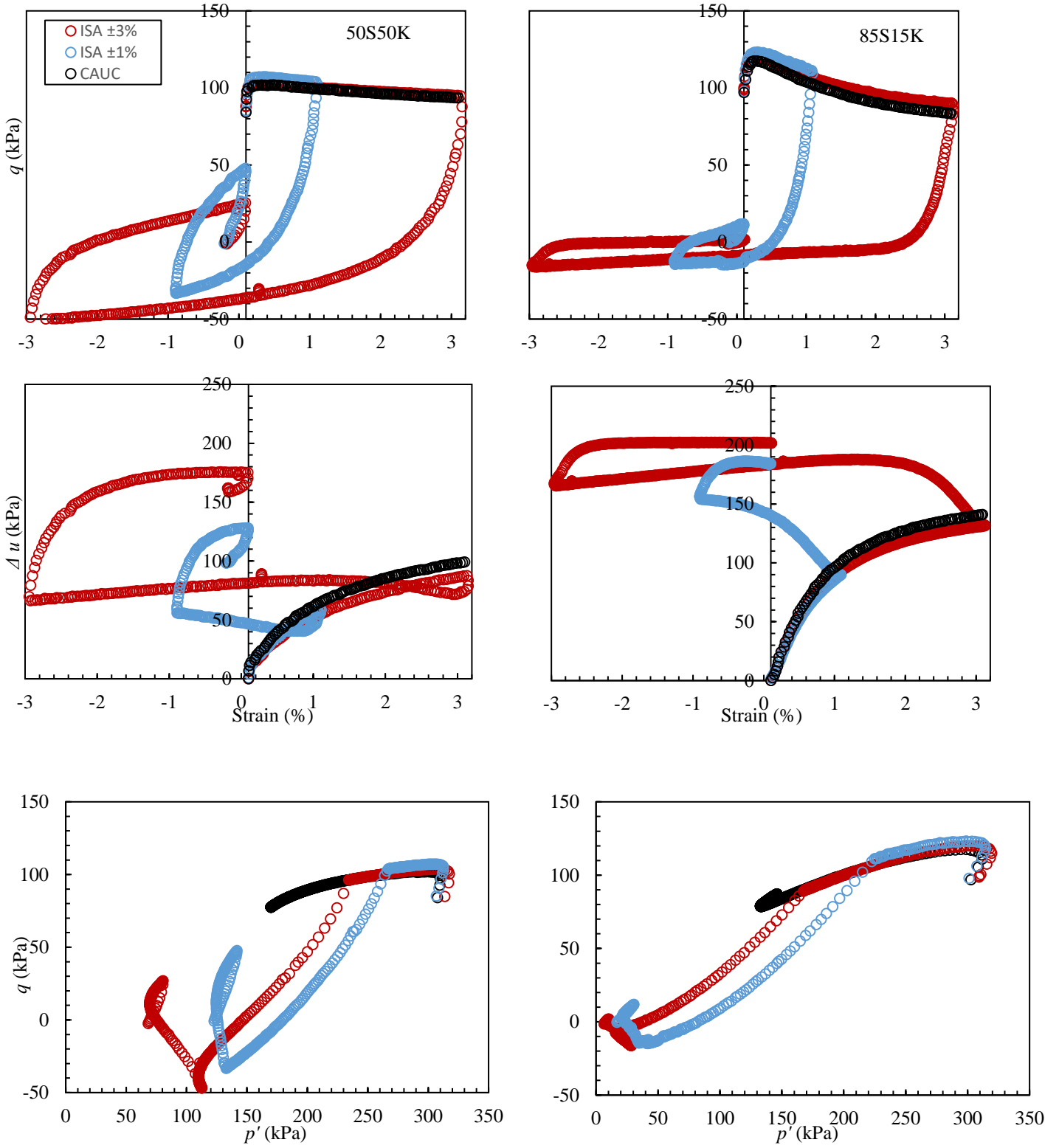**Figure 4.2 1** Stress-strain, shear induced pore pressure vs ISA strain and ISA stress path for normally consolidated undisturbed, ±1% & ±3% ISA cycle.

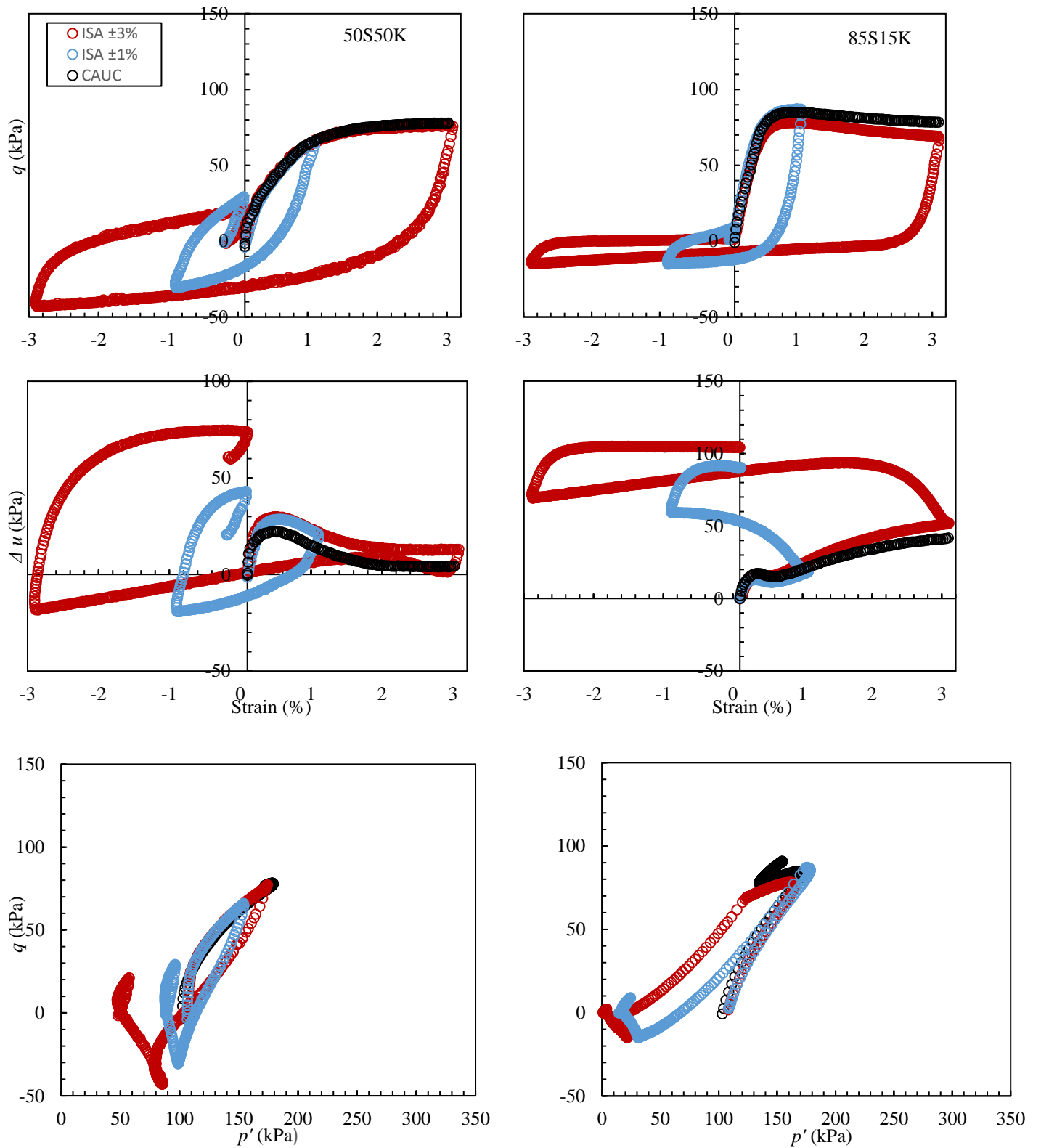**Figure 4.2 2** Stress-strain, shear induced pore pressure vs ISA strain and ISA stress path for OCR=3.6 undisturbed, ±1% & ±3% ISA cycle.
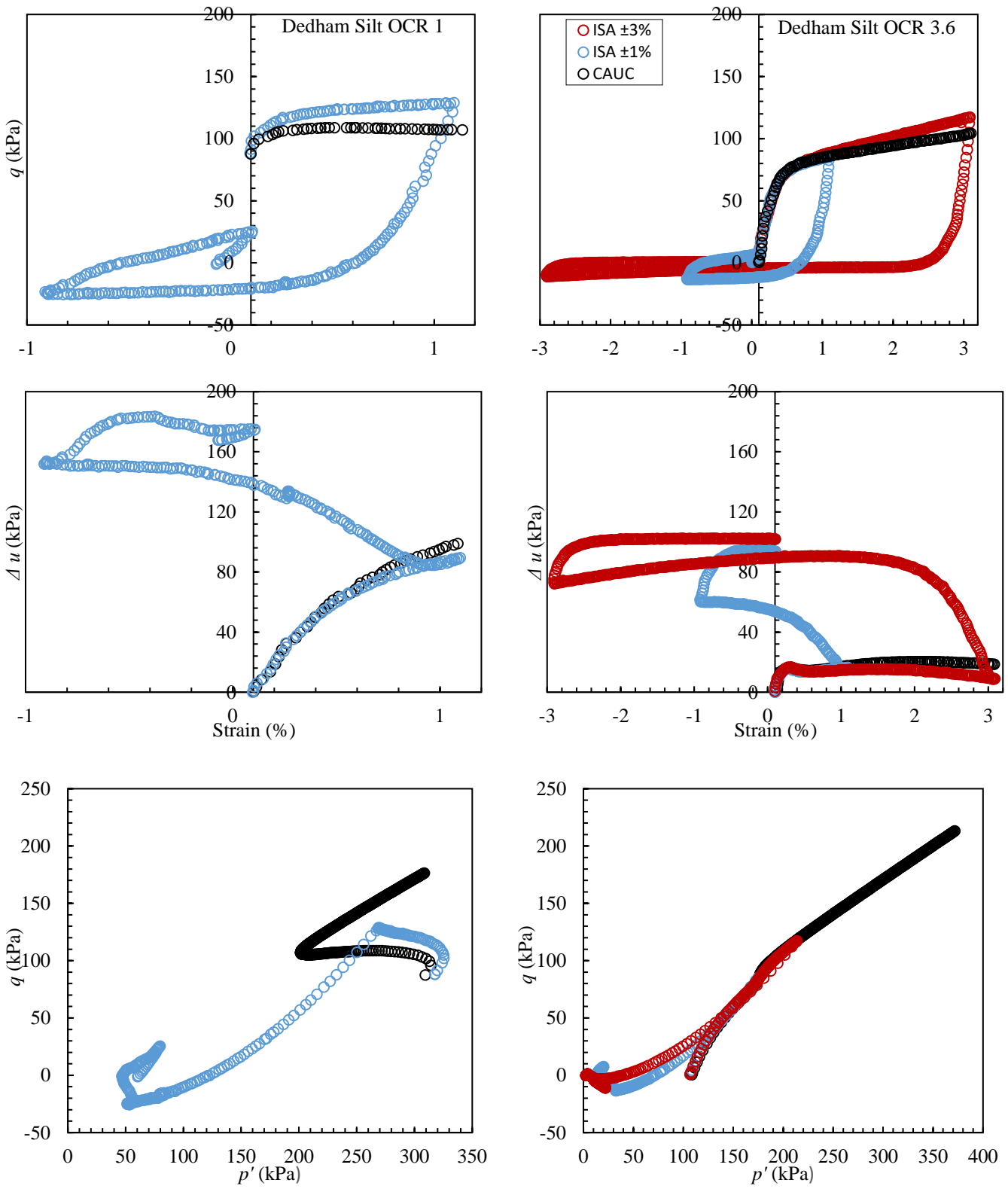
Figure 4.2 3 Stress-strain, shear induced pore pressure vs ISA strain and ISA stress path for OCR=1 & OCR=3.6, undisturbed and ±1% & ±3% ISA cycle
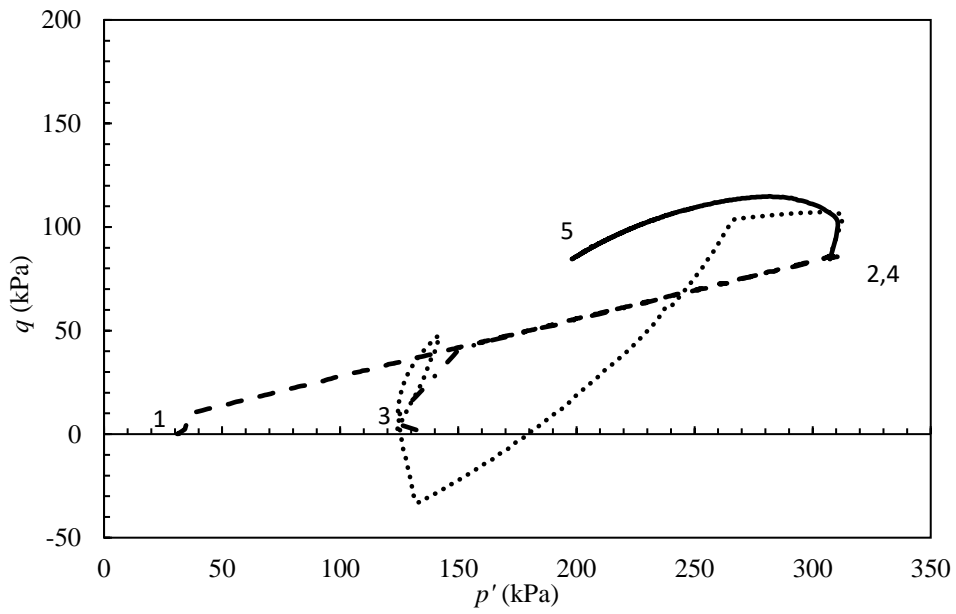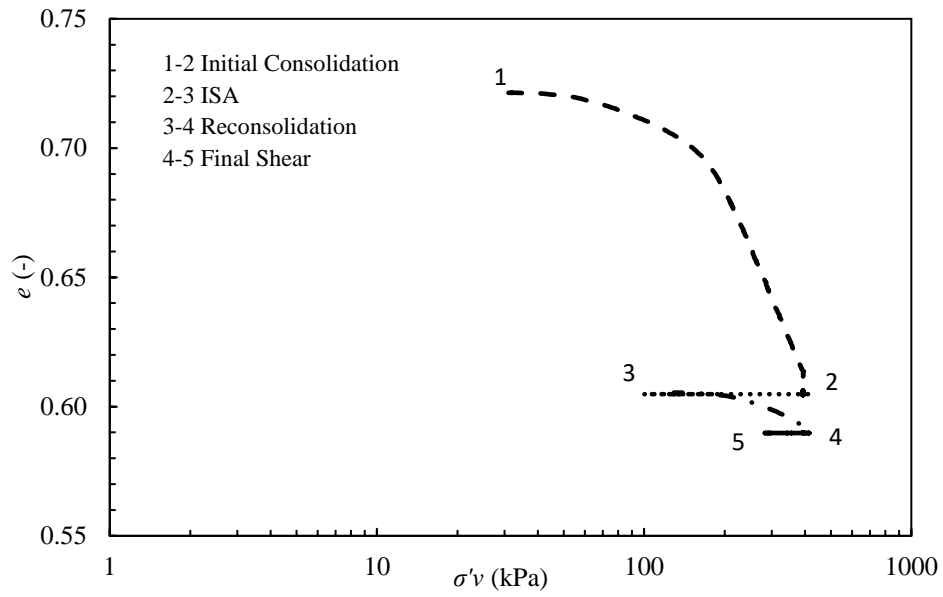
Figure 4.2 4 Complete compression curve and stress path for normally consolidated 50S50K, ±1.0% ISA test with post-ISA recompression consolidation
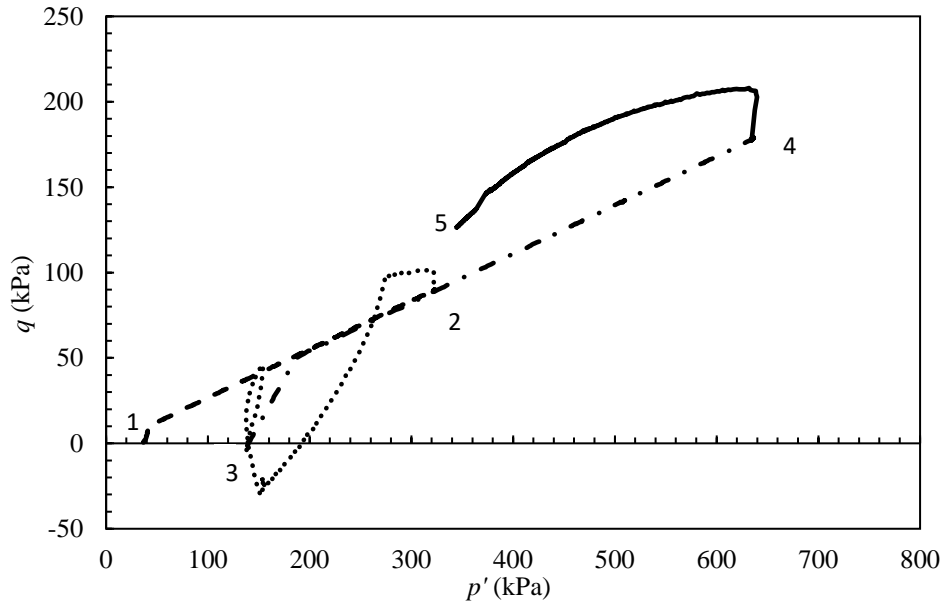
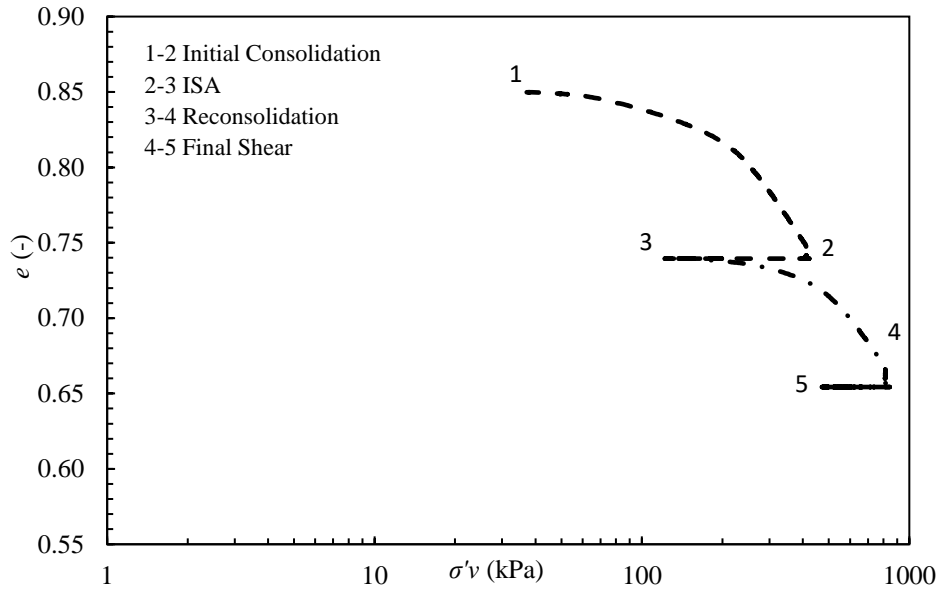**Figure 4.2 5** Complete compression curve and stress path for normally consolidated 50S50K, ±1.0% ISA test with post-ISA SHANSEP
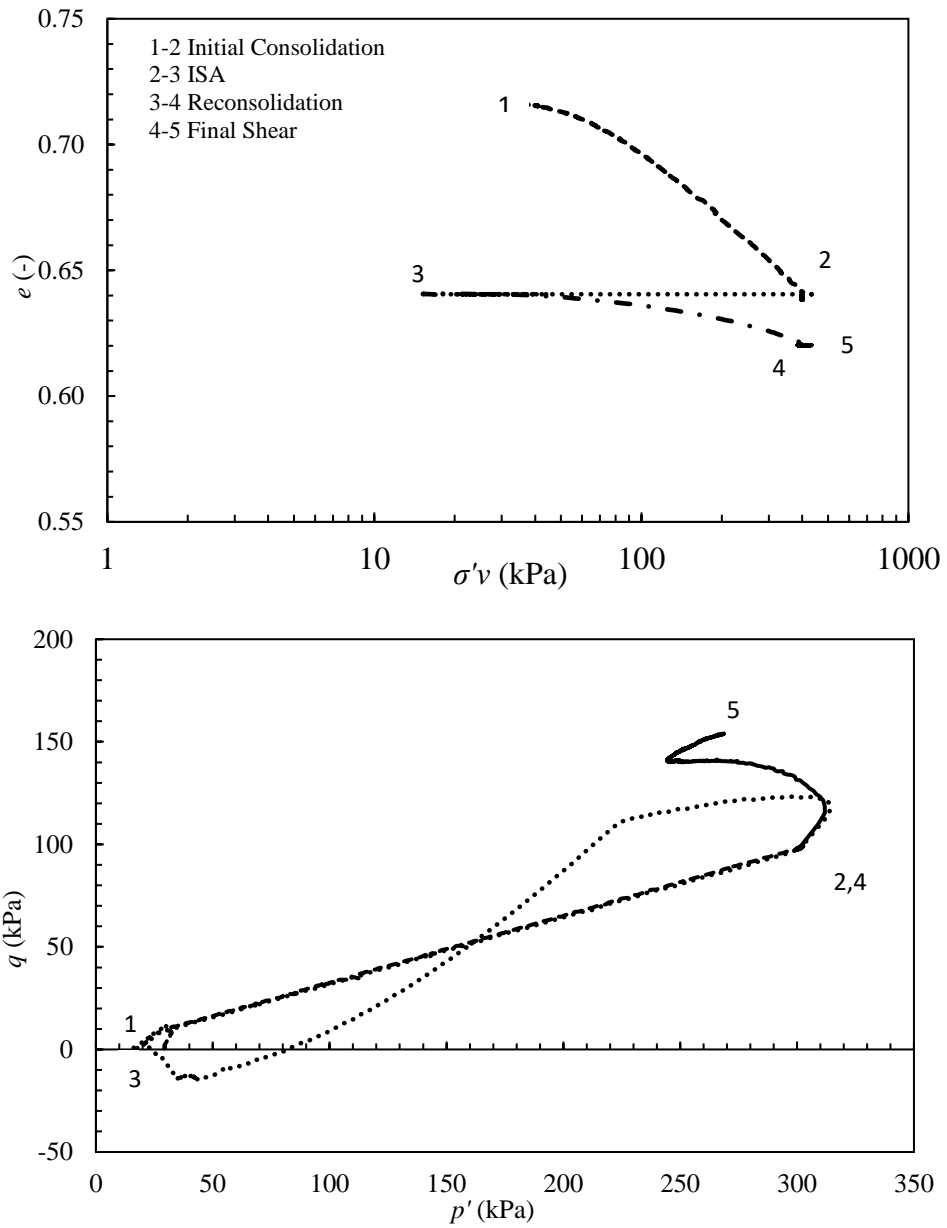
Figure 4.2 6 Complete compression curve and stress path for normally consolidated, ±1.0% ISA test on 85S15K with post-ISA recompression consolidation.

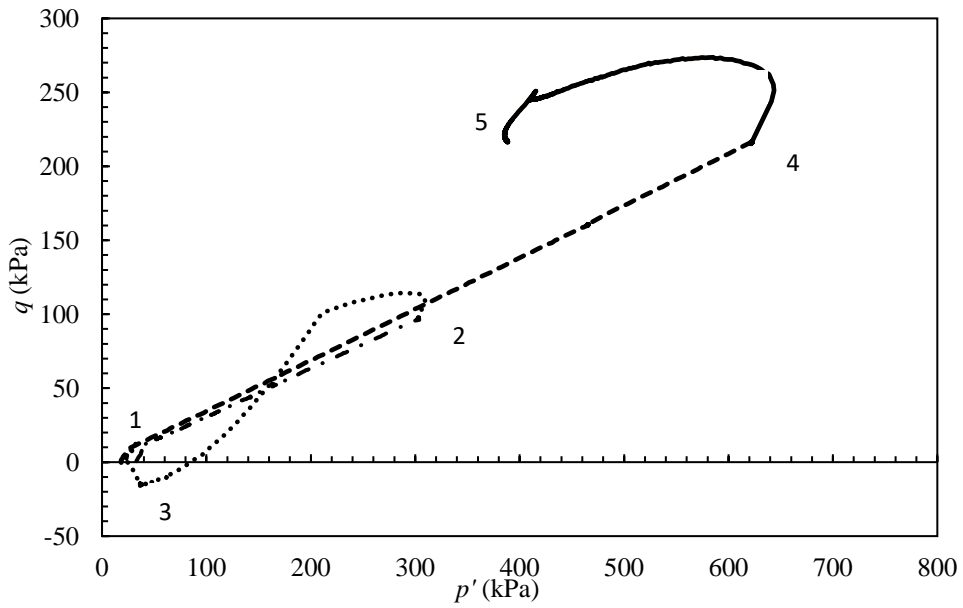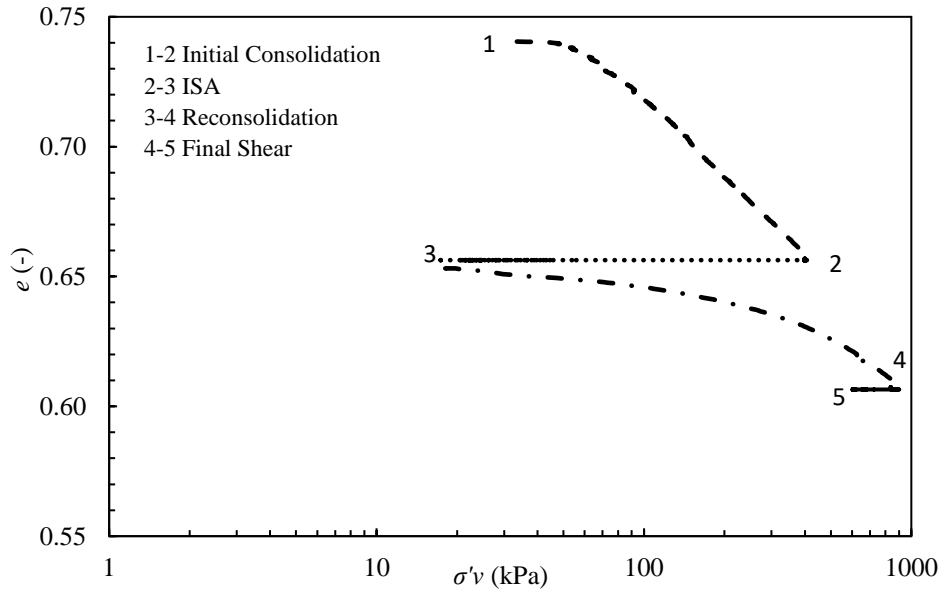**Figure 4.2 7** Complete compression curve and stress path for normally consolidated, ±1.0% ISA test on 85S15K with post-ISA SHANSEP.

73

Figure 4.2 8 Stress-strain, normalized stress-strain, and shear induced pore pressure plots for normally consolidated undisturbed, ±1% ISA and SHANSEP tests

Figure 4.2 9 Stress paths and normalized stress paths for normally consolidated undisturbed, ±1% ISA and SHANSEP tests.

Figure 4.2 10 Stress-strain, normalized stress-strain, and shear induced pore pressure plots for normally consolidated undisturbed, ±3% ISA and SHANSEP tests

Figure 4.2 11 Stress paths and normalized stress paths for normally consolidated undisturbed, ±3% ISA and SHANSEP tests.
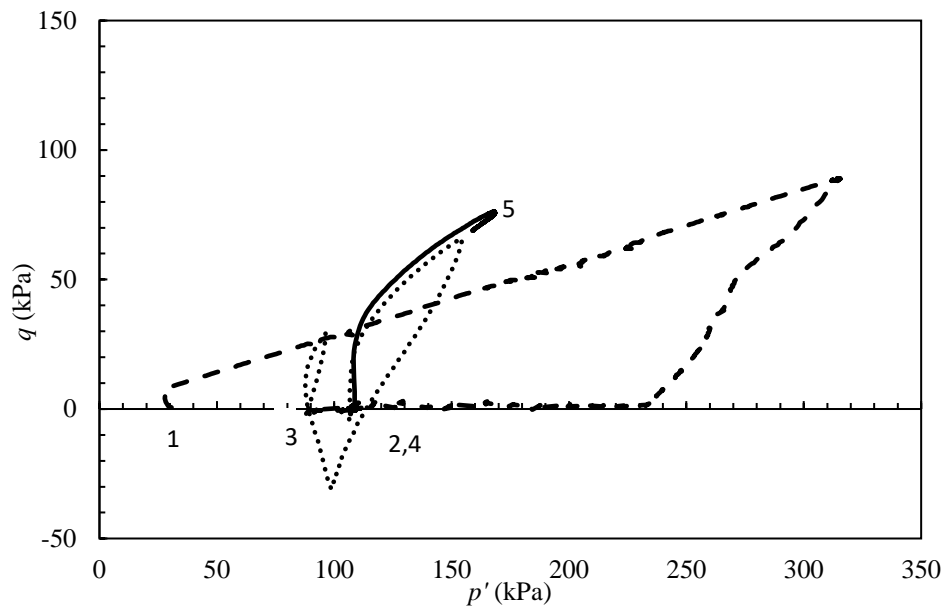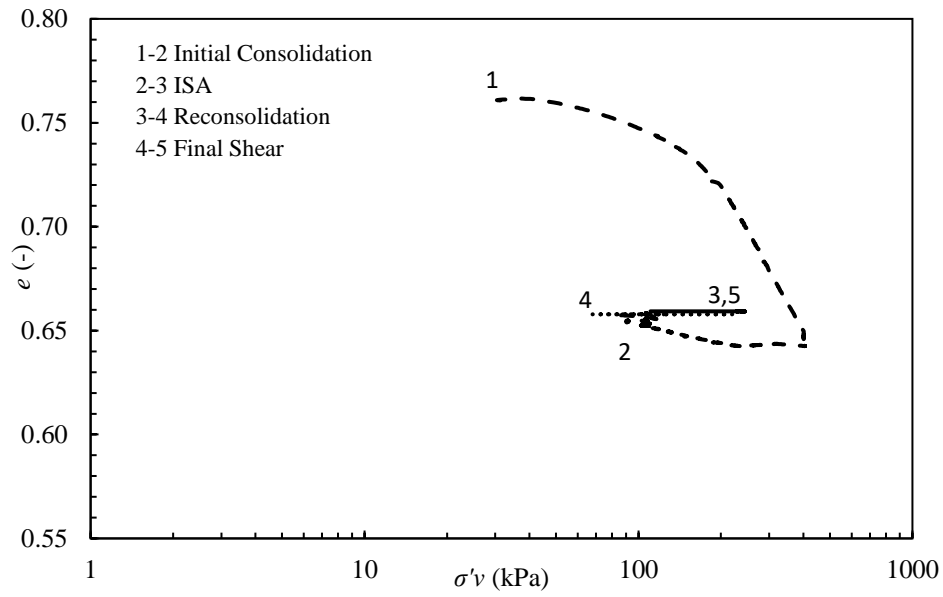
Figure 4.2 12 Complete compression curve and stress path for an OCR = 3.6, ±1.0% ISA test on 50S50K specimen with post-ISA recompression consolidation.
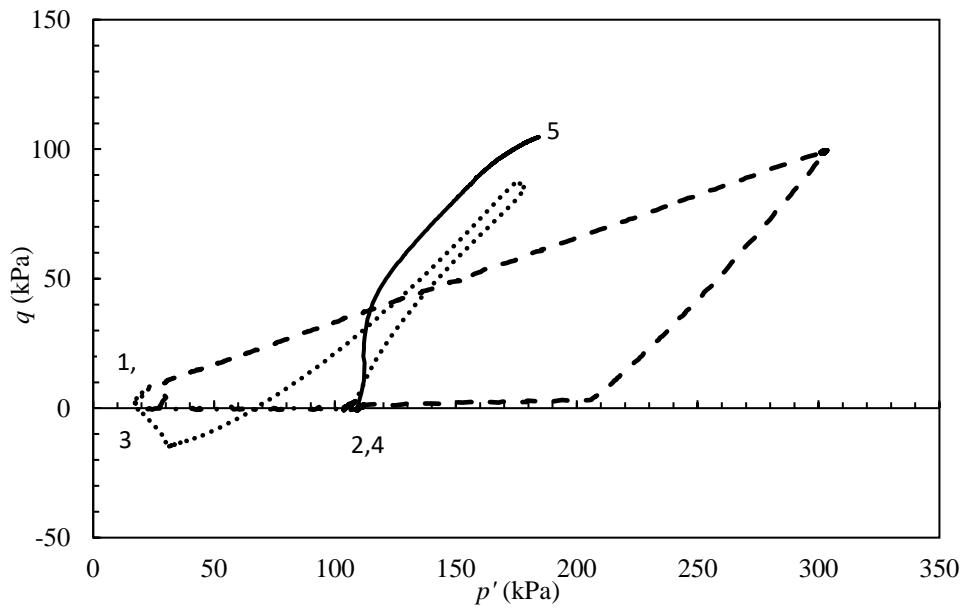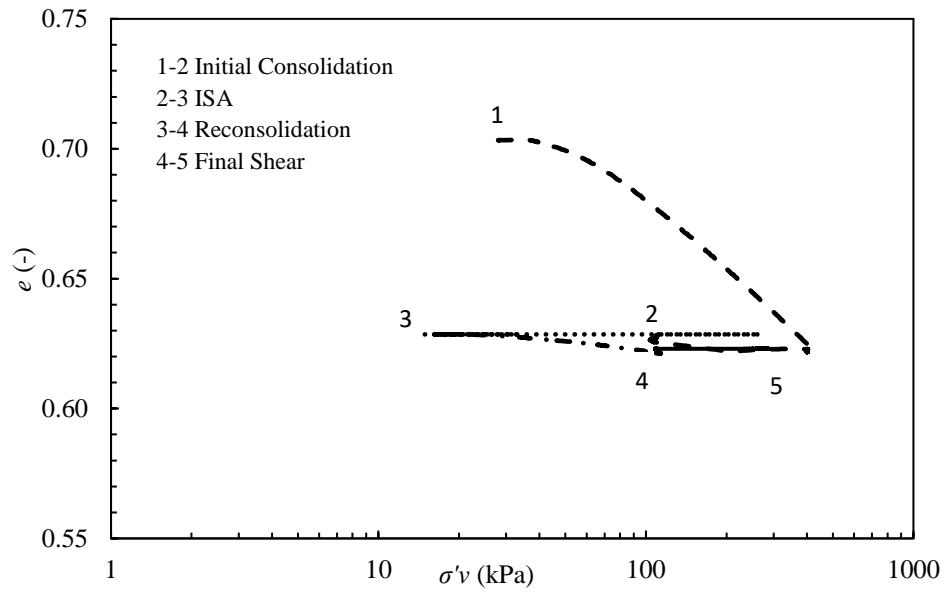
Figure 4.2 13 Complete compression curve and stress path for an OCR = 3.6, ±1.0%
ISA test on 85S15K specimen with post-ISA recompression consolidation.
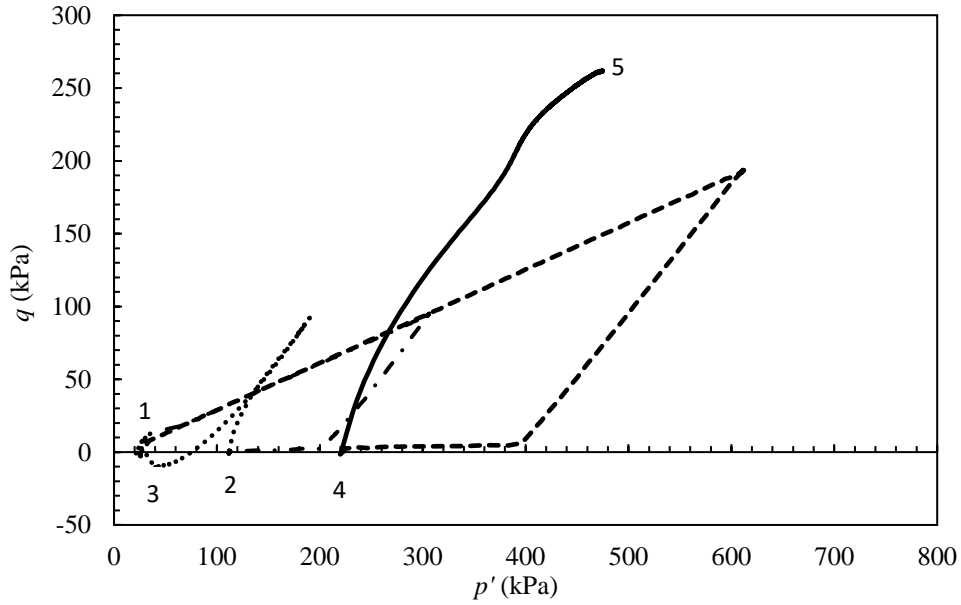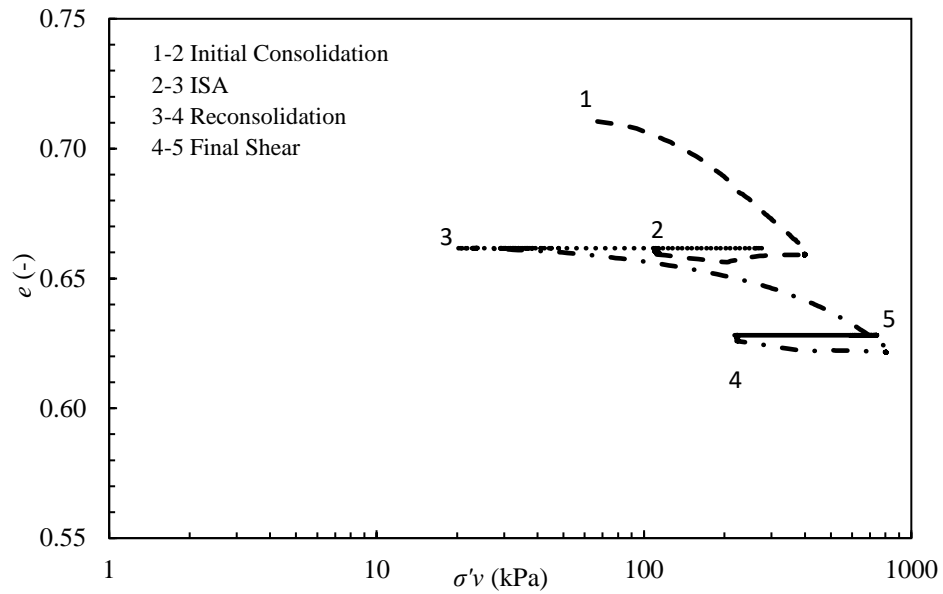
Figure 4.2 14 Complete compression curve and stress path for an OCR = 3.6, ±1.0% ISA test on 85S15K specimen with post-ISA SHANSEP.
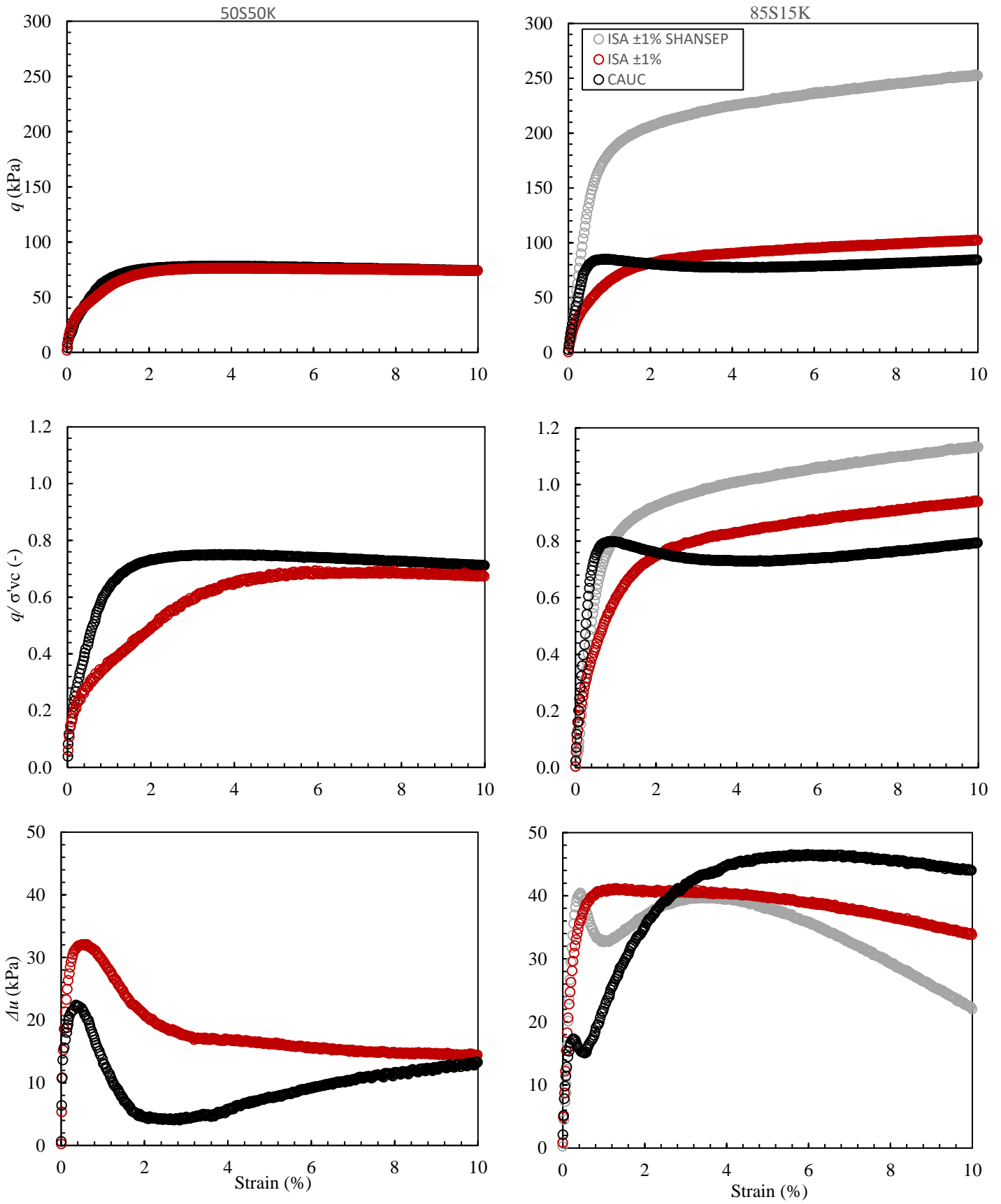
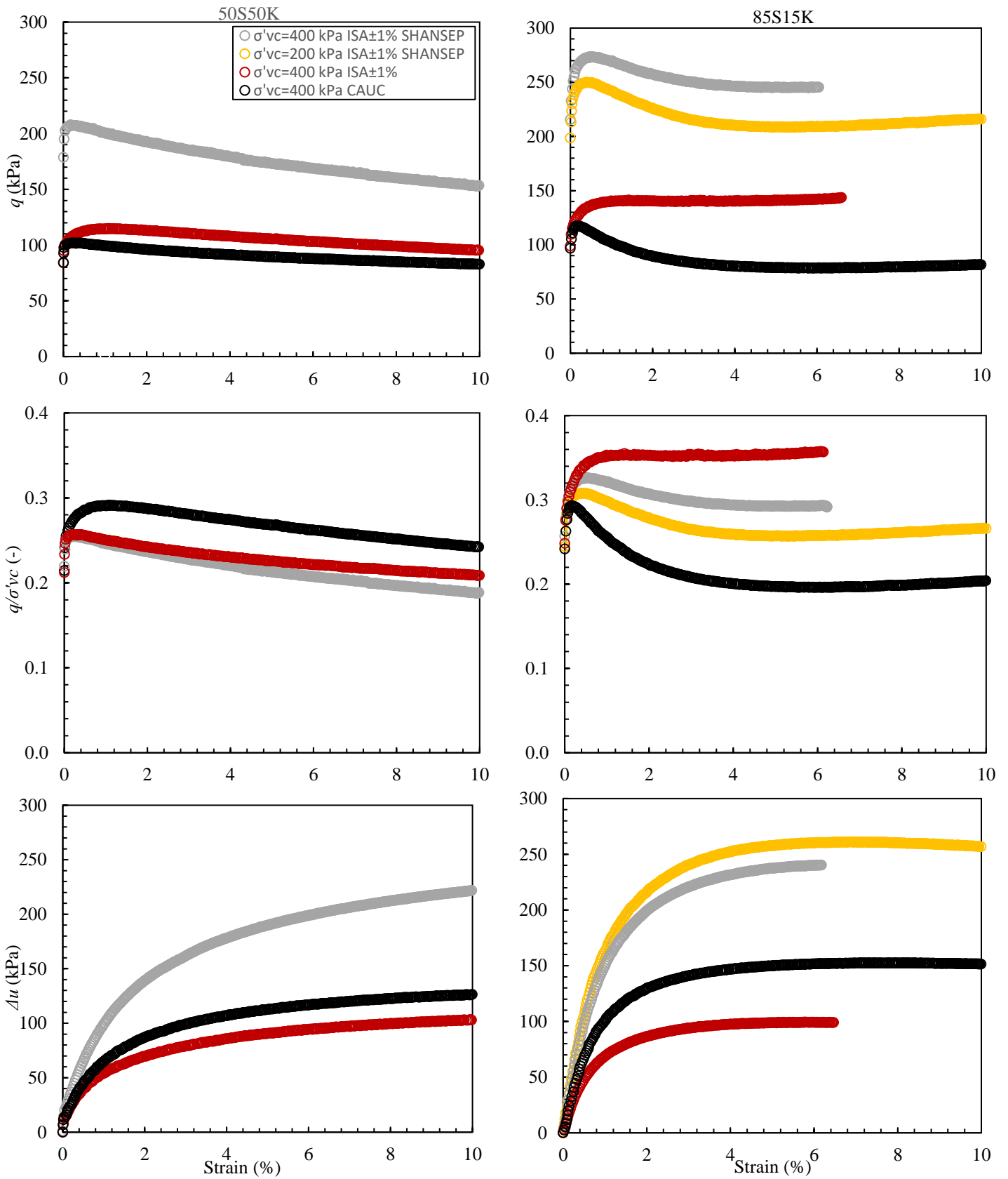**Figure 4.2 15** Stress-strain, normalized stress-strain, and shear induced pore pressure plots for OCR=3.6 undisturbed, ±1% ISA and SHANSEP tests
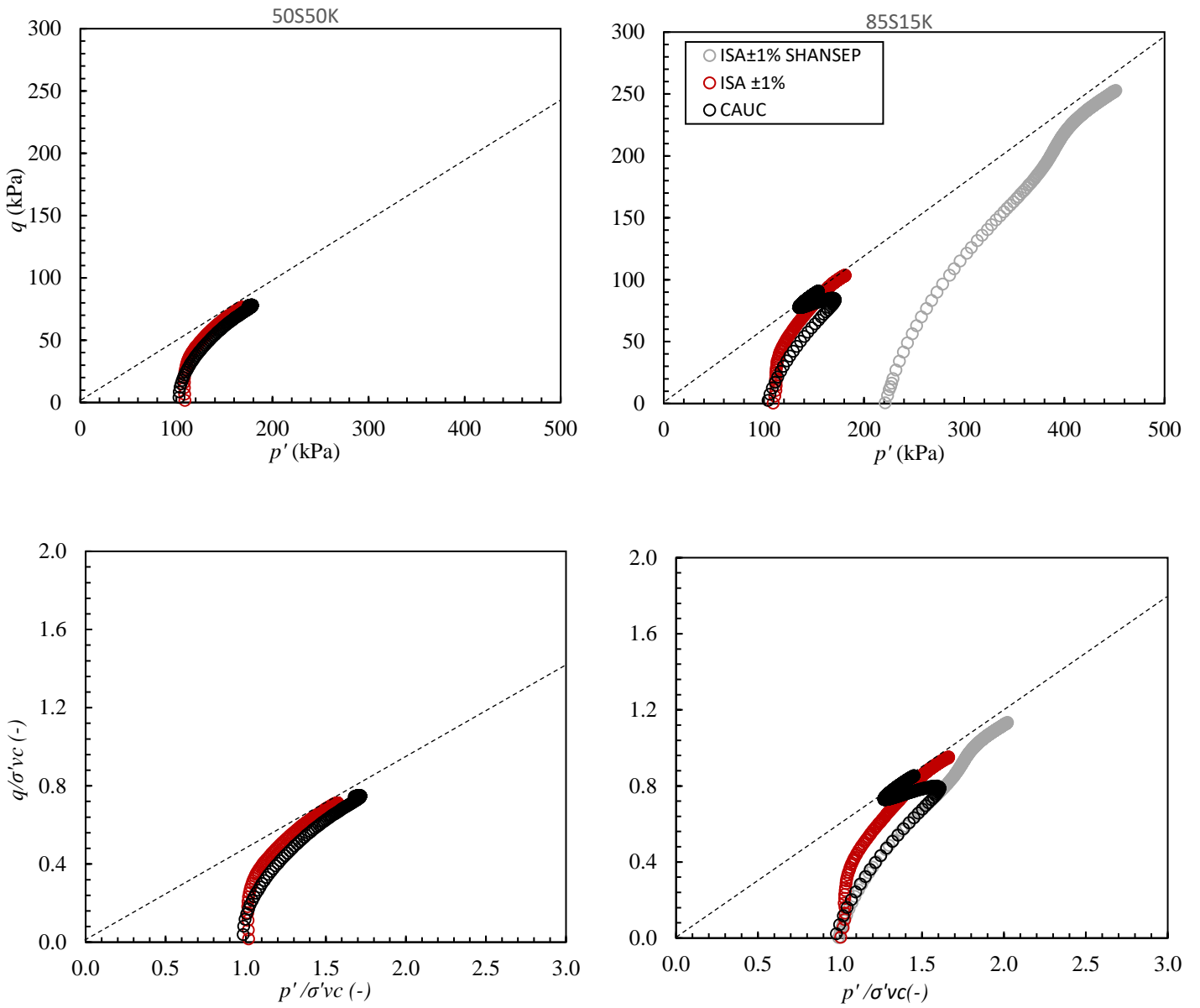
Figure 4.2 16 Stress paths and normalized stress paths for OCR =3.6 undisturbed, ±1% ISA and SHANSEP tests
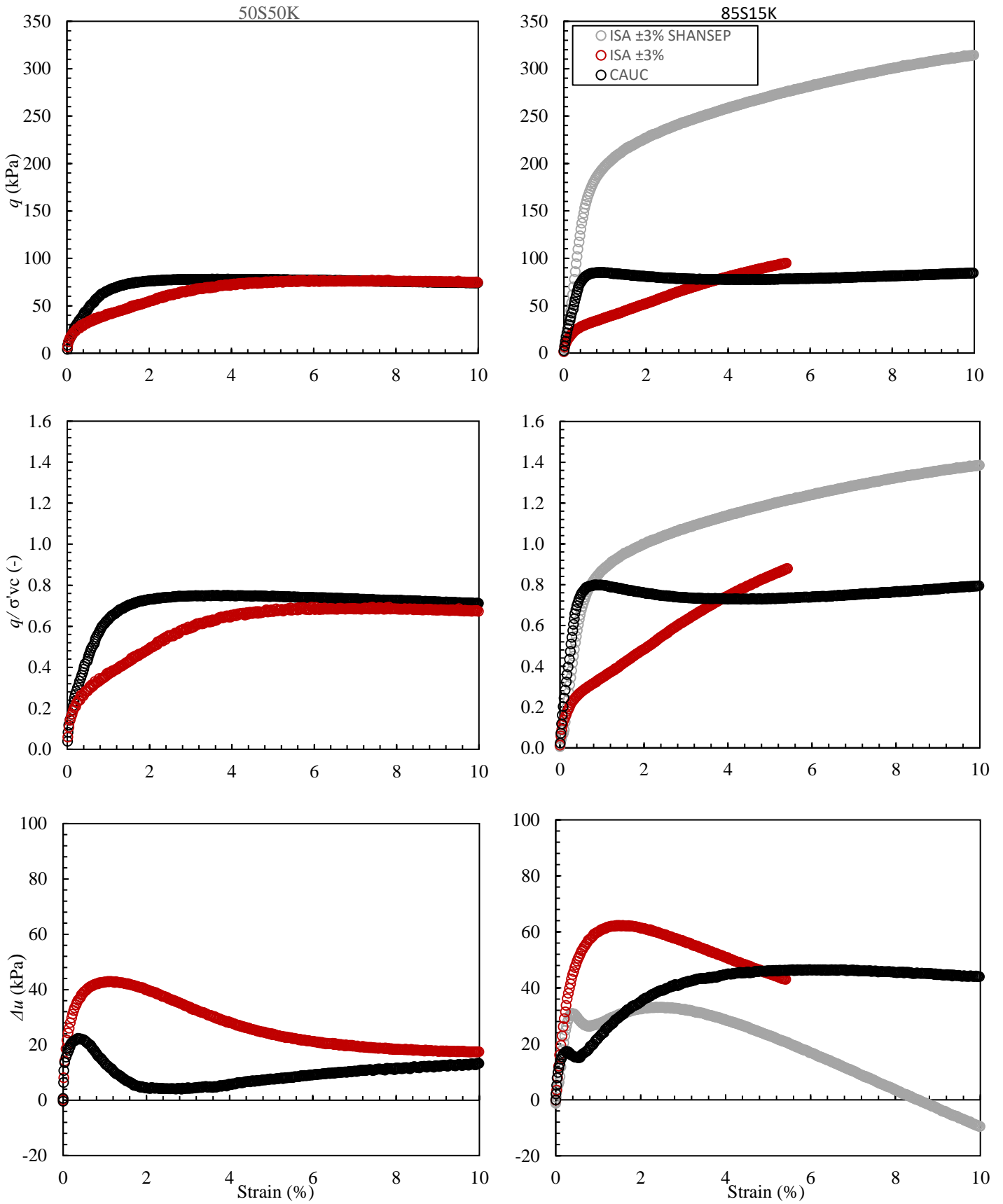
Figure 4.2 17 Stress-strain, normalized stress-strain, and shear induced pore pressure plots for OCR =3.6 undisturbed, ±3% ISA and SHANSEP tests
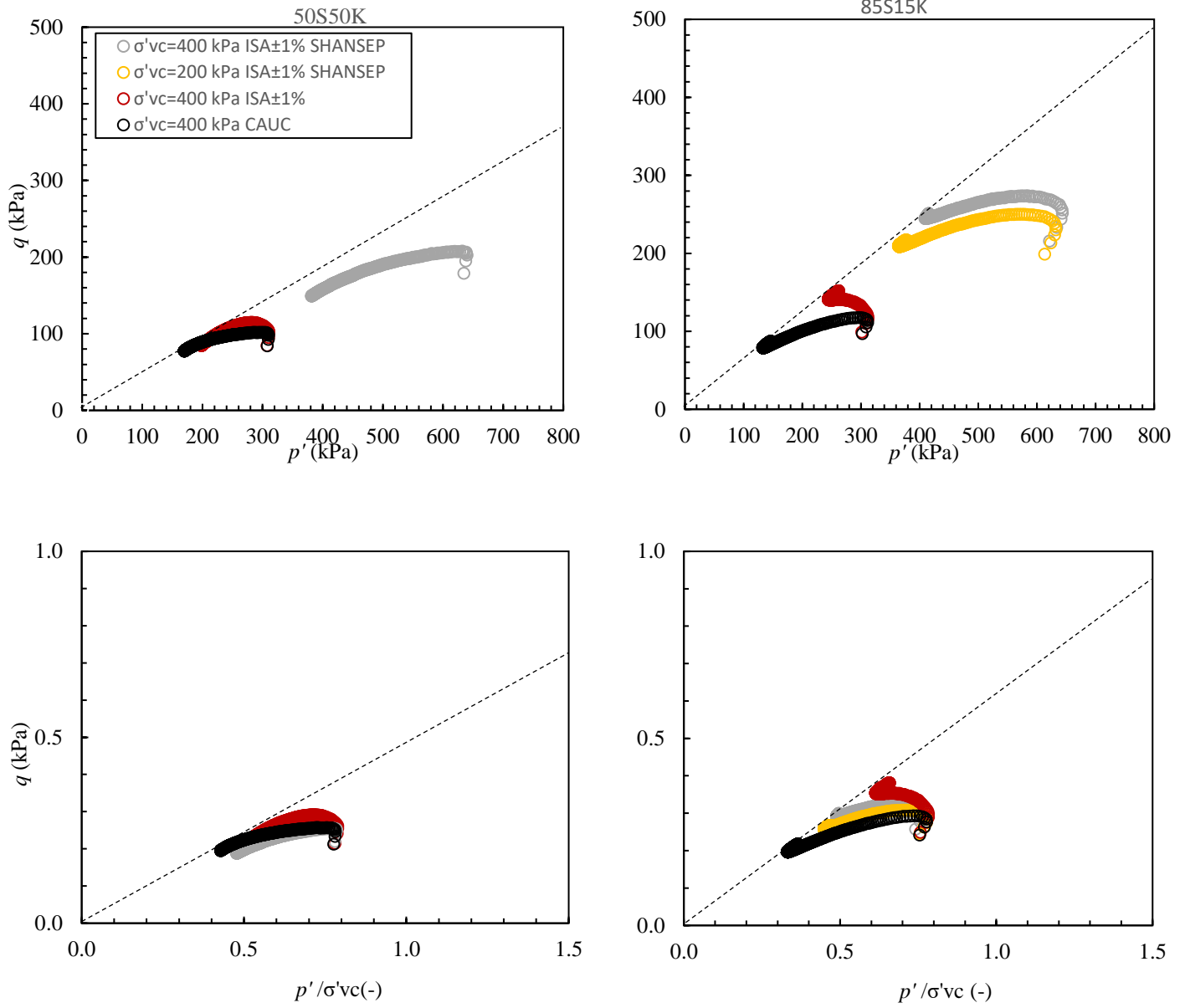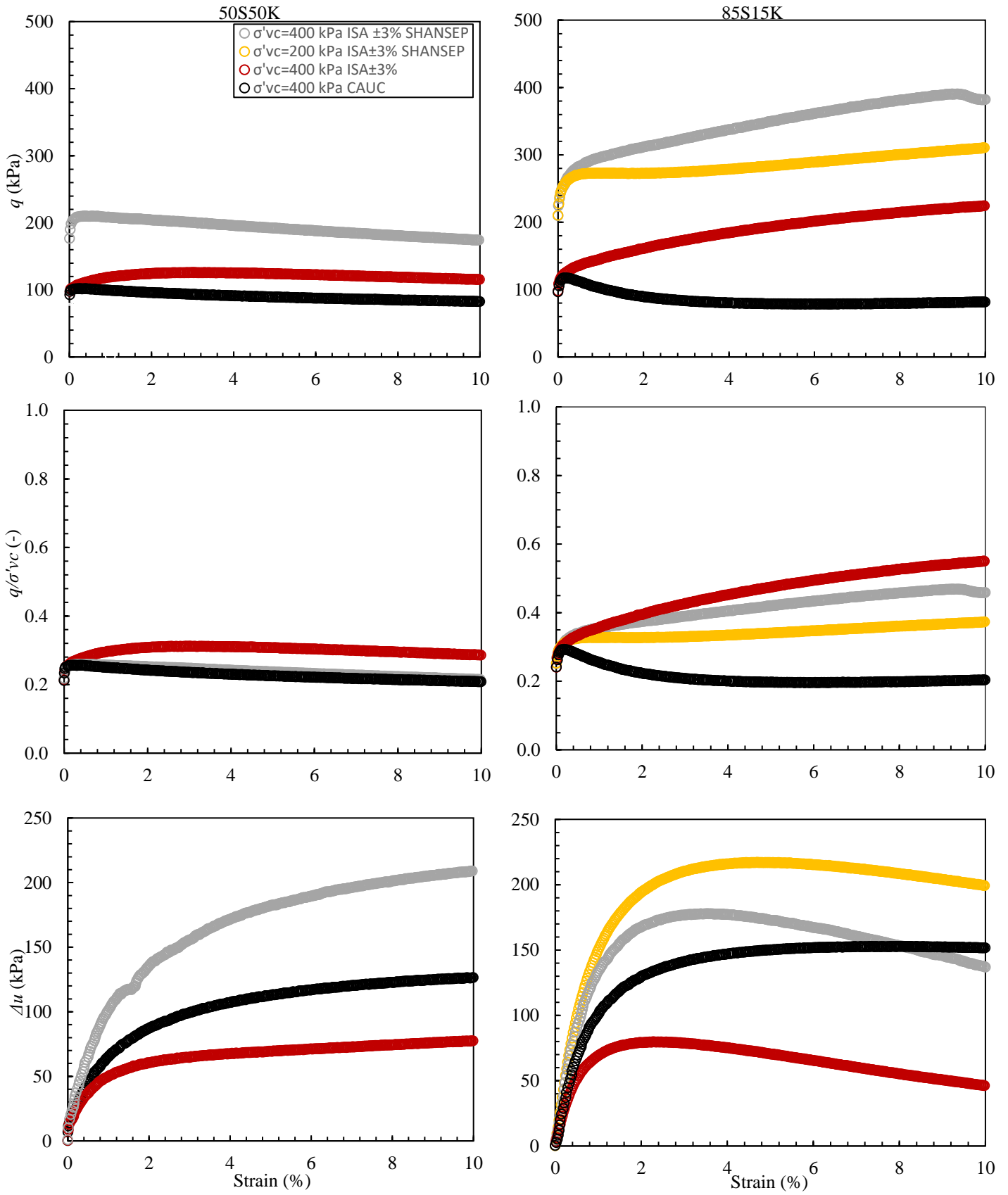
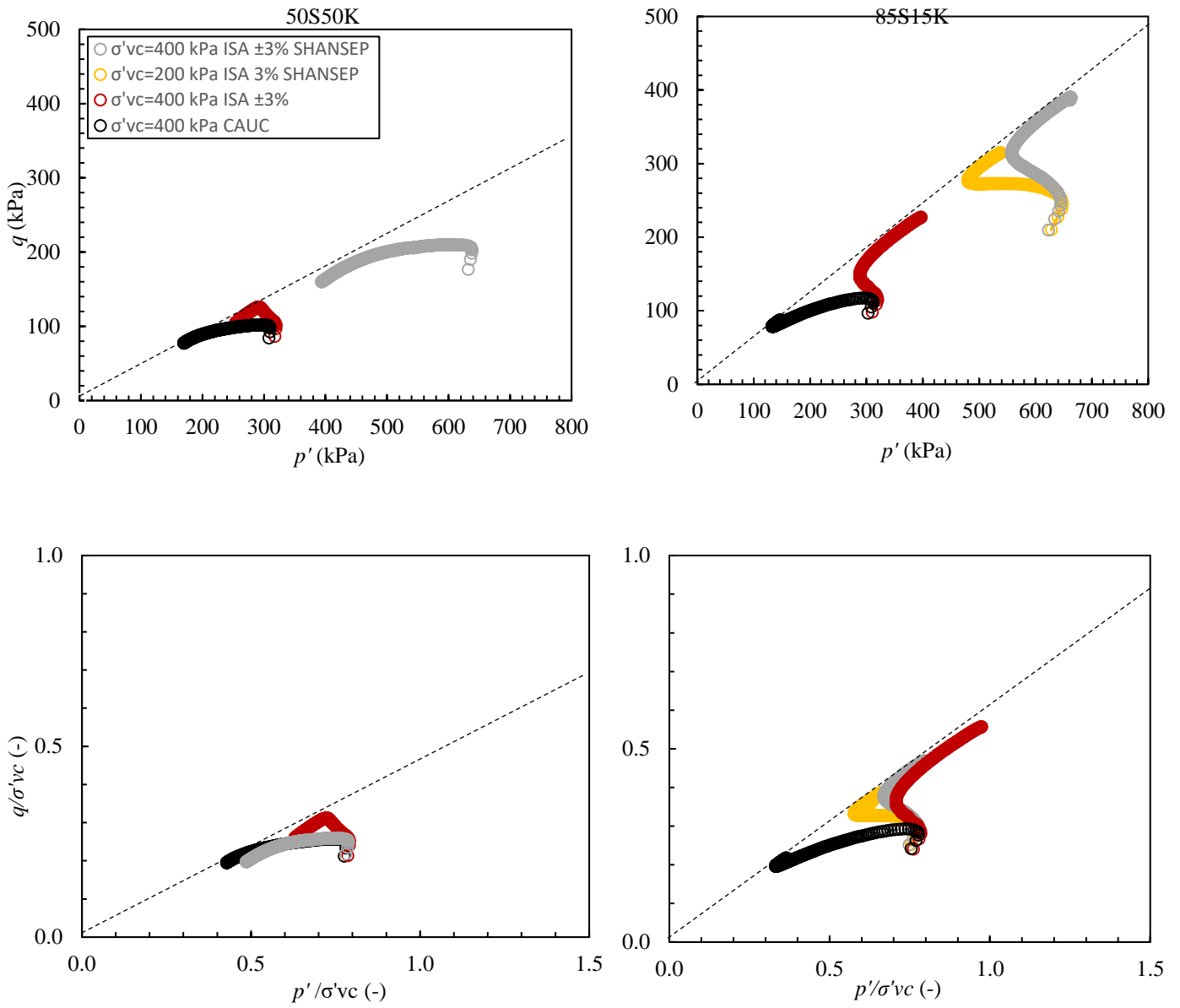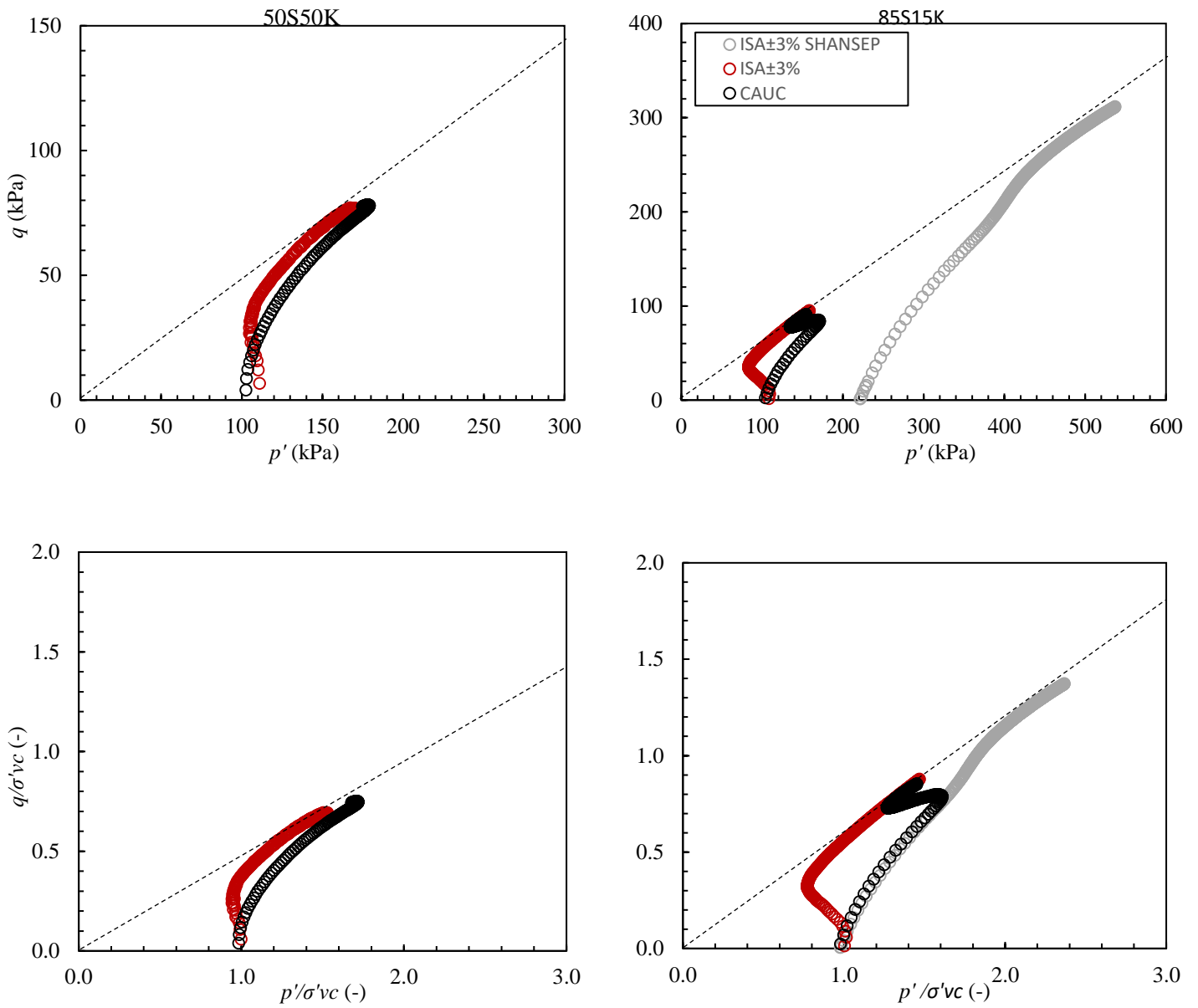**Figure 4.2 18** Stress paths and normalized stress paths for OCR= 3.6 undisturbed, ±3% ISA and SHANSEP tests.
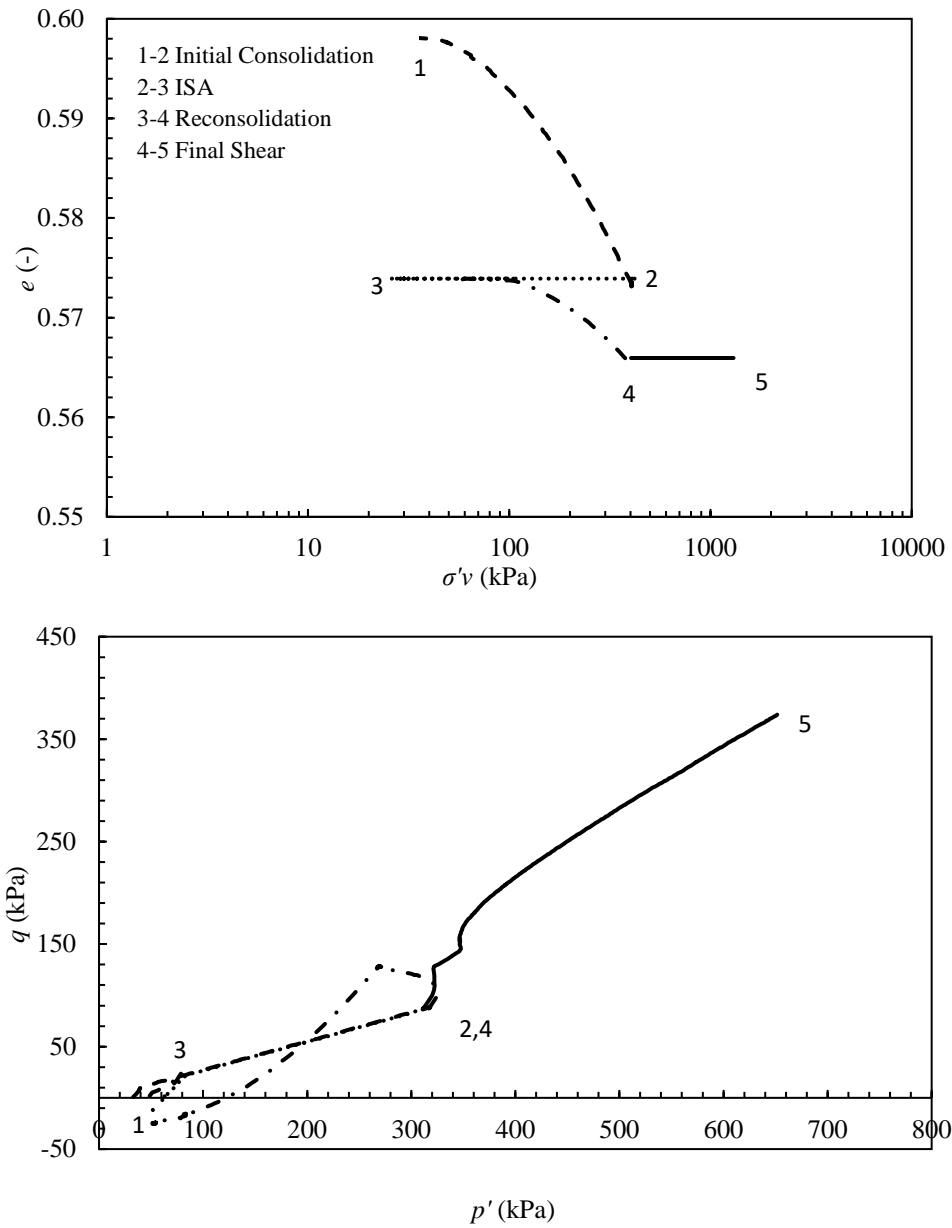
Figure 4.2 19 Complete compression curve and stress path for normally consolidated Dedham Silt, ±1.0% ISA test with post-ISA recompression
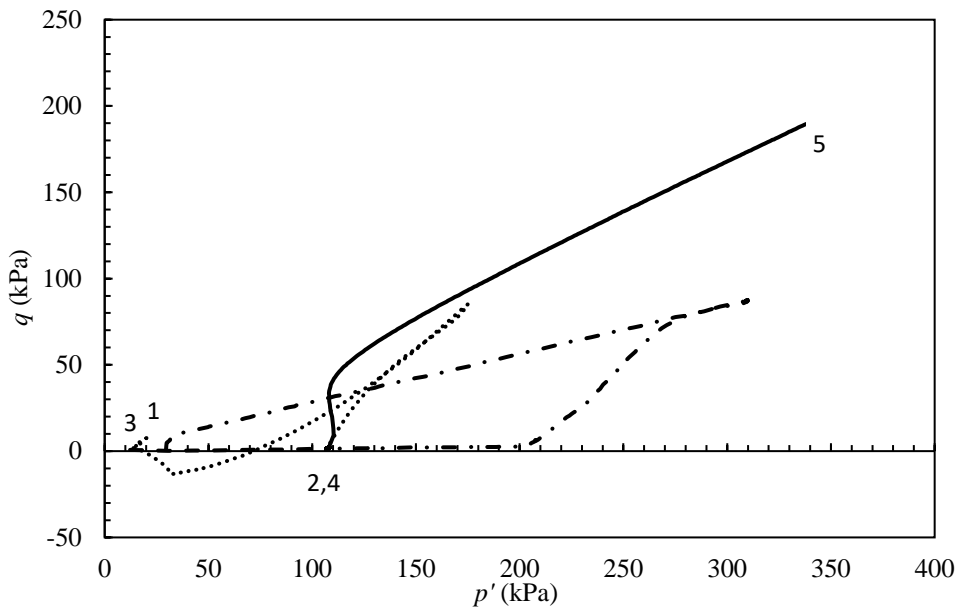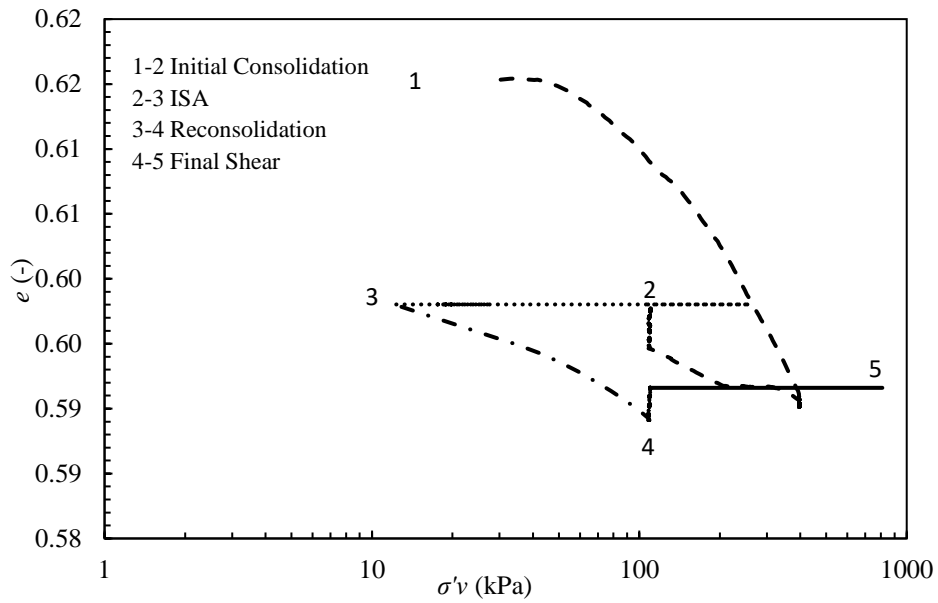
Figure 4.2 20 Complete compression curve and stress path for OCR=3.6 Dedham Silt, ±1.0% ISA test with post-ISA recompression
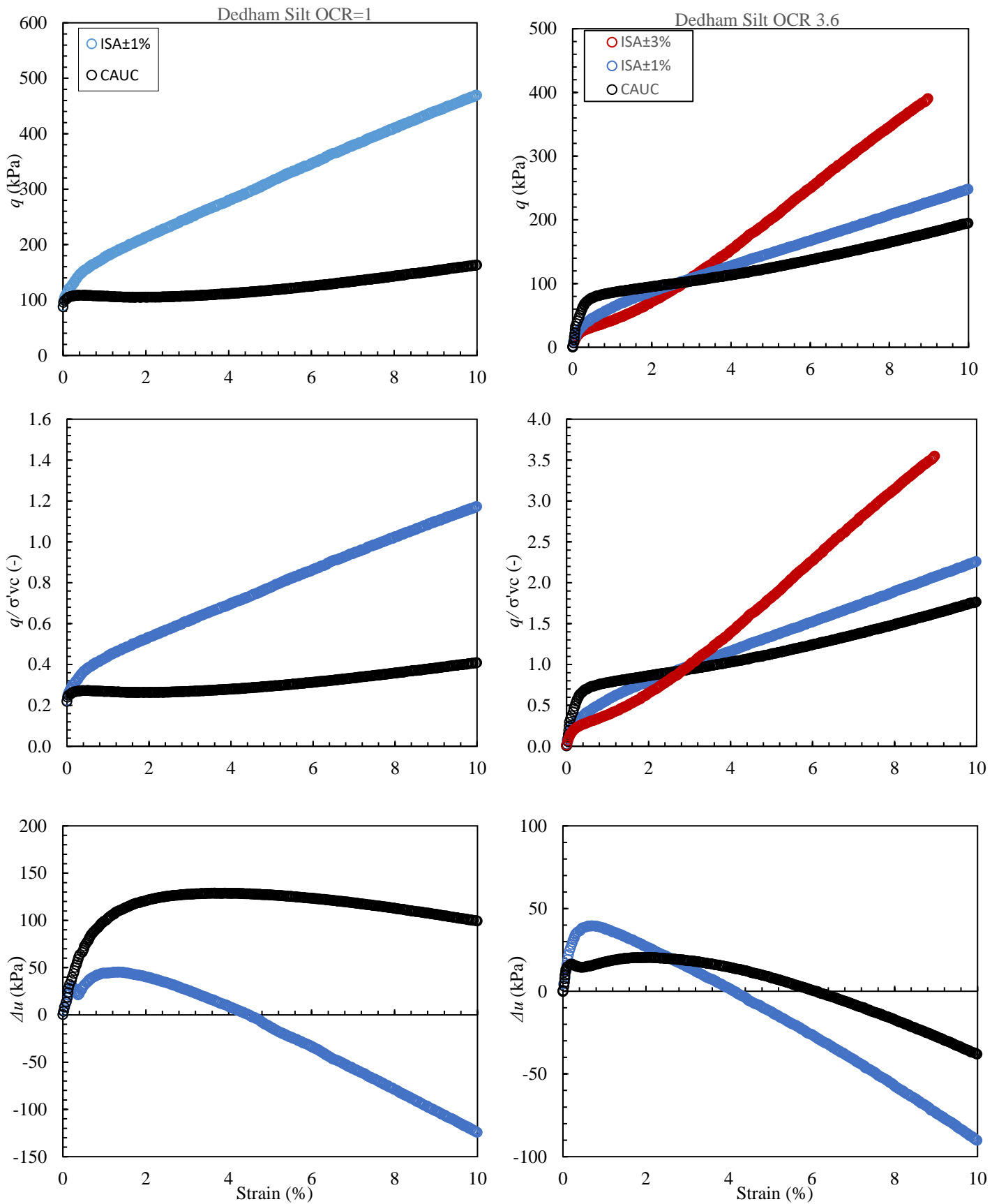
Figure 4.2 21 Stress-strain, normalized stress-strain, and shear induced pore pressure plots for Dedham Silt OCR=1 & OCR =3.6 undisturbed, ±1% & ±3% ISA with recompression
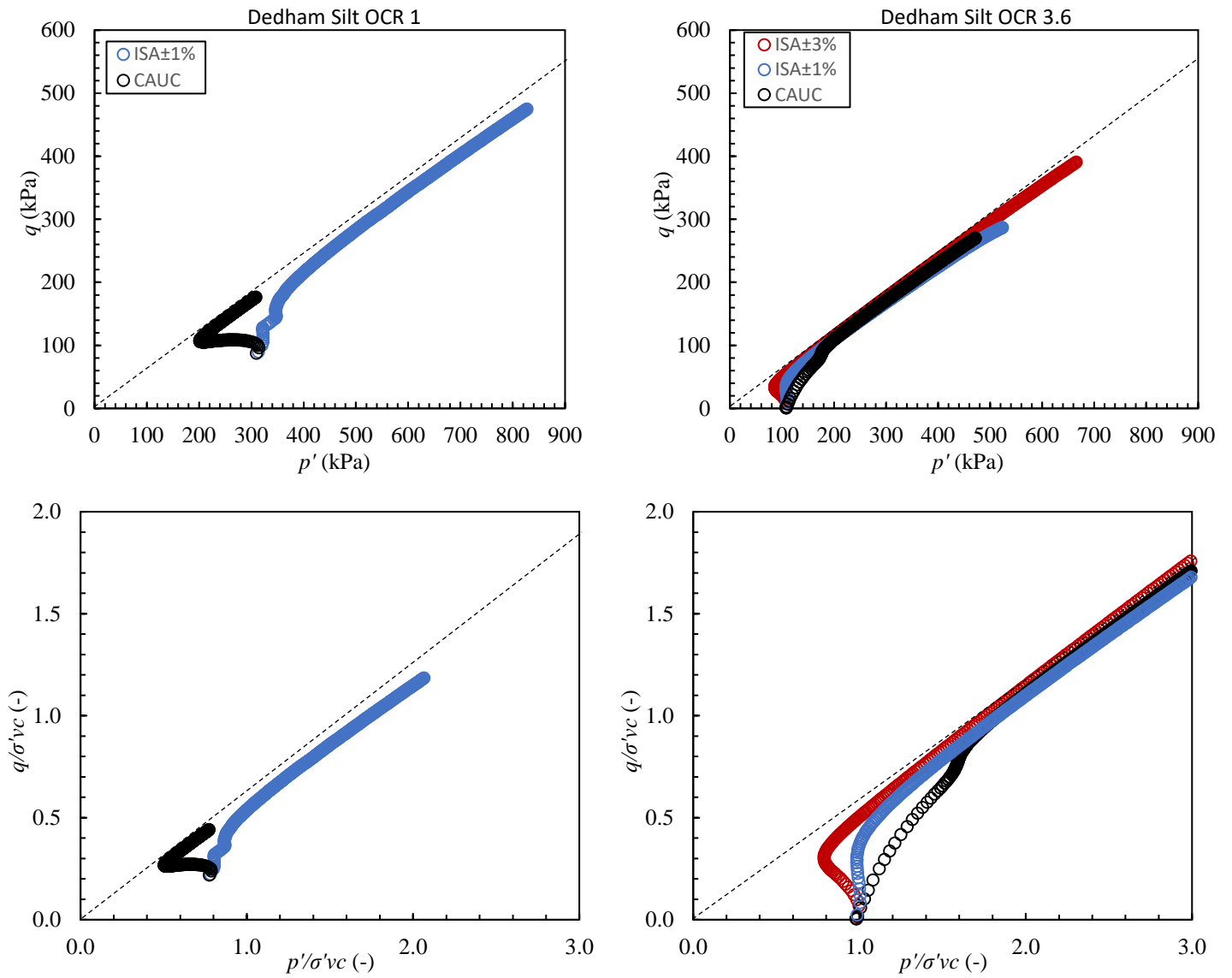
Figure 4.2 22 Stress paths and normalized stress paths for Dedham Silt OCR=1 & OCR= 3.6 undisturbed, ±1% & ±3% ISA with recompression

4.3 Shear Wave Velocity

This section presents and analyzes results of shear wave velocity and small strain shear modulus measurements obtained from laboratory triaxial cells equipped with bender elements. The tests were conducted on reconstituted specimens of 85S15K and 50S50K to study the influence of ISA straining and post-ISA Recompression and SHANSEP consolidation procedures after ISA disturbance on shear wave velocity and small strain shear modulus of the test soils. A shear wave velocity-stress state backbone curve was developed for each soil. The change in the shear wave velocity and small strain shear modulus due to both ISA disturbance and post-ISA reconsolidation procedure was evaluated relative to the backbone curve. The backbone curve was developed using the following equation as introduced in the Section 2.6:

$$G_{vh} = V_{vh}{}^2 \rho_t = S_{vh} e^{-m} (\sigma'_v \sigma'_h)^n \qquad \text{Eq. 4.3.1}$$

where

G_{vh} = small strain shear modulus

V_{vh} = shear wave velocity

ρ_t = total density

S_{vh} = "structure" term

σ'_v = vertical effective stress

σ'_h = horizontal effective stress

In order to determine the coefficients S_{vh}, m, and n the shear wave velocity ideally needs to be measured at known states of σ'_v, σ'_h, and e for: 1) various stress states but with little change in void ratio to determine n, i.e. unload-reload cycles, 2) the same effective

stress state but at different void ratios to determine m, and 3) normalization of G_{vh} by F(e) to confirm n and to determine S_{vh}. These known states were achieved by performing K_0-consolidated tests in a triaxial stress path cell equipped with bender elements with multiple unload-reload loops and frequent measurement of the shear wave velocity.

Table 4.3.1 summarizes the triaxial testing loading schedule used for development of the shear wave velocity – stress state framework. The symbols in Figure 4.2.1a shows at which σ'_v values the shear wave velocity was measured which were recorded using an input frequency of 5 kHz. Figure 4.2.1b plots the small strain shear modulus G_{vh} versus stress squared for which G_{vh} was computed as the product of V_{vh} squared and the corresponding specimen total density for each shear wave velocity measurement. Figure 4.3b also plots the data analyzed (solid lines) using the following procedure as described by Hight and Leroueil (2003) and Lukas (2017):

1) Determine G_{vh}, V_{vh}, ρ_t, e, σ'_v, and σ'_h at various normally consolidated (OCR = 1) and over consolidated (OCR > 1) states during the test

2) From plot of G_{vh} versus $\sigma'_v\sigma'_h$ for the unload-reload cycles perform a best fit regression for the equation $y = ax^b$ to determine the value of n in Equation 4.3.1

3) From plot of $G_{vh}/(\sigma'_v\sigma'_h)^n$ versus e perform a best fit regression for the equation $y = ax^b$ to determine the value of m in Equation 4.3.1

4) From plot of G_{vh}/e^{-m} versus $\sigma'_v\sigma'_h$ perform a best fit regression for the equation $y = ax$ to determine the value S_{vh} in Equation 4.3 and confirm the value of n, denoted as $n*$.

Table 4.3.2 presents the resulting Equation 4.3.1 coefficients which define the backbone curves for the 50S50K and 85S15K soils.

For the ISA tests, shear wave velocity was measured at selected stages for each test including: the end of consolidation also known as the pre-ISA shear wave velocity ($V_{vh,0}$), end of ISA ($V_{vh,ISA}$) and end of post-ISA reconsolidation ($V_{vh,p-ISA}$) as summarized in Table 4.3.3.

90

Figure 4.3.2 presents the G_{vh}, V_{vh} and G_{vh}/e^{-m} versus $\sigma'_v\,\sigma'_h$ for normally consolidated 85S15K with ±1% & ±3% ISA straining followed by Recompression and SHANSEP post-ISA consolidation. It can be observed that the value of G_{vh} and V_{vh} during ISA disturbance is reduced significantly relative to the pre-ISA undisturbed stress state. Table 4.3.3 summaries the ratio of V_{vh} at the end of ISA ($V_{vh,ISA}$) to the pre-ISA value ($V_{vh,ISA}/V_{vh,0}$). A maximum reduction in $V_{vh,ISA}/V_{vh,0}$ ratio equal to 0.29 is observed for normally consolidated (σ'_{vmax}=400kPa) 85S15K specimen subjected to ±3% ISA. However, the specimen normally consolidated to pre-ISA σ'_{vmax}=200 kPa with ±3% ISA shows much smaller reduction in $V_{vh,ISA}/V_{vh,0}$ equal to 0.71. Post-ISA reconsolidation G_{vh} and V_{vh} values return to pre-ISA undisturbed states exhibiting that the specimen has fully recovered the disturbance according to these measures. This is also demonstrated by the $V_{vh,p\text{-}ISA}/V_{vh,0}$ ratio which equals to 1 for post-ISA Recompression but is greater than 1 for SHANSEP consolidation. However, the G_{vh} and V_{vh} for 85S15K plot very close to the backbone curve demonstrating minimal destruction during ISA disturbance, again according to these measures.

For OCR=3.6, the reduction in G_{vh} and V_{vh} during ISA disturbance is smaller than normally consolidated specimen with $V_{vh,ISA}/V_{vh,0}$ equal to 0.72 for ±3% ISA specimen. Figure 4.3.3 shows the G_{vh}, V_{vh} and G_{vh}/e^{-m} versus $\sigma'_v\,\sigma'_h$ for 85S15K OCR=3.6. Even though G_{vh} and V_{vh} are reduced during ISA disturbance in reference to the pre-ISA undisturbed behavior, the values plot on the backbone curve exhibiting full recovery of these parameters destruction.

Figure 4.3.4 presents the G_{vh}, V_{vh} and G_{vh}/e^{-m} versus $\sigma'_v\,\sigma'_h$ for normally consolidated 50S50K ±1% & ±3% ISA Recompression and SHANSEP consolidation. Unlike 85S15K, the specimen undergoes very small reduction in G_{vh} and V_{vh} during ISA with $V_{vh,ISA}/V_{vh}$ equal to 0.86 and 0.90 for ±1% & ±3% ISA respectively. The post-ISA Recompression specimen

recovers G_{vh} and V_{vh} back to the pre-ISA undisturbed state. ISA with SHANSEP consolidation, however, results in higher G_{vh} and V_{vh}. Similarly, for higher OCR=3.6 the specimen exhibits very small reduction in G_{vh} and V_{vh} which is recovered back to the pre-ISA undisturbed state after post-ISA reconsolidation.

The normally consolidated 85S15K underwent significant reduction in G_{vh} and V_{vh} along with σ'$_v$σ'$_h$ which decreases for higher OCR. The post-ISA Recompression brings G_{vh} and V_{vh} back to the pre-ISA undisturbed state but the SHANSEP consolidation results in higher values of G_{vh} and V_{vh}. The end of ISA G_{vh} and V_{vh} values plot on the backbone curve depicting very small or no destruction during the ISA disturbance. Plotting close to the backbone curve is consistent with the specimens being reconstituted and presumed to possess no structure. The normally consolidated and OCR=3.6 50S50K specimens experienced very small reduction in G_{vh} and V_{vh} during ISA disturbance which was recovered during post-ISA reconsolidation.

Table 4.3 1 Shear wave framework loading schedule for triaxial test

Loading Step	Loading/ Unloading	Target σ'_v (kPa)	Strain Rate (%/hr)	Target OCR (-)	Target K_0 (-) 50S50K	Target K_0 (-) 85S15K
1	Loading	100	0.2	1	--	0.51
2	Unloading	20	0.1	5	--	1.12
3	Loading	200	0.2	1	0.56	0.51
4	Unloading	25	0.1	8	1.40	1.41
5	Loading	400	0.2	1	0.56	0.51
6	Unloading	50	0.1	8	1.40	1.41
7	Loading	600	0.2	1	0.56	0.51

Note: The 50S50K cakes were consolidated to 200 kPa so no 100 kPa unload was performed.

Table 4.3 2 Shear Wave Framework Parameters from Equation 4.3.1

Soil	n	m	S_{vh}	$n*$
50S50K	0.226	1.53	4.24	0.218
85S15K	0.249	1.52	1.99	0.248

Table 4.3 3 Shear wave velocity values for pre-ISA ($V_{vh,0}$), end of ISA ($V_{vh,ISA}$), and after post-ISA ($V_{vh,p\text{-}ISA}$) reconsolidation and post-ISA reconsolidation $\Delta e/e_0$ values

Soil	OCR	Test Type		$V_{vh,0}$ (m/s)	$V_{vh,ISA}$ (m/s)	$V_{vh,ISA}/V_{vh,0}$	$V_{vh,p\text{-}ISA}$ (m/s)	$V_{vh,p\text{-}ISA}/V_{vh,0}$	$\Delta e/e_0$ (-)
85S15K	1.0	ISA (±1%)	Recompression	175	97	0.55	177	1.01	0.031
			SHANSEP	180	88	0.48	-	-	0.065
		ISA (±3%)	Recompression	178	55	0.31	189	1.06	0.067
			SHANSEP	180	53	0.29	234	1.30	0.093
	3.6	ISA (±1%)	Recompression	140	91	0.65	142	1.01	0.011
			SHANSEP	143	91	0.63	226	1.58	0.054
		ISA (±3%)	Recompression	137	60	0.44	141	1.02	0.047
			SHANSEP	141	101	0.72	225	1.60	0.095
50S50K	1.0	ISA (±1%)	Recompression	-	-	-	-	-	-
			SHANSEP	218	188	0.86	266	1.22	0.099
		ISA (±3%)	Recompression	165	149	0.90	202	1.22	0.047
			SHANSEP	149	161	1.08	202	1.36	0.110
	3.6	ISA (±1%)	Recompression	185	169	0.91	185	1.00	0.002
			SHANSEP	-	-	-	-	-	-
		ISA (±3%)	Recompression	180	145	0.80	180	1.00	0.010
			SHANSEP	-	-	-	-	-	-
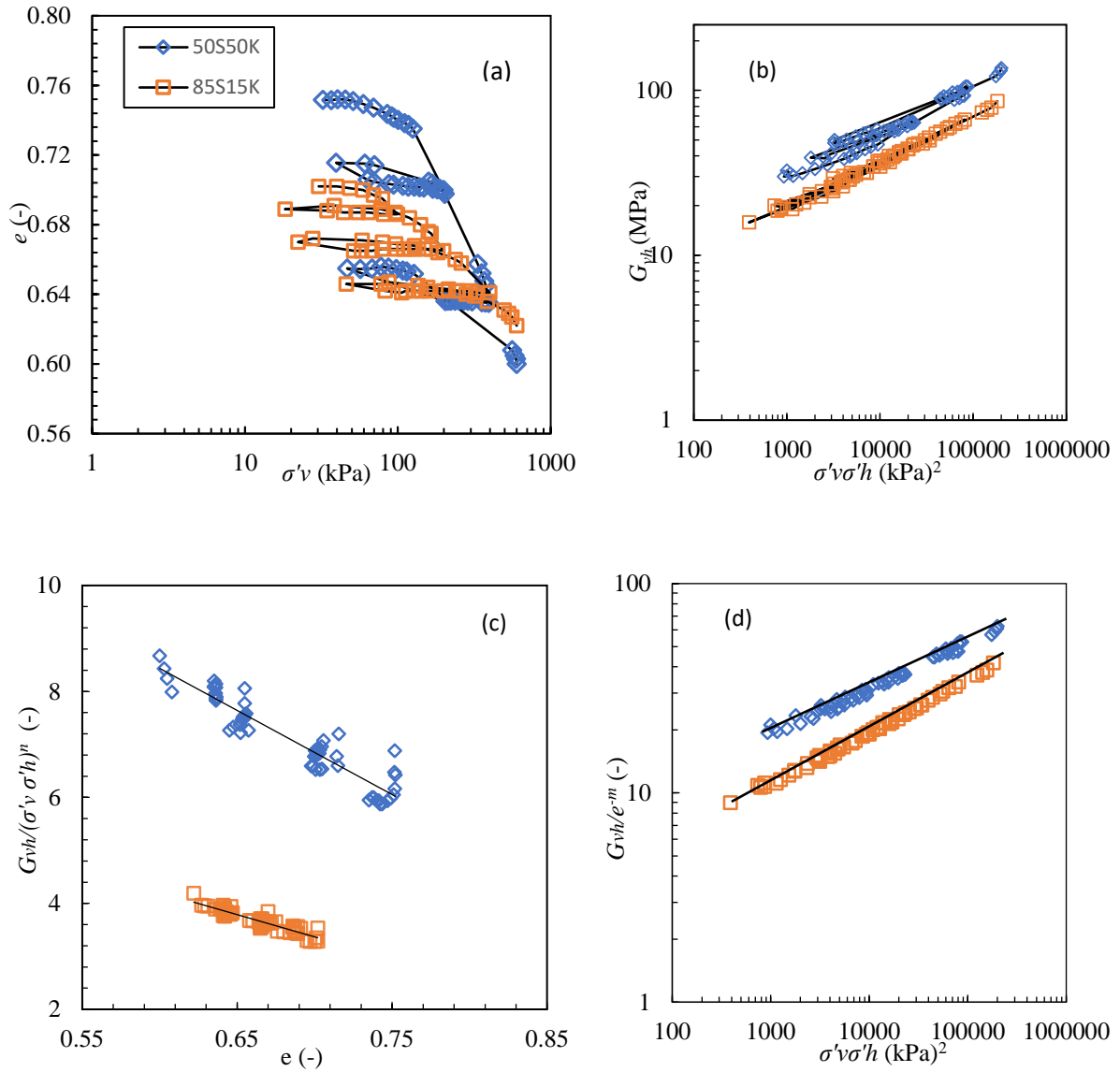
Figure 4.3 1 Shear wave framework for 85S15K and 50S50K: (a) void ratio versus effective stress at the measured shear wave velocity during K_0 consolidation. Equation 4.3.1 parameters (b) n, (c) m, and (d) S_{vh} and confirmation of n.
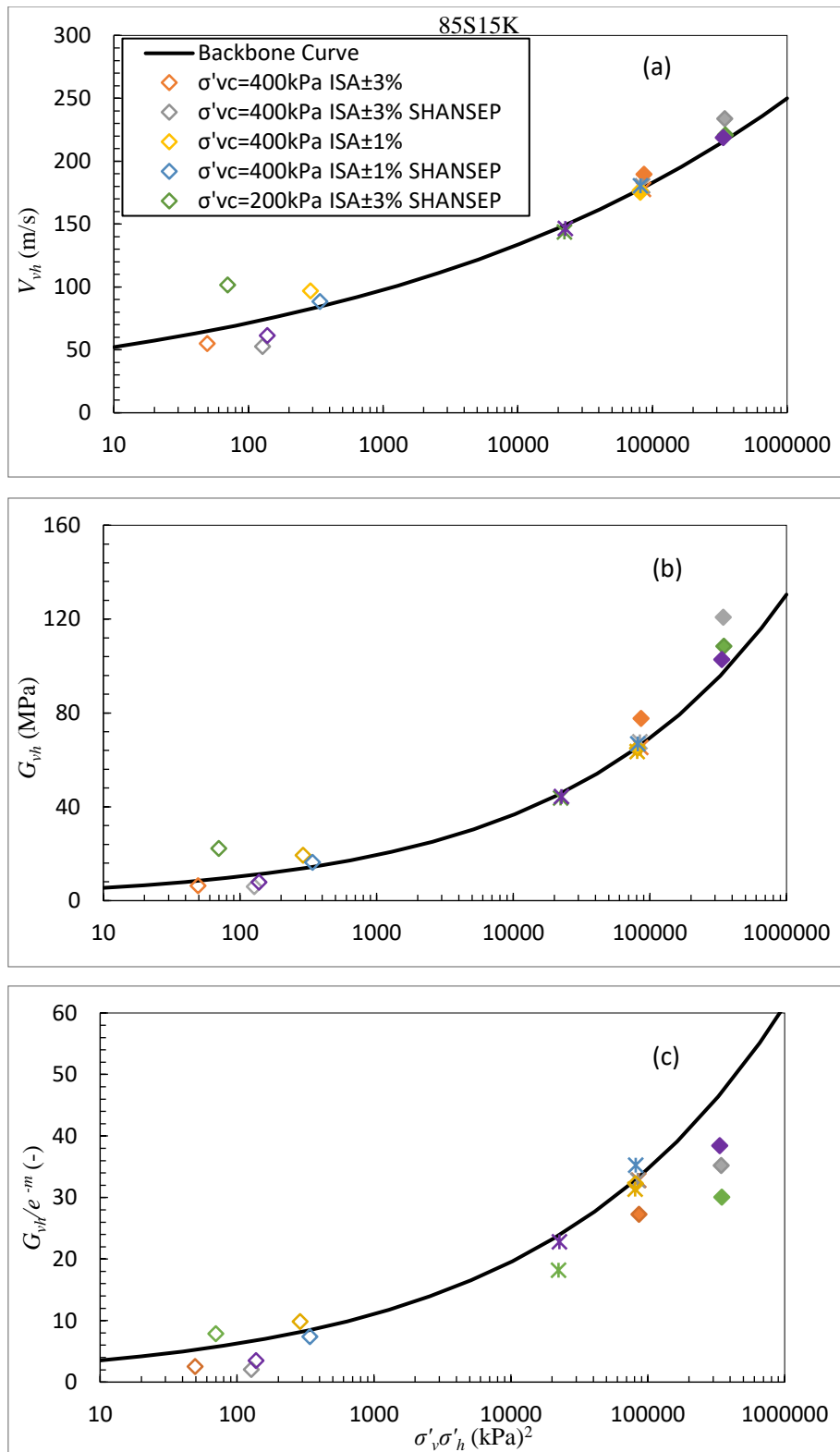
Figure 4.3 2 Backbone curve of 85S15K normally consolidated (a) V_{vh} versus $\sigma_v'\sigma_h'$ (b) G_{vh} versus $\sigma_v'\sigma_h'$ (c) G_{vh}/e^{-m} versus $\sigma_v'\sigma_h'$ with pre-ISA (crisscross symbols), end of ISA, and post-ISA (shaded symbols) data from ±1% & ±3% ISA Recompression and SHANSEP consolidation
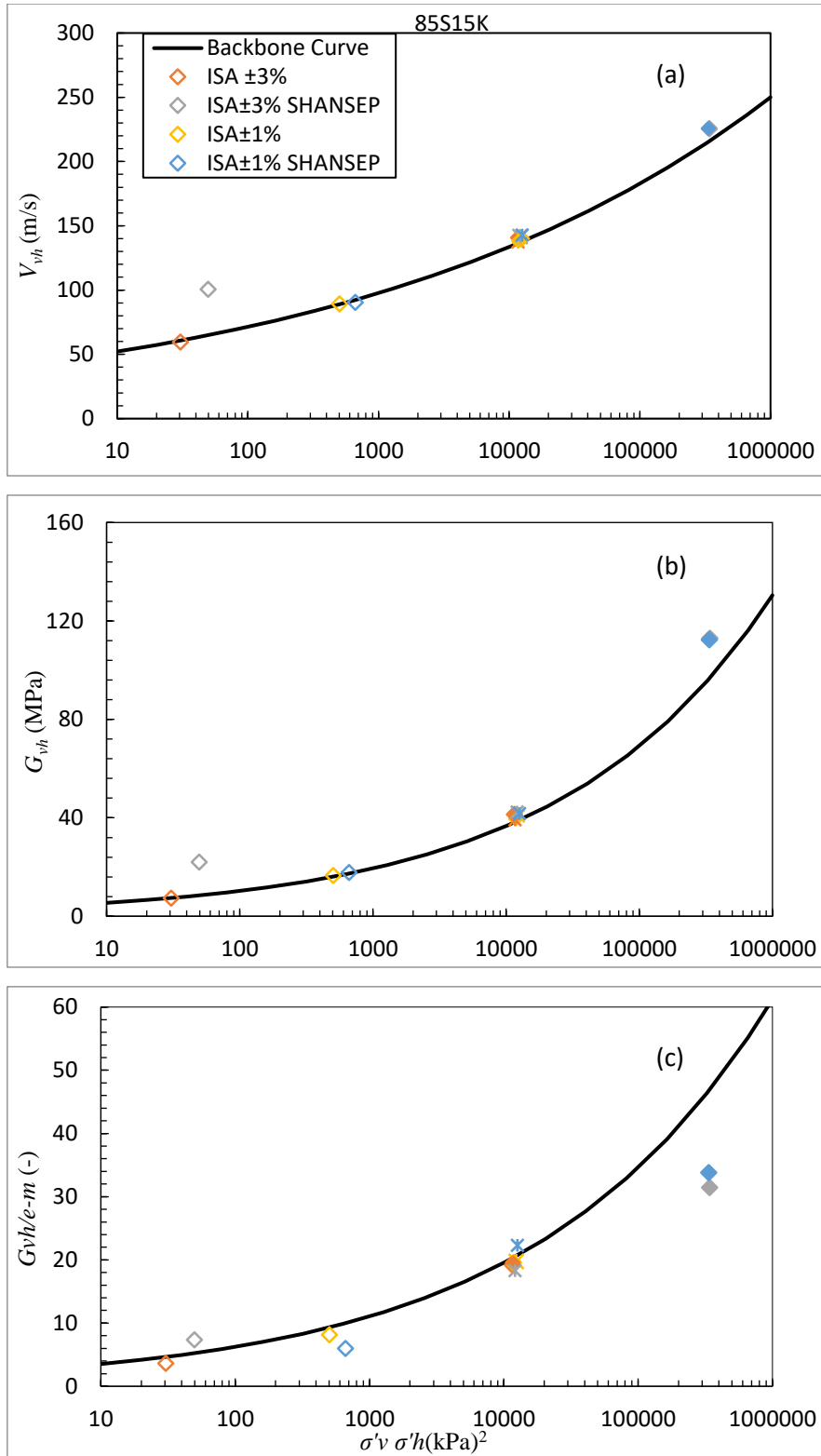
Figure 4.3 3 Backbone curve of 85S15K OCR=3.6 (a) V_{vh} versus $\sigma_v'\sigma_h'$ (b) G_{vh} versus $\sigma_v'\sigma_h'$ (c) G_{vh}/e^{-m} versus $\sigma_v'\sigma_h'$ with pre-ISA (crisscross symbols), end of ISA, and post-ISA (shaded symbols) data from ±1% & ±3% ISA Recompression and SHANSEP consolidation
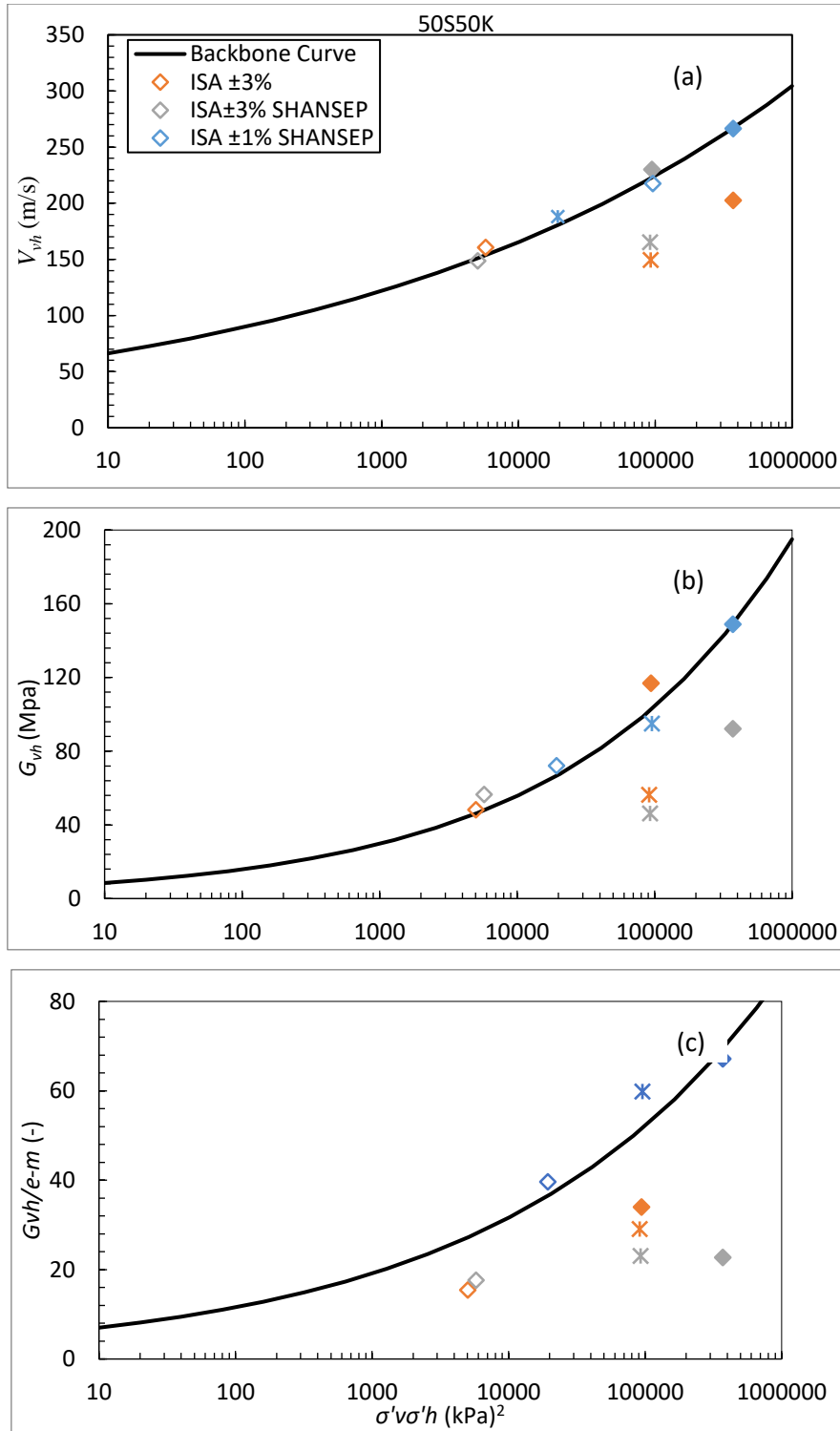
Figure 4.3 4 Backbone curve of normally consolidated 50S50K (a) V_{vh} versus $\sigma_v'\sigma_h'$ (b) G_{vh} versus $\sigma_v'\sigma_h'$ (c) G_{vh}/e^{-m} versus $\sigma_v'\sigma_h'$ with pre-ISA (crisscross symbols), end of ISA, and post-ISA (shaded symbols) data from ±1% & ±3% ISA Recompression and SHANSEP consolidation
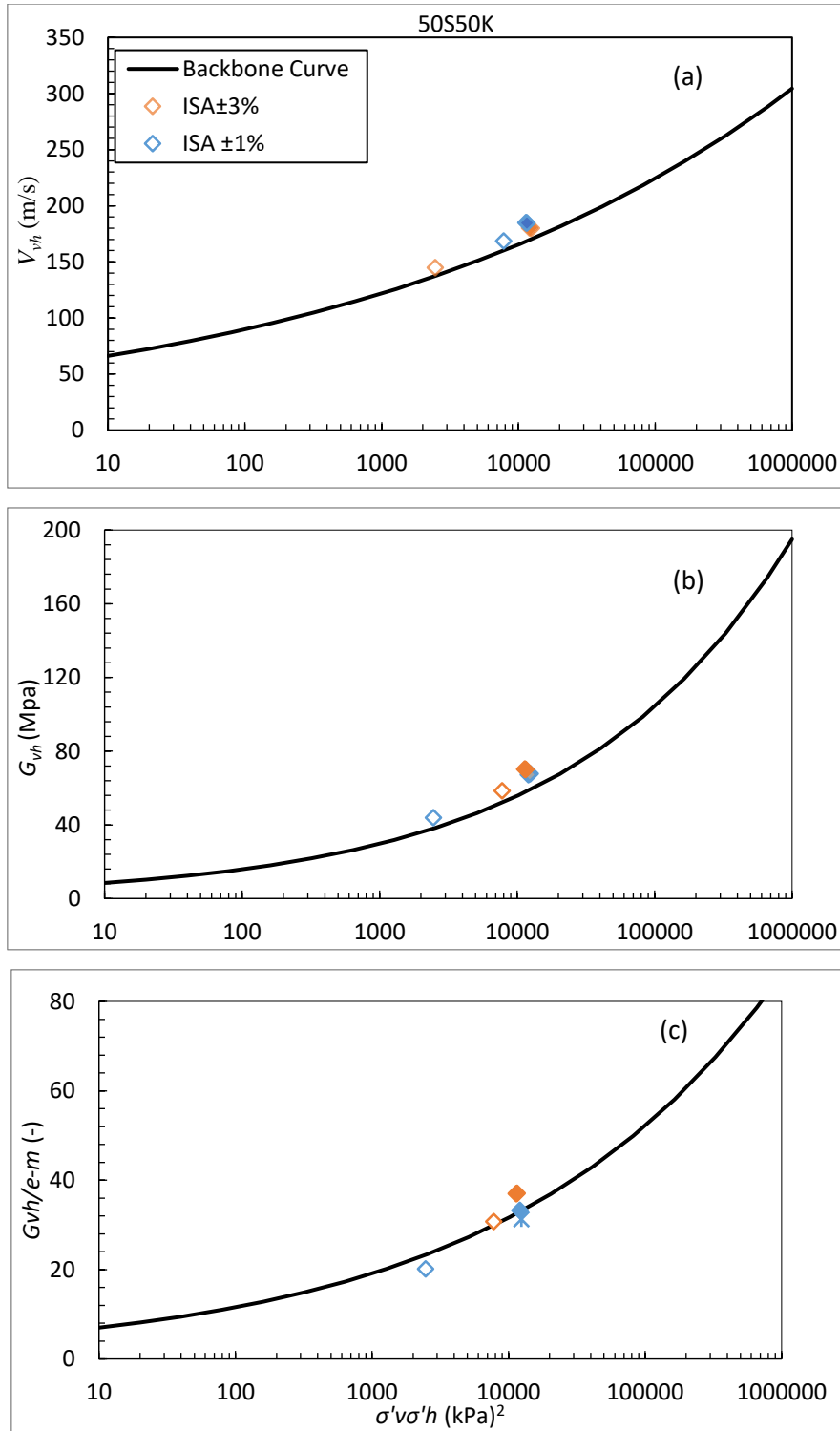
Figure 4.3 5 Backbone curve of 50S50K OCR=3.6 (a) V_{vh} versus $\sigma_v'\sigma_h'$ (b) G_{vh} versus $\sigma_v'\sigma_h'$ (c) G_{vh}/e^{-m} versus $\sigma_v'\sigma_h'$ with pre-ISA (crisscross symbols), end of ISA, and post-ISA (shaded symbols) data from ±1% & ±3% ISA Recompression and SHANSEP consolidation
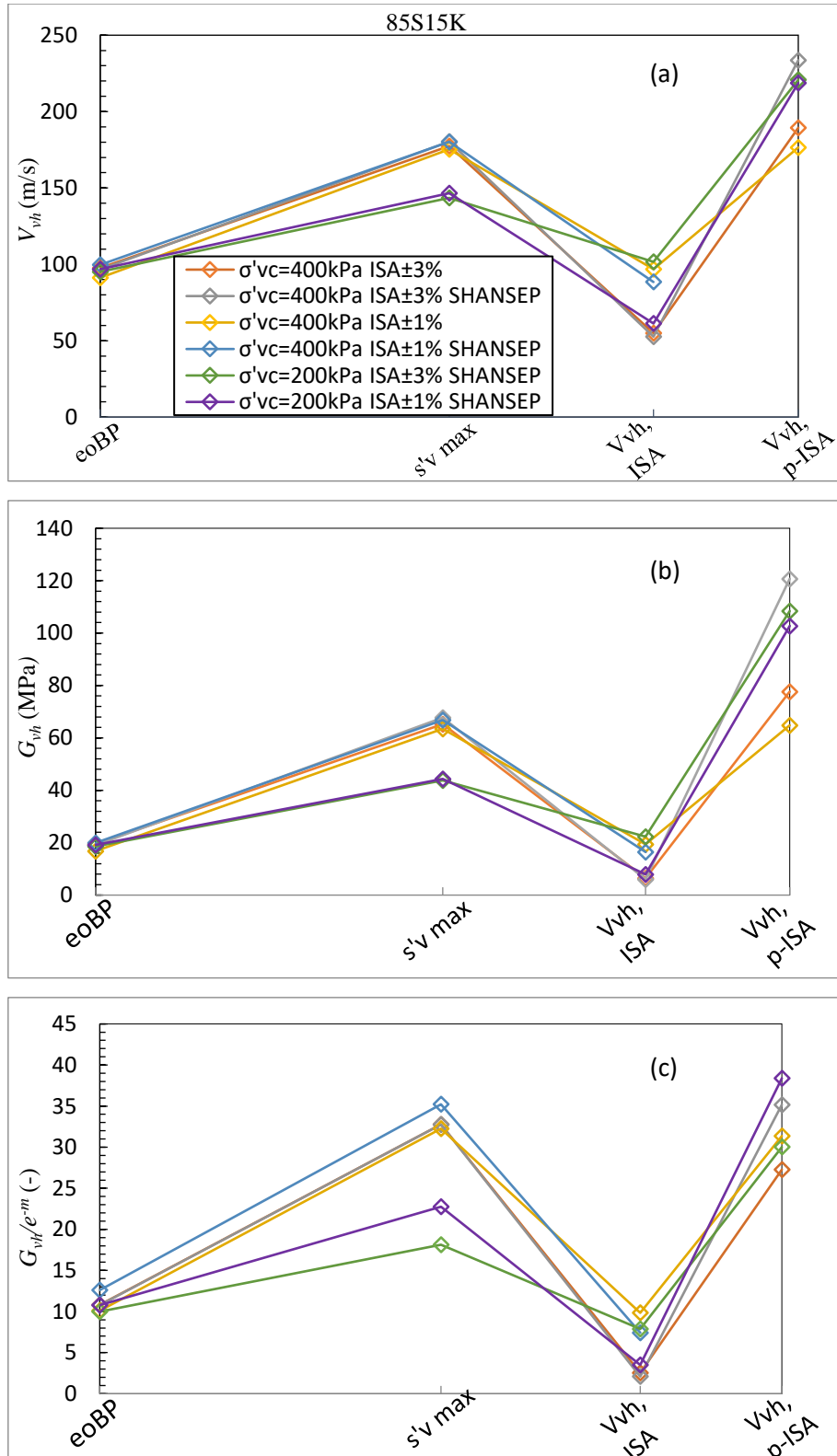
Figure 4.3 6 Shear wave velocity at various ISA test stages for normally consolidated 85S15K (a) V_{vh} (b) G_{vh} (c) G_{vh}/e^{-m} (e_{0BP} = end of back pressure, σ'_{vc} = pre-ISA, $V_{vh,ISA}$ = end of ISA, and $V_{vh,p\text{-}ISA}$ = after post-ISA reconsolidation).
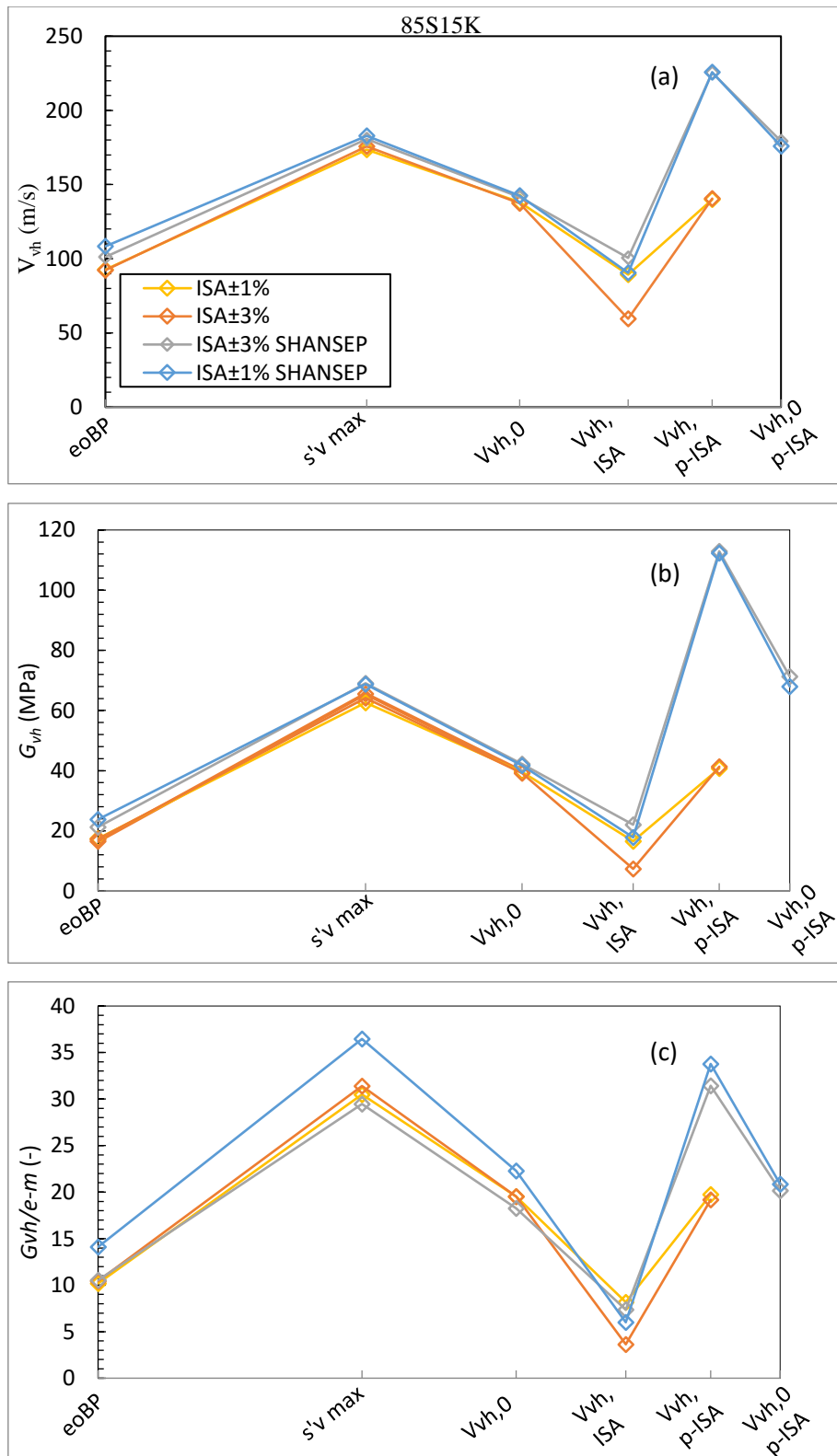
Figure 4.3 7 Shear wave velocity at various ISA test stages for 85S15K OCR=3.6 (a) V_{vh} (b) G_{vh} (c) G_{vh}/e^{-m} (e_{0BP} = end of back pressure, σ'_{vc}=pre-ISA(loading), $V_{vh,0}$ = pre-ISA(unloading), $V_{vh,ISA}$ = end of ISA, Vvh,p-ISA = after post-ISA SHANSEP, $V_{vh,0\text{-}ISA}$ = after post-ISA reconsolidation).
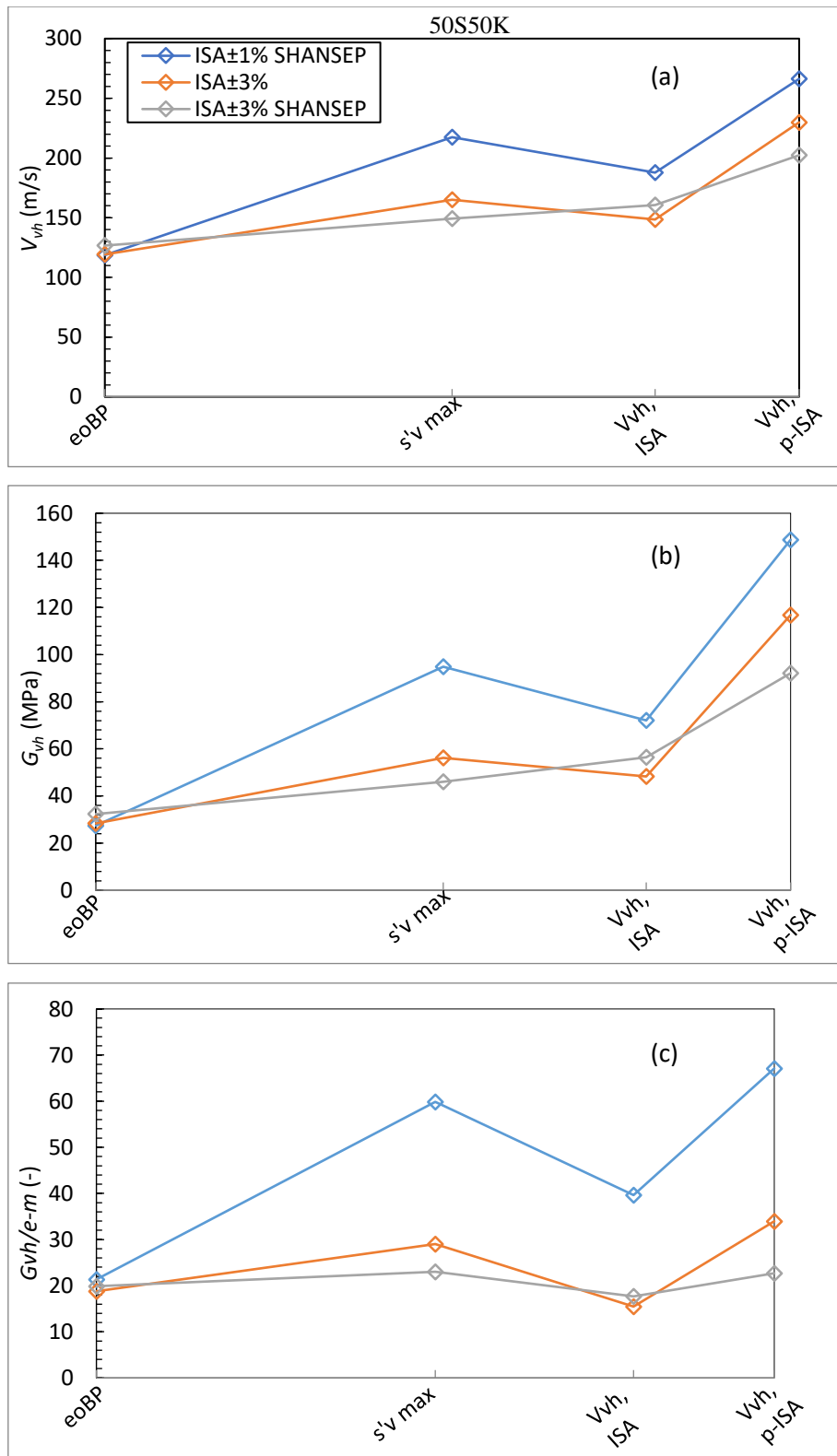
Figure 4.3 8 Shear wave velocity at various ISA test stages for normally 50S50K (a) V_{vh} (b) G_{vh} (c) G_{vh}/e^{-m} (e_{0BP} = end of back pressure, σ'_{vc}=pre-ISA, $V_{vh,ISA}$ = end of ISA, $V_{vh,p-ISA}$ = after post-ISA reconsolidation).

Figure 4.3 9 Shear wave velocity at various ISA test stages for 50S50K OCR=3.6 (a) V_{vh} (b) G_{vh} (c) G_{vh}/e^{-m} (e_{0BP} = end of back pressure, σ'_{vc}=pre-ISA(loading), $V_{vh,0}$ = pre-ISA(unloading), $V_{vh,ISA}$ = end of ISA, $V_{vh,p\text{-}ISA}$ = after post-ISA reconsolidation).

CHAPTER 5. SUMMARY AND CONCLUSION

5.1 Summary

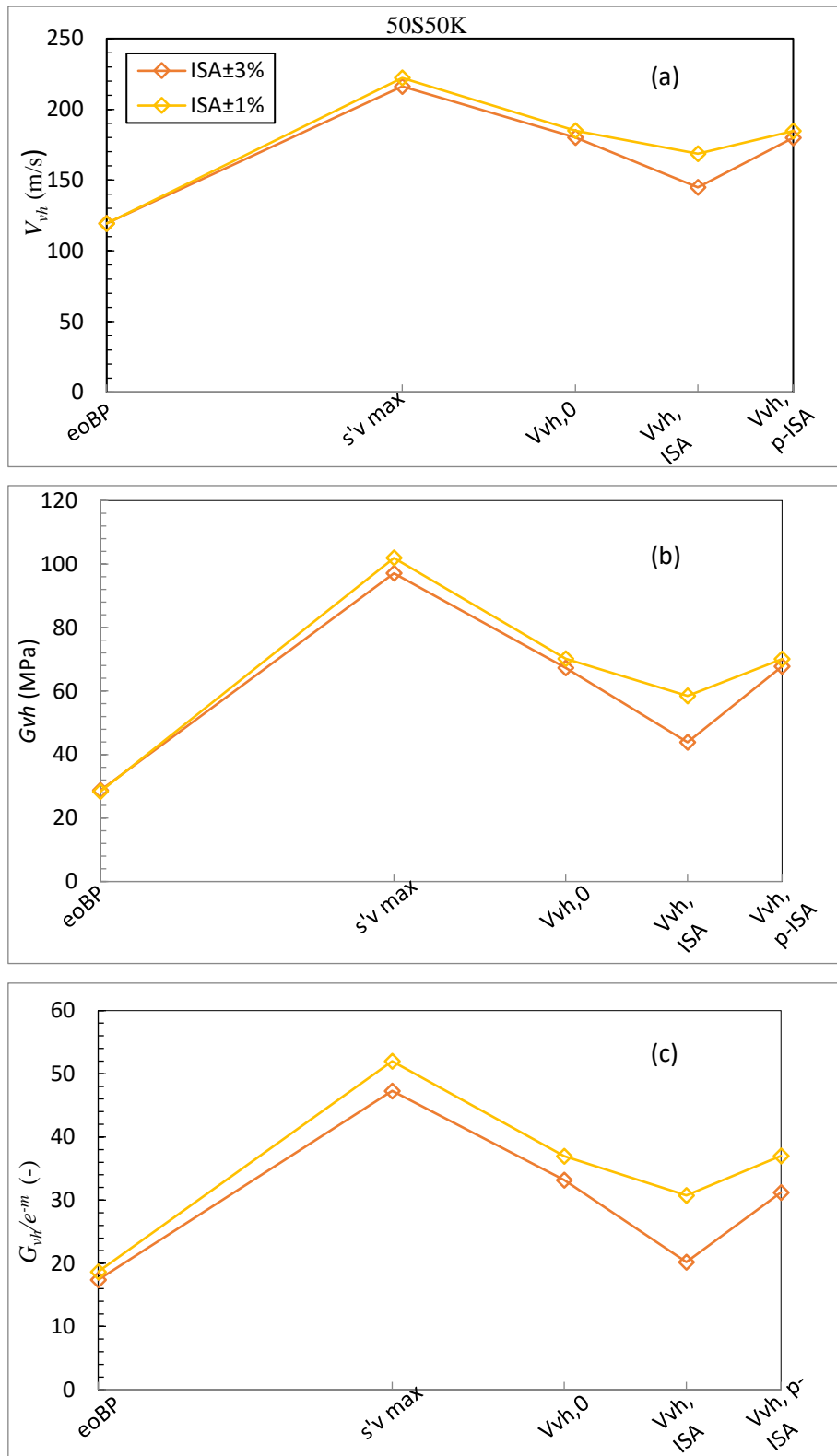This thesis presents methods and test results from triaxial testing of reconstituted silt samples subjected to simulated tube sampling disturbance. The test soils consisted of two synthetic soils 85S15K consisting of 85% silt and 15% kaolin and 50S50K consisting of 50% silt and 50% kaolin and one natural soil known as Dedham Silt. The plasticity index for the soils were 16% for 50S50K, 4% for 85S15K and non-plastic for Dedham Silt. The reconstituted specimens were prepared using the vacuum split mold technique and were tested in a triaxial stress path cell system equipped with bender elements using ideal sampling approach (ISA) framework to simulate tube sampling.

The first part of the laboratory testing was to perform anisotropically consolidated undrained triaxial compression tests (CAUC) at various consolidation stress levels on test soils with the end of consolidation vertical effective stress (s'vc) ranging from 100 to 800 kPa. The objective of these tests was to evaluate the influence of stress level on the normalized undrained shear strength of the test soils. 85S15K specimens initially showed contractive behavior during undrained shear for all preshear consolidation stress levels but changed to dilative behavior at larger strains towards the end of the tests. The normalized undrained shear strength generally does not increase with an increase in stress level. Similarly, 50S50K specimens all exhibited contractive behavior through the entire shearing phase of the tests. The near perfect linear regression fit through the undrained shear strength ($s_u = q_{max}$) versus preshear vertical effective stress for 85S15K (S = s_u/s'vc = 0.30) and 50S50K (S = 0.26) indicated little to no dependency of the normalized undrained stress strength with consolidation stress level. Unlike the other two test soils, Dedham silt specimens exhibited fully dilative behavior during undrained shear for all consolidation stress levels and did not reach a peak shear stress value.

85S15K consolidated to $\sigma'_{vc} > 400$ kPa, showed a gain in the post peak normalized shear stress with an increase in strain once the stress paths reached the failure envelope. If the specimens were subjected to continuing shearing to much higher strains, then the post peak normalized shear stress would exceed the peak shear stress reached during the initial contractive behavior phase. This demonstrates the tendency for low plasticity silts to exhibit dilative behavior not only increases with a decrease in plasticity but also with an increase in consolidation stress level. The later effect is presumably due to the continuing decrease in void ratio with increasing consolidation stress level. Using the Brandon et al. (2006) failure criteria for 85S15K, the peak excess pore pressure and k_f line methods showed consistency in an increase in normalized undrained shear strength with an increase in consolidation stress level. For 50S50K the normalized undrained shear strength does not show any trend with an increase in consolidation stress level. Dedham silt showed a decreasing trend in normalized undrained shear strength with increasing consolidation stress level for peak deviator ($\sigma_1 - \sigma_3)_{max}$, peak principal stress ratio $(\sigma_1'/\sigma_3')_{max}$, k_f line and limiting strain (5%) failure criteria.

The second part of the laboratory testing included normally consolidated (overconsolidation ratio OCR = 1) and OCR = 3.6 specimens that were subjected to two levels of ISA axial strain cycles ±1.0%, and ±3.0% followed by either Recompression or SHANSEP reconsolidation and then sheared undrained. The objective of this test program was to study the effect of Recompression and SHANSEP consolidation procedures on post ISA behavior of the test soils. The effect of ISA disturbance is much more significant for the low plasticity 85S15K soil than the low plasticity 50S50K clay. 85S15K and Dedham silt showed significant loss in effective stress during ISA disturbance in reference to the undisturbed behavior and much larger than 50S50K. Although this loss in effective stress decreased with increase in OCR.

For normally consolidated 85S15K and the lower ISA straining of ±1.0%,, Recompression consolidation resulted in an increase in the undrained shear strength and eliminated the contractive behavior of the undisturbed specimen resulting in dilative behavior. The SHANSEP consolidation procedure recovers to some extent the undisturbed behavior and reduces the dilative behavior exhibited by the Recompression specimen, however, it overestimated the undrained shear strength of the soil. For higher OCR and ISA disturbance SHANSEP consolidation does not mitigate the ISA disturbance and the specimens have a greater tendency for post-ISA dilation behavior. For 50S50K, SHANSEP consolidation is more effective in recovering the undisturbed behavior compared to 85S15K but overestimates the undrained shear strength. Dedham Silt in all cases shows highly dilative behavior but ISA straining removes the initial contractive phase for the OCR = 1 behavior while it creates an initially softer response (i.e., lower slope in the stress-strain curve) for the OCR = 3.6 specimens with ±1% & ±3% ISA straining.

The third part of the laboratory testing included measurement of shear wave velocity and small strain modulus during undisturbed and ISA tests performed on 85S15K and 50S50K. The objective of these measurements was to evaluate the influence of ISA straining, post-ISA Recompression and SHANSEP consolidation procedures after ISA disturbance on shear wave velocity V_{vh} and small strain shear modulus G_{vh} of the test soils. For normally consolidated 85S15K ISA straining followed by Recompression and SHANSEP post-ISA consolidation, the values of G_{vh} and V_{vh} during ISA disturbance reduced significantly relative to the pre-ISA undisturbed stress state. This reduction in G_{vh} and V_{vh} during ISA was higher for specimens consolidated at higher consolidation stress levels and subjected to higher levels of disturbance but smaller with higher OCR and plasticity of the soil. Post-ISA reconsolidation G_{vh} and V_{vh} values returned to the pre-ISA undisturbed states exhibiting that the specimen has fully recovered the disturbance according to these measures. Even though

G_{vh} and V_{vh} are reduced during ISA disturbance in reference to the pre-ISA undisturbed behavior, the values plot on the backbone curve exhibiting full recovery of the ISA induced degradation of these parameters.

5.2 Conclusions

The CAUC tests results of 85S15K and 50S50K indicated little to no dependency of the normalized undrained stress strength with consolidation stress level, however, as observed in 85S15K, increase in consolidation stress level increases the tendency for the low plasticity silts to exhibit dilative behavior. Overall, ISA tests results showed that the effect of Recompression and SHANSEP consolidation procedures on post ISA behavior (i.e. recovering the undisturbed behavior) of intermediate soils is dependent on the plasticity of the soil, to some extend on the pre-ISA consolidation stress (as observed in 85S15K), level of ISA disturbance experienced by the specimen and the overconsolidation ratio.

The G_{vh} and V_{vh} measurements showed that the reduction due to ISA disturbance for 85S15K and 50S50K could be used as an indicator of sample disturbance in similar types of silts. The amount of reduction in G_{vh} and V_{vh} was found to be dependent on plasticity of soil, level of disturbance and OCR. However, once specimens are reconsolidation back to the initial effective stress state it appears that G_{vh} and V_{vh} values are largely fully recovered and do not indicate any influence of the induced disturbance. Furthermore, since these observations are limited to two kinds of silts tested, more research incorporating different types of silts is needed to fully understand the effect of sample disturbance on G_{vh} and V_{vh} of the soil.

REFERENCES

American Society of Testing and Materials (ASTM), (2011). *Annual Book of Standards, Section 4 Construction, Vol. 4.08, Soil and Rock (I): D420 – D5876.* West Conshohocken, PA. Baligh, M. M., A. S. Azzouz and C. T. Chin. (1987), "Disturbances due to ideal tube sampling", Journal of Geotechnical Engineering 113(7), 739–757.

Bjerrum, L. and K.H. Andersen. (1972), "In situ measurements of lateral pressures in clay", *Proceedings of the 5th European Conference on Soil Mechanics and Foundation Engineering*, Madrid, Spain, 11–20.

Carroll, Roselyn. (2013), "The engineering behavior of Irish silts", PhD thesis, University College Dublin.

Clayton, C. R. I., D. W. Hight and R. J. Hopper. (1992), "Progressive destructuring of Bothkennar clay: implications for sampling and reconsolidation procedures," *Géotechnique* 42(2), 219–239.

Clayton, C.R.I., Siddique, A., and Hopper, R.J. (1998). "Effects of Sampler Design on Tube Sampling Disturbance - Numerical and Analytical Investigations," *Géotechnique*, 48(6), 847-867.

DeGroot, D.J., Lunne, T. and Tjelta, T.I. (2010). "Recommended best practice for geotechnical site characterization of offshore cohesive sediments." Invited Keynote Paper. *Proceedings of the 2nd International Sym. on Frontiers in Offshore Geotechnics*. Perth, Western Australia, 33-57.

Donohue, S., and Long, M. (2010). "Assessment of sample quality in soft clay using shear wave velocity and suction measurements," *Géotechnique*, 60(11), 883-889.

Fleming, L. N. and J. M. Duncan. (1990), "Stress-deformation characteristics of Alaskan silt", *Journal of Geotechnical Engineering*, ASCE 116(3), 377–393.

Hardin, B.O., and Blandford, G.E. (1989). "Elasticity of particulate materials," *Journal of Geotechnical Engineering*, 115(6), 788-805.

Hight, D. W. and S. Leroueil. (2003), "Characterization of soils for engineering purposes", *Characterization and Engineering Properties of Natural Soils: Proceedings of the International Workshop*, Vol. 1, Singapore, 255–360.

Jamiolkowski, M., Lancellotta, R. & Lo Presti, D.C.F. (1995). "Remarks on the Stiffness at Small Strains of Six Italian Clays." *Pre-failure Deformation of Geomaterials*, Shibuya, Mitachim & Miura (eds.), Vol. 1, 817–836. Balkema: Rotterdam.

Ladd, C.C, and DeGroot, D.J. (2003) "Recommended practice for soft ground site characterization: Arthur Casagrande lecture," *Proceedings of the 12th Panamerican Conference on Soil Mechanics and Geotechnical Engineering*, Cambridge, MA. 1-63.

Ladd, C.C. and Foott, R. (1974). "New design procedure for stability of soft clays." *Journal of the Geotechnical Engineering Division*, *ASCE*, 100(7), 763–786.

Ladd, C.C., and Lambe, T.W., (1963). "The Strength of 'Undisturbed' Clay Determined from Undrained Tests," *American Society for Testing and Materials, STP 361*, 342-371.

Landon, M.M., DeGroot, D.J., and Sheahan, T.C. (2007). "Non-Destructive sample quality assessment of a soft clay using shear wave velocity," *Journal of Geotechnical and Geoenvironmental Engineering*, 133(1), 424-432.

Long, M. (2006a), "Sample disturbance effects on medium plasticity clay/silt", *Proceedings of the Institute of Civil Engineers - Geotechnical Engineering* 159(2), 99–111.

Long, Michael, Gisli Gudjonsson, Shane Donohue and Knut Hagberg. (2010), "Engineering characterisation of Norwegian glaciomarine silt", *Engineering Geology* 110(3-4), 51–65.

Lukas, W. (2017). "An Experimental Investigation of the Influence of Sampling on the behavior of Intermediate Soils" (Doctoral dissertation).

Lukas, W.G., DeGroot, D.J., Zhang, G., DeJong, J.T., and Krage, C.P. (2017). "Influence of laboratory simulated tube sampling disturbance on undrained shear behavior of a low plasticity synthetic intermediate soil." *Proc. 19th Int. Conf. on Soil Mechanics and Geotechnical Engineering*, Seoul, Korea, Sept 2017.

Lunne, Tom, Toralv Berre, Knut H Andersen, Stein Strandvik and Morten Sjursen. (2006), "Effects of sample disturbance and consolidation procedures on measured shear strength of soft marine Norwegian clays," *Canadian Geotechnical Journal* 43(7), 726–750.

Pennington, D.S., Nash, D.F.T., and Lings, M.L. (1997). "Anisotropy of G0 shear stiffness in Gault clay." *Géotechnique*, 47(3), 391-398.

Sandven, R. (2003), Geotechnical properties of a natural silt deposit obtained from field and laboratory tests, in "Characterization and Engineering Properties of Natural Soils: *Proceedings of the International Workshop*", Vol. 2, Singapore, pp. 1121–1148.

Santagata, M. C. and J. T. Germaine. (2002), "Sampling disturbance effects in normally consolidated clays", *Journal of Geotechnical and Geoenvironmental Engineering* 128(12), 997–1006.

Santagata, M. C., J. V. Sinfield and J. T. Germaine. (2006), "Laboratory simulation of field sampling: comparison with ideal sampling and field data", *Journal of Geotechnical and Geoenvironmental Engineering* 132(3), 351–362.

Santagata, M. and J. T. Germaine. (2005), "Effect of OCR on sampling disturbance of cohesive soils and evaluation of laboratory reconsolidation procedures", *Canadian Geotechnical Journal* 42(2), 459– 474.

Siddique, A., S.M. Farooq and C. R. I. Clayton. (2000), "Disturbance due to tube sampling in coastal soils", *Journal of Geotechnical and Geoenvironmental Engineering* 126(6), 568–575.